論文 / 著書情報
Article / Book Information

題目(和文)	
Title(English)	Establishment of component design approaches to ensure anchor rods yielding in exposed steel column bases
著者(和文)	楊暁雨
Author(English)	Xiaoyu Yang
出典(和文)	学位:博士（工学）, 学位授与機関:東京工業大学, 報告番号:甲第11832号, 授与年月日:2022年3月26日, 学位の種別:課程博士, 審査員:吉敷 祥一,元結 正次郎,河野 進,西村 康志郎,佐藤 大樹
Citation(English)	Degree:Doctor (Engineering), Conferring organization: Tokyo Institute of Technology, Report number:甲第11832号, Conferred date:2022/3/26, Degree Type:Course doctor, Examiner:,,,,
学位種別(和文)	博士論文
Type(English)	Doctoral Thesis

A thesis submitted for the degree of

Doctor of Engineering

Establishment of Component Design Approaches to Ensure Anchor Rods Yielding in Exposed Steel Column Bases

Yang Xiaoyu

Supervisor: Prof. Kishiki Shoichi

Department of Architecture and Building Engineering

Tokyo Institute of Technology

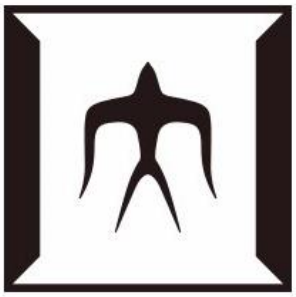

Feb. 2022

Abstract

Exposed column bases are extensively used in low-to-medium rise steel structures. As a connection type between steel column and reinforced concrete foundation, they can transfer weight, seismic load, and wind loads from the superstructure to the sub-system, which makes exposed column bases in the most severe stress state. Moreover, the stress transfer mechanism in the column base is extremely complicated at various failure modes. Among all of the failure modes, one of them stated in the Japanese design recommendations is the yielding of anchor rods, with corresponding demands for the design of superstructures fully established. However, when considering the yielding of anchor rods, the anchorage of anchor rods must be kept. In other words, concrete breakout failure owing to the pull-out of anchor rods must be prevented. Also, with the tensile yielding of the anchor rods, in the compression side of exposed column bases, the bearing failure of the foundation concrete must be prevented. While in the current design recommendations in Japan, the statement of the calculation of concrete breakout failure strength and bearing stress was not clear. Furthermore, the experimental studies on them were limited in number. Thus, an experimental study was conducted with full-scaled exposed column base specimens. By analyzing the experiment results, the design approaches of concrete breakout failure strength and bearing stress are proposed.

In Chapter 2, experiment plan and results are introduced. There are ten full-scaled exposed column base specimens in total. Experiment parameters include the number of column longitudinal rebar, embedded length of anchor rods, type of anchor rods, strength of concrete foundation, etc. In the loading process, significant concrete breakout failure cracks were observed, which also caused the deterioration of strength. As a result, the concrete breakout failure strength calculated by the current design recommendation in Japan is higher than the experiment result about twice. As for the full-plastic moment, the calculation value using the current design recommendation fits the experiment result well. Furthermore, the influences of the parameters on the concrete breakout failure strength and bearing stress were clarified.

In Chapter 3, the design approach of concrete breakout failure is introduced. Based on the analysis of experiment results, the contribution of column rebar and the timing of concrete breakout failure are clarified. The current Column Base Recommendation in Japan overestimates the number of effective column rebar in the evaluation of concrete breakout failure strength. Not all of the column rebar in the concrete breakout failure area is contributed to the strength. Furthermore, in the case of exterior column-type column bases, the number of effective column rebar is related to the number of foundation beams. With the proposed consideration of effective column rebar number, in the calculation of maximum strength, using the current reduction factor 0.7 applying to the strength of column rebar fit experiment results well. Regarding the contribution of concrete, the strength at the instant when conical cracks occurred is experimentally obtained, after the crack occurred, the strength decreased and stabilized till the ultimate state. In the design of anchor rods considering the concrete breakout failure, to prevent the occurrence of conical cracks, it is proposed that only the contribution of concrete should be counted. After the crack occurred, the strength of effective column rebar can be added to calculate the ultimate strength. This proposal is proved available by the database containing previous experiment results related to concrete breakout failure.

In Chapter 4, the design approach of concrete bearing stress is introduced. The applicability and accuracy of current evaluation methods of bearing stress in the case of exposed column bases are discussed. Previous experiment data relate to exposed column base and anchor rods yielding are collected and analyzed. A method to normalize the experiment data is proposed. As for the evaluation result, the method stated in a recommendation of Architectural Institute of Japan can evaluate the strength most conservatively. About the method stated in a recommendation of American Concrete Institute and Kutani & Masuda's equation, they fit the LRFD design philosophy well. While considering the design philosophy in Japan, a relatively more conservative equation was proposed and it could reduce the number of overestimated specimens to approximately 19.3%.

In all, by conducting the experiments and analyzing the experiment results, the

component design approaches are proposed to prevent concrete breakout failure and bearing failure in the exposed column bases. Following the design route of exposed column bases in Japan, considering the proposed calculation methods of concrete breakout failure and bearing stress, the yielding of anchor rod could be ensured.

Contents

Chapter 1.
Introduction

1. Introduction

Exposed column bases are extensively used in low-to-medium rise steel structures. As shown in Figure 1-1, exposed column bases are composed of the steel column welded with steel base plate, and fixed with the foundation concrete by the steel anchor rods. They serve as a connection type between steel column and reinforced concrete (RC) foundation. Exposed column bases could transfer weight, seismic load, and wind load from the superstructure to the sub-system. However, the stress transfer mechanism in the column base is extremely complicated at various failure modes. One of the failure modes mentioned in the Japanese design recommendations [1-1] involves the yielding and fracture of anchor rods. To ensure this failure mode, the pull-out failure of the anchor rods—one of the reasons responsible for the concrete breakout failure—and bearing failure of foundation concrete must be prevented. However, in Japan, the current design recommendation regarding the concrete breakout failure and bearing strength in the case of exposed column bases is not clear, and the studies that have focused on these topics are limited in number. Thus, an experimental study was conducted with full-scaled exposed column bases applied to cyclic loading to clarify the problems mentioned above.

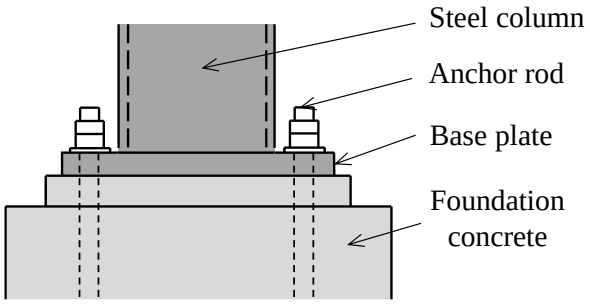

Figure 1-1 Component of exposed column bases

1.1 Research background and literature review

As exposed column bases transfer all the loads from the superstructure to the foundations, the stress state of exposed column bases is the most severe. In previous earthquakes, significant failure of exposed column base was observed. In the 2011 Tohoku earthquake, as illustrated in Photo 1-1 [1-2], fracture of anchor rods was observed.

Photo 1-1 Anchor rods fracture in 2011 Tohoku earthquake [1-2]

For the failure modes of the exposed column bases, based on the energy dissipation ability, the failure modes could be summarized into two types: brittle failure and ductile failure. In the design of exposed column bases, brittle failure should be strictly prohibited due to the sudden loss of strength and energy dissipation capacity. Several typical brittle modes in exposed column bases were summarized as shown in Figure 1-2. They contained the fracture of anchor rods, bearing failure of foundation concrete, concrete breakout failure, and bearing failure in the anchorage parts. On the other hand, several ductile failure modes are permitted in the design of exposed column bases. As shown in Figure 1-3, ductile failure modes contained the yielding of base plates, yielding of steel column, and

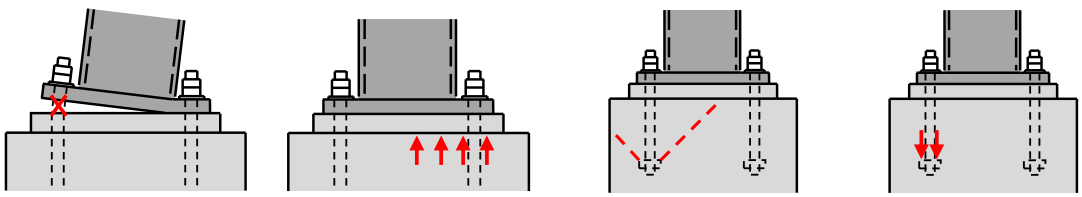

Figure 1-2 Brittle failure modes in exposed column bases

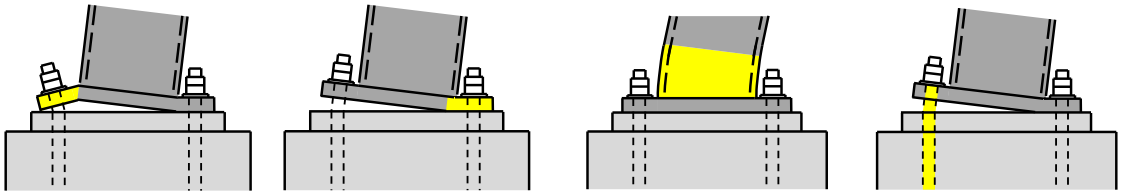

Figure 1-3 Ductile failure modes in exposed column bases

yielding of anchor rods. Due to the better energy dissipation ability compared to the brittle failure modes, there is relatively more research conducted to figure out the behavior related to the ductile failure modes. About the failure mode of yielding of base plates, the thickness of base plates will determine the strength, stiffness, and consequently the failure mode of exposed column bases. The thickness of base plates is associated with the ductility and hysteretic behavior of the exposed column bases [1-3]. Further, the thickness of base plate is also related to the distance from the edge of steel column to base plate. When the ratio of thickness to the distance becomes larger, the bending of base plate becomes less significant in the stress distribution[1-4]. The size of base plates will also influence the structural behavior. An experimental study on exposed column bases with different sizes of base plates was conducted. The size had a slight influence on the ductility of the connection and ultimate strength [1-5]. Related to the yielding of anchor rods, in the previous studies, the initial stiffness, ultimate strength, and post-yield behavior of the exposed column base, which influence the connection performance and affect the structural behavior, have been also documented in [1-6]-[1-9].

However, in the different design recommendations, the permittable ductile failure modes are also different. Thus, the exposed column base design recommendations were summarized and discussed by the different failure modes and further demands to ensure these failure modes.

1.2 Design recommendations about exposed column base

As there are many ductile failure modes of exposed column bases, in the current design recommendation of exposed column bases, permittable failure modes are different in the US [1-10], [1-11], EU [1-12], and Japan. In the design recommendations of exposed column bases in the US and EU, the yielding of base plates was also stated as a permittable failure mode of exposed column bases. However, in Japan, the design based on the yielding of base plates was not stated.

In Japan, a design process of exposed column bases is presented in the AIJ Guidebook on Design and Fabrication of Column Base in Steel Structure (Column Base Recommendation) [1-1]. Figure 1-4 shows the current design process of column bases used in Japan. From the frame view, plastic hinges are allowed in the column base, and the anchor rods applied in the column base should be ductile (with guaranteed and sufficient elongation ability). If this requirement is not satisfied, the column base must be designed to remain elastic under severe earthquakes (case C). The strength of the steel column ${}_cM_{pc}$ is ensured with the appropriate choice of the connection factor α, which guarantees the energy dissipation of seismic members by preventing early fracture at the connection. The connection factor α is usually set to values between 1.3 and 1.5 as indicated by the Japanese instruction manual of technical standards on building structures related to the Building Standards Law (Instruction Manual) [1-13]. The relation of the maximum strength between the column base ${}_{cb}M_u$ and the steel column ($\alpha \cdot {}_cM_{pc}$) is considered as a premise in the design. Regarding the evaluation of ${}_{cb}M_u$, it is assumed to be equal to the full plastic moment of column base ${}_{cb}M_p$. In the Column Base Recommendation [1-1], ${}_{cb}M_p$ is calculated by accumulating the strength by considering the influence of axial force on the column base. As indicated in mode C of Figure 1-4, if the maximum strength of the column base ${}_{cb}M_u$ is smaller than ${}_cM_{pc}$, then there would be no plastic hinge allowed in the column base. Both the lower part of steel column and column base must be kept elastic in the ultimate state. This mode is not recommended in practice because of the difficulty in the design of structures. Regardless of the ductility of

the anchor rods, if ${}_{cb}M_u$ is greater than ($\alpha \cdot {}_cM_{pc}$), the plastic hinge will form in the steel column as indicated in Figure 1-4 (modes B-1 and B-2). By limiting the width-to-thickness ratio of the steel column, local buckling could be prevented with guaranteed sufficient plastic deformation at the bottom of the steel column. The last type is the column base hinged mode (mode A) as indicated in Figure 1-4. If ductile anchor rods are

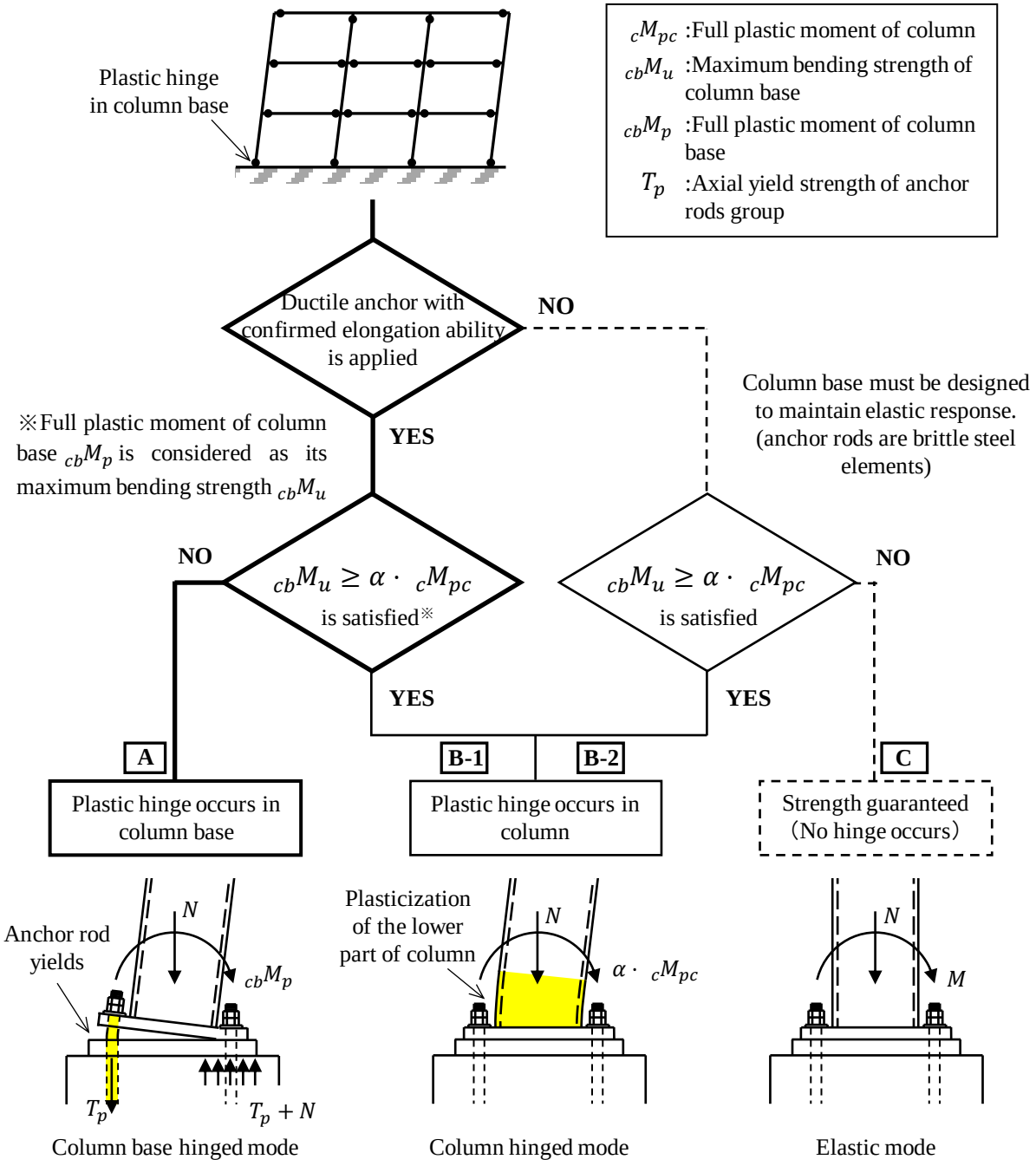

Figure 1-4 Failure mode of column base in a frame with the plastic hinge formed according to the recommendations of Architectural Institute of Japan [1-1]

Table 1-1 Relations between the column and anchor's strength, hysteresis curve, and yielding position

Mode	Column	Anchor	Hysteresis curve	Yielding position
A	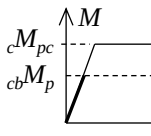	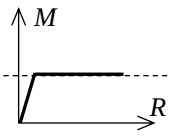	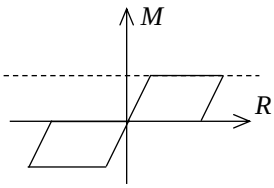	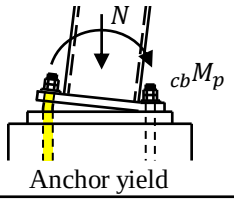
B-1	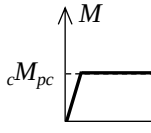	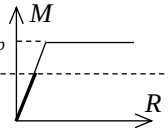	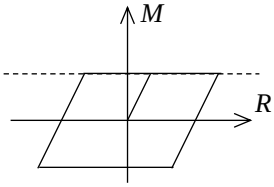	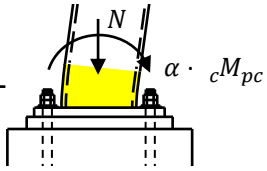
B-2	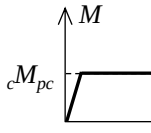	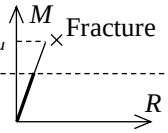	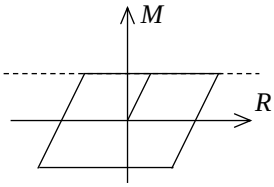	
C	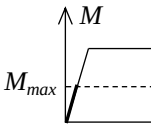	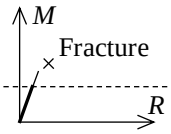	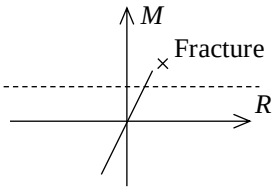	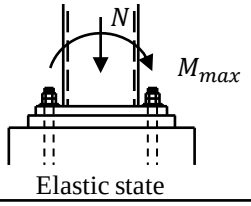

applied, and the maximum strength of column base $_{cb}M_u$ is less than ($\alpha \cdot {}_cM_{pc}$), the plastic hinge will occur in the column base and the anchor rods will yield. A summary of the relations between the column and anchor strength, hysteresis curve, and yielding positions of these modes is outlined in Table 1-1.

To consider the effect of plastic deformation capacity on demanded horizontal strength of structures, in the current Building Standard Law of Japan, a coefficient of structural characteristics D_s (0.25–0.50 for steel structures) was set. The coefficient D_s is a reduction factor in the calculation of the demanded horizontal strength. Smaller D_s values indicate that the structure undergoes a larger plastic deformation capacity. In the case of anchor rods yielding, slip behavior will occur owing to the elongation of the anchor rods. Furthermore, the inflection point will shift downward, which will cause the damage concentration on the top of the column and the beam of the 2nd floor. In that way,

an increase of 0.05 in the coefficient of structural characteristics D_s is necessary. In addition, to attain the rotation capacity of the column base, it is necessary to ensure that the elongation capacity of anchor rods is attained. It is required that the threaded part will not fracture before a sufficient plastic deformation develops on the shaft part. In this way, the section area ratio of the threaded part to the shaft part is strictly controlled to be greater than the yield ratio of material. The upper limit of yield ratio of the anchor rods is controlled to be 80% [1-14]. Generally, there are two fabrication methods of thread in the anchor rods, namely, rolled threads (ABR), and machined threads (ABM) [1-15]. For ABR, the strength of thread increases owing to the roll threading. Additionally, the section area of the threaded part, A_e, is similar to the shaft part A_b ($A_e/A_b \approx 0.95$); accordingly, the threaded and shaft parts could yield at almost the same time. Until a complete plastic deformation occurs on the shaft part, a fracture will not occur on the anchor rods. In this respect, elongation of the anchor rods is close to the material (approximately equal to 20%). For ABM, the section area of threaded part is smaller than that of shaft part owing to the machine threading effect. To ensure that section area ratio of the threaded to the shaft part, metric fine thread was adopted, the upper limit of yield ratio of the anchor rods was controlled to 75%.

In Japan, the yielding of anchor rods is specially permitted in the design of exposed column bases. Generally, in the design of connections of steel structures, the strength of

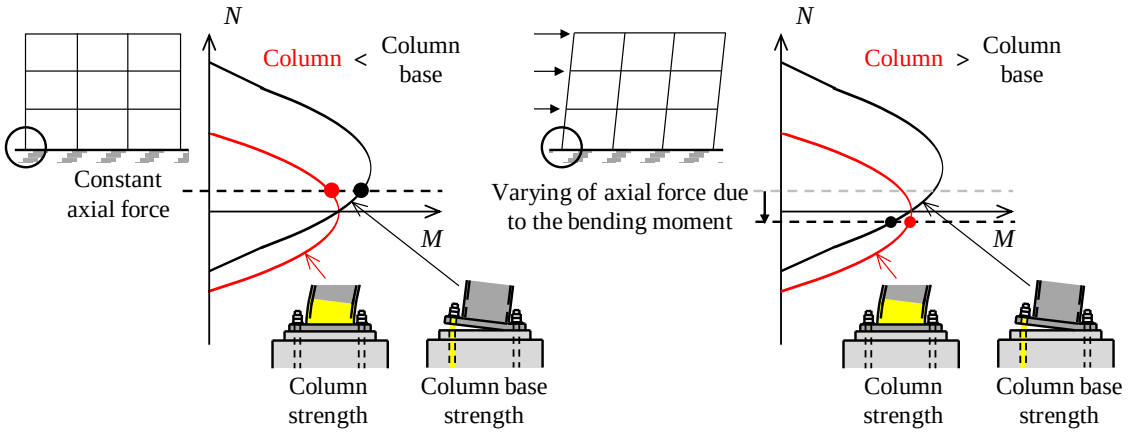

(a) Constant axial force (b) Varying axial force

Figure 1-5 Strength relation of steel column and column bases in different axial froce states

connections should be designed larger than the corresponding structural component. For example, in the beam-to-column connections, the strength of welding should be larger than the strength of beams. Damage must be prevented on the connections. However, the reason exposed column bases become an exception is that it is difficult to ensure the yielding of column for the edge columns due to the variance of axial force caused by bending moment. As shown in Figure 1-5, the full-plastic strength of exposed column base and steel column is correlated with the axial force. When there is no lateral force on the structures (no bending moment influencing the axial force on the column/column base), the axial force is constant. In this state, with the special design, the strength of steel column could be designed to be smaller than exposed column bases as illustrated in Figure 1-5(a). However, when the lateral force occurred, owing to the bending moment, the axial force on the column and column base will change. It will further influence the strength relation between the steel column and column base, in some cases, the strength relation of steel column and column base might be reversed, as illustrated in Figure 1-5(b). As it is hard to predict the varying range of axial force in earthquakes, in the design of exposed column base, even the yielding of steel column was designed to be the expected failure mode, ductile anchor rods are still recommended to be used in the column base in case of the above situation, to prevent the brittle fracture of anchor rods.

With the above consideration, the exposed column base could be designed as the failure mode of anchor rods yielding. However, to ensure the yielding of anchor rods, the concrete breakout failure and bearing failure of the foundation concrete must be prevented. Due to the insufficient statement of these two failure modes, an experimental study was conducted to clarify them to ensure the yielding of anchor rods.

1.3 Scope of thesis

In chapter 2, the experiment plan and results of ten full-scale exposed column base specimens are introduced. The experiment results are discussed by different parameters. Results related to the concrete breakout failure and bearing stress were also summarized.

In chapter 3, a design approach of concrete breakout failure is proposed. Experiment results related to the concrete breakout failure are analyzed to clarify the contribution of column longitudinal rebar and concrete in the strength of concrete breakout failure in exposed column bases. Based on the experiment results, the mechanism of concrete breakout failure was proposed and confirmed available by a database containing previous experiments about concrete breakout failure.

In chapter 4, a design approach of concrete bearing stress is proposed. Current calculation methods of bearing stress in exposed column bases are summarized. A database of exposed column bases experiments is established. By normalizing and analyzing the experiment results in the database, the accuracy and applicability of current bearing stress design approaches are evaluated, furthermore, considering the design philosophy in Japan, a more conservative design approach is proposed.

In chapter 5, the conclusions of each chapter are summarized. Following the design flow of exposed column bases in Japan, with the proposed component design approaches of concrete breakout failure and bearing failure, the exposed column base could be designed with the failure mode of anchor rods yielding.

References

[1-1] Architectural Institute of Japan: 2017, AIJ Guidebook on Design and Fabrication of Column Base in Steel Structure, Maruzen, Tokyo, 2017 (in Japanese).

[1-2] Kishiki S., Yamada S., et al., Damage to column bases and roof joints in steel school buildings due to the 2011 Tohoku earthquake. AIJ J. Technol. Des. Vol. 19, No.42, 585-590, 2013.6

[1-3] Astaneh A., et al. Behavior and design of base plates for gravity, wind and seismic loads. Proceedings of the National Steel Construction Conference, AISC, Chicago, Illinois, 1992

[1-4] DeWolf J. T. Column base plates. Structural Engineering Practive, Vol. 1, No. 1, pp. 39-51, 1982.

[1-5] Bruda J., Itani A. Studies of seismic behavior of steel base plates. Report No. CCEER 99-7, Center for Civil Engineering Earthquake Research, Dept. of Civil Engineering, Univ. of Nevada, Nevada, 1999.

[1-6] Aviram A, Stojadinovic B, Kiureghian A. Performance and reliability of exposed column base plate connections for steel moment resisting frames. PEER Rep. 2010/107, Pacific Earthquake Engineering Research Center, Berkeley, CA.

[1-7] Kanvinde A, Grilli D, Zareian, F. Rotational stiffness of exposed column base connections: Experiments and analytical models. J Struct Eng 2012, 549 –560.

[1-8] Yamada S. Influence of the elasto-plastic behavior of column bases on the ultimate earthquake resistance of multi-story steel moment frames. Proc., 12th World Conf. on Earthquake Engineering, New Zealand Society for Earthquake Engineering, Wellington, New Zealand, 2000.

[1-9] Yamada S, Akiyama H. Influence of the rigidity of column bases on the ultimate earthquake resistance of multi-story steel moment frames. J. Struct. Constr. Eng. 1997; 496: 113–118. (in Japanese).

[1-10] AISC. Steel Design Guide 1: Base plate and anchor rod design. 2nd edition, 2006.

[1-11] AISC. STEEL CONSTRUCTION MANUAL. 15th edition, 2017.

[1-12] Eurocode 3: Design of steel structures. Part 1-8: Design of joints, British

Standards, 2005.

[1-13] Instruction manual of building structures' technical standards affiliated with the Building Standards Law, 2015 (in Japanese).

[1-14] JIS G 3138, Rolled steel bars for building structure, 2005 (in Japanese).

[1-15] JIS B 1220, Set of anchor bolt for structures, 2015 (in Japanese).

Chapter 2.
Experimental study on exposed column bases

2. Experimental study on exposed column bases

To ensure the anchor rods yielding in the exposed column base, the pull-out of anchor rods and bearing failure of foundation concrete must be prevented. However, the current design recommendation did not state the calculation methods clearly. To clarify the concrete breakout failure mechanism and bearing stress in the case of exposed column bases, ten full-scale specimens of exposed column bases with foundation beam were specially designed and tested. In this chapter, the experiment plan and results were listed.

2.1 Experiment plan

2.1.1 Specimens and parameters

To clarify the concrete breakout failure mechanism and bearing stress in the case of exposed column bases, totally ten column base specimens were designed. They were divided into three series (A, B, C) owing to the different sizes of their structural components. The specimen consisted of a square hollow section (SHS) column, RC column, footing, and RC foundation beam. The shape of the B-series specimens was taken as an example as illustrated in Figure 2-1. Overview and dimension of test specimens are illustrated in Figure 2-2 and 2-3. The matrix of the parameters is listed in Table 2-1. The

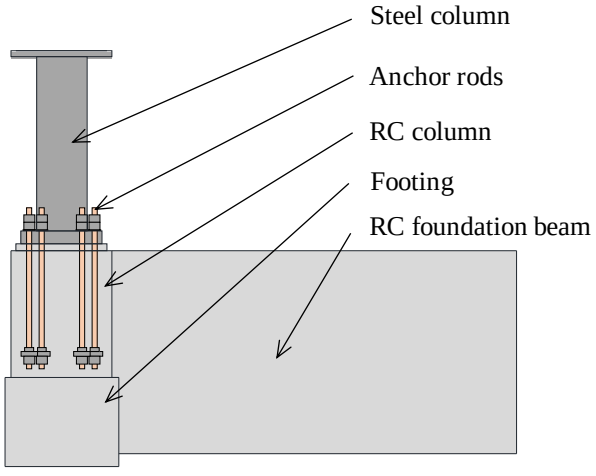

Figure 2-1 Shape and component of B-series specimens

parameters include the number of column rebars, embedded depth of anchor rods,

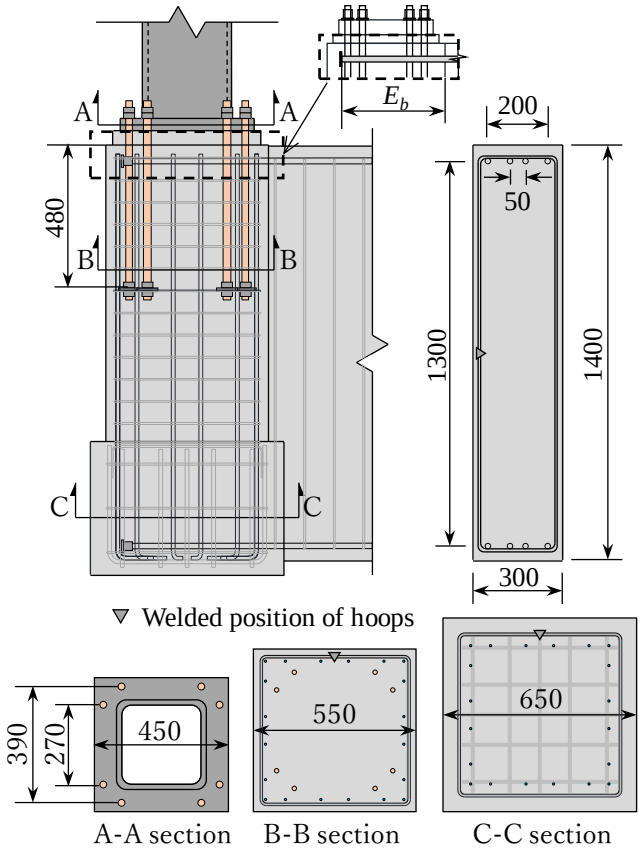

Figure 2-2 Details of A-series specimens

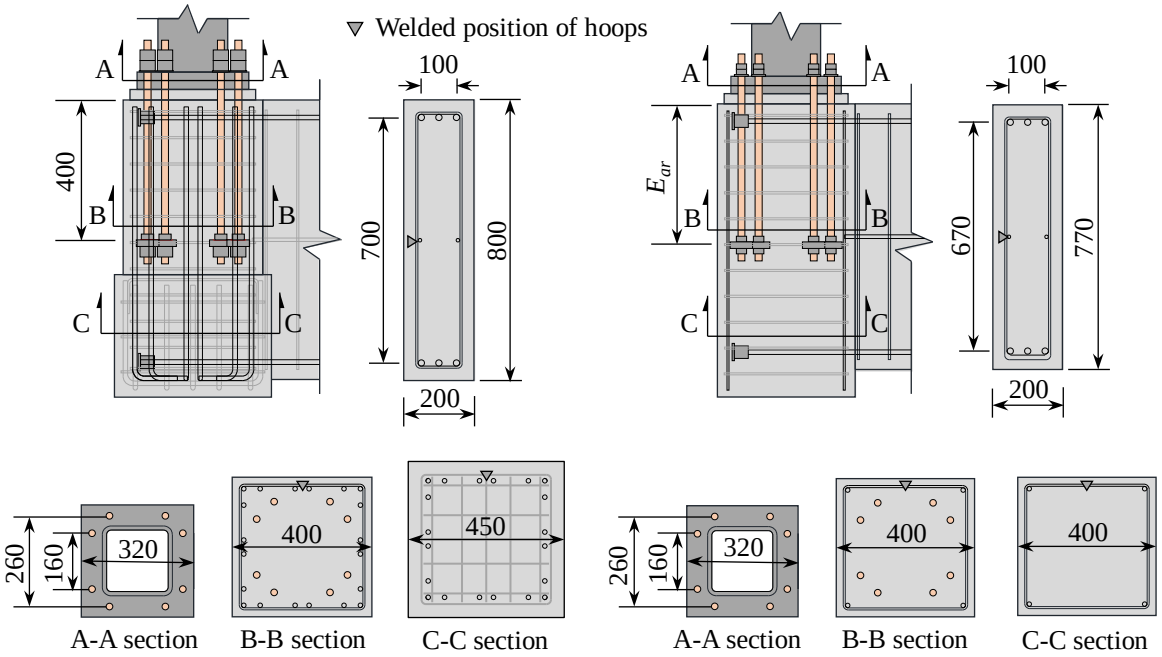

Figure 2-3 Details of B and C-series specimens

Table 2-1 Parameter matrix

Specimen	E_b [mm]	R_b [mm]	Grade of beam rebar	σ_b [N/mm^2]	E_{ar} [mm] (E_{ar}/R_{ar})	D_b [mm]	Anchor rods' grade (R_{ar})
A16-390-20d	490	16	SD390	21	480(20)	1400	M24 ABR490 (24)
A16S-390-20d	370						
B19-390-20d	350	19	SD390	21	400(20)	800	Φ19-PC Grade C (20)
B16-490-20d		16	SD490	21			
B16-590-20d		16	USD590	21			
B16H-590-20d		16	USD590	36			
C16-590-20d	350	16	USD590	21	400(20)	770	M20 ABR490 (20)
C16-590-30d					600(30)		
C16-590-39d					780(39)		
C16-590-39db							D19-SD345 (20)

Note: E_b: Embedded length of beam main rebar; R_b: Nominal diameter of beam main bar; σ_b: Nominal compression strength of concrete; E_{ar}: Embedded length of anchor rod; D_b: Beam depth; R_{ar}: Nominal diameter of anchor rod.

Table 2-2 Section property of specimens

Beam Section	**Beam main bar**	**Hoops**
A-Series	4-D16 (SD390)	12-D6(SD295) @100
B-Series	3-D16~D19 (SD390, SD490, USD590)	15-D6(SD295) @100
C-Series	3-D16 (USD590)	15-D6(SD295) @100
B-B Section	**Column rebar**	**Hoops**
A-Series	20-D13(SD390)	18-D6 (SD295) @75
B-Series	20-D13 (SD295)	12-D6 (SD295) @75
C-Series	4-D6 (SD295)	12-D6 (SD295) @75

Note: D6, 13, 16, 19: Deformed rebar with its nominal diameter as 6, 13, 16, 19mm, respectively. The nominal yield strength F_y of SD295, SD390, SD490, USD590 are 295, 390, 490, 590N/mm^2, respectively.

compression strength of concrete, and beam rebar. Specimens were named according to the format: Series-Diameter of beam rebar-Nominal strength of beam rebar-Embedded length of anchor rod. As an example, specimen A16-390-20d indicates that the specimen was in A-series, the nominal diameter of the beam rebar was 16 mm and had nominal yield strength of 390 N/mm^2. Additionally, 20d indicates that the embedded lengths of the anchor rods were 20 times their nominal diameters. Additionally, the symbols S and H in the name refer to the short-embedded length of the beam rebar and the higher compression strength of concrete, respectively. About specimen C16-590-39db, db represented that the deformed bar was used as the anchor rods. The detail of reinforcement arrangement in foundation beam and RC column is listed in Table 2-2. Welded hoops were used in the specimens to mitigate the complex reinforcement in the concrete. The weld position was illustrated in Figure 2-2 and 2-3 by triangle marks. The parameters and specimen properties will be introduced by the order of series.

In A-series, the parameter was the embedded length of beam rebar in concrete column. In B-series, the parameters included the diameter and grade of beam rebar and nominal compression strength of concrete. In C-series, the parameters that differed were embedded length of anchor rods and type of anchor rods. The embedded length (equal to

20 times the nominal diameter of the anchor rod) was set by the requirements of the current Japanese Building Design Code [2-1]. Additional tests were conducted with embedded lengths equal to 30 and 39 times the nominal diameter of the anchor rod to clarify their influences on the concrete breakout failure strength. Specimens in B and C-series with different numbers of column rebars were also compared to investigate their influences on concrete breakout failure strength.

The differences associated with the various series of specimens are presented below. A-series contained two specimens. The SHS column, □-300×12 (BCR295, i.e., specified minimum yield stress F_y = 295 N/mm^2), with a 40 mm thick base plate (SM490, i.e., F_y=325N/mm^2) was fixed to a RC column by 8-M24 ABR490 anchor rods (i.e., F_y = 325 N/mm^2). Regarding the anchorage of anchor rods, circular anchor plates with a diameter of 70 mm and a thickness of 15 mm were used. Embedded lengths of anchor rods were equal to 20 times their nominal diameters.

Four specimens were in B-series, the sections of steel column, concrete column, and foundation beam were smaller than those in A-series. The SHS column, □-200×12 (BCR295), with 50 mm thick base plate were fixed to the RC column by 8-Φ19 PC steel bars Grade C (i.e., F_y = 1080 N/mm^2) [2-2]. To confirm the behavior of the column rebar, stronger anchor rods were chosen to maintain the elastic state during the loading procedure. Regarding the anchorage of the anchor rods, circular anchor plates with 65 mm diameter and 19 mm thickness were used based on the need of PC steel bars. The embedded lengths of the anchor rods were 20 times their nominal diameters.

C-series also contained four specimens, the scale was similar to the B-series specimens, and 8-M20 (ABR490) anchor rods were used to fix the base plate to the RC column. The differences between the B and C-series specimens included the foundation beam depth which was 30 mm less than the B-series, and there was no footing on the C-series specimens. Additionally, there was no column transverse rebars, only 4-D6 rebars were set in the corner of the column as the support of hoops.

2.1.2 Setup, loading protocol, and measurement plan

Figure 2-4 and 2-5 shows the experiment setup. In the experiment process, positive loading was defined as the loading which tended to close the knee joint (closing side), and negative loading was defined as the loading which tended to open the knee joint (opening side). To carry out the experiment with the largest possible size of specimens, in A-series, the setup was specifically developed such that specimens were set in an upside-down orientation inclined at an angle of 45°, as shown in Figure 2-4 and Photo

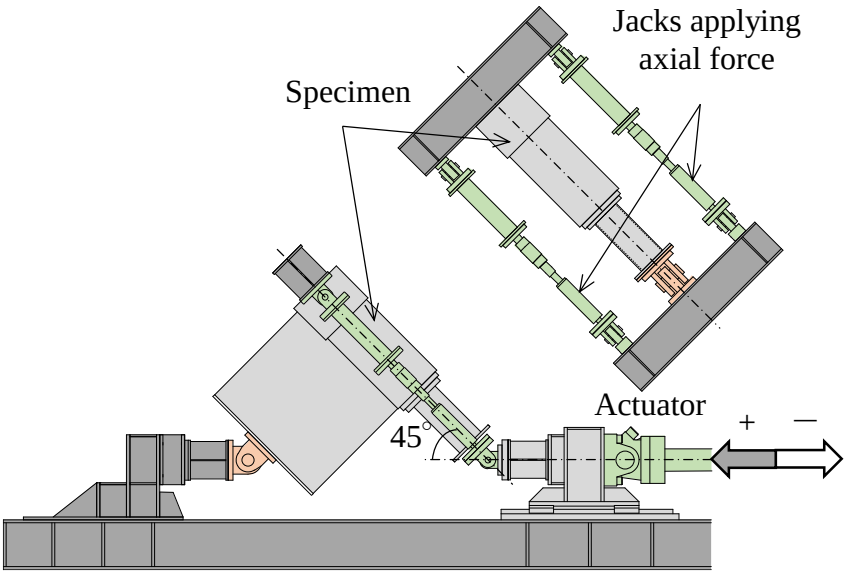

Figure 2-4 Experimental setup of A-series specimens

Photo 2-1 Experimental setup of A-series specimens

2-1. Free-end of the RC foundation beam was connected with a pin and reaction jigs. On the other side, the steel column was connected to the actuator through the horizontal pin-roller jig. Cyclic loading was applied on the specimens. Additionally, two hydraulic jacks parallel to the column were set to apply a constant compressive force equal to 300 kN to the column, which was assumed as a dead load from superstructure in practice. Furthermore, owing to the setup, the axial force exerted on the column base was varied as the loading direction changed. The axial force and moment distribution in the closing

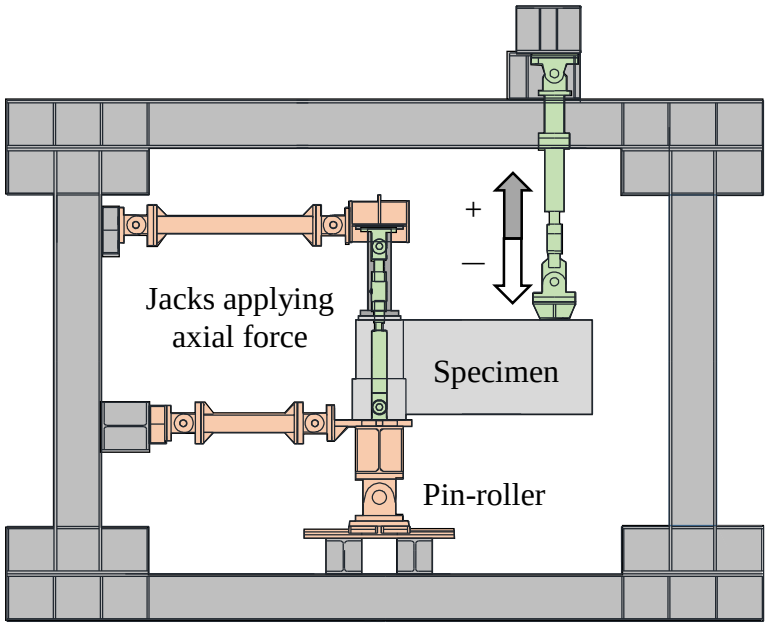

Figure 2-5 Experimental setup of B&C-series specimens

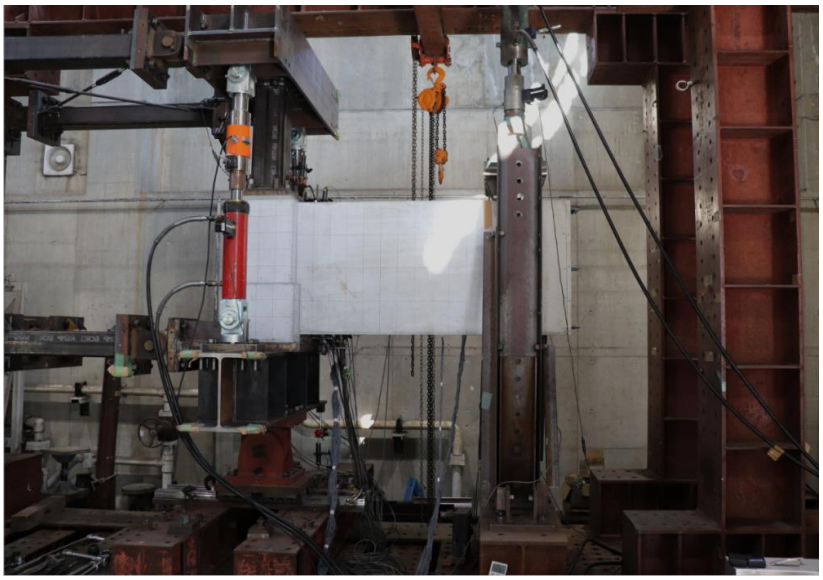

Photo 2-2 Experimental setup of B&C-series specimens

side is illustrated in Figure 2-6(a).

For the setup of A-series specimens, as the 45 degrees setup, the axial force of the specimens will change in the loading process with the variance of shear force applied on the specimens. To eliminate the effect of varying axial force on the exposed column bases, experiment setup of B and C-series was specially designed as illustrated in Figure 2-5 and Photo 2-2. Furthermore, the number of specimens was increased to clarify the influence of other parameters. One hydraulic jack connected with the foundation beam applied cyclic loading on the specimen. A constant compressive axial force equal to 300 kN was also applied on the column by the two sets of hydraulic jacks parallel to the column. A pin-roller jig was set in the bottom part of the specimen as support. The axial force and moment distribution on the closing side is shown in Figure 2-6(b).

Cyclic loading was conducted to control the story drift R which varied from 1/400, 1/200, and 1/150 at two cycles per amplitude. Subsequently, one cycle from R varied from 1/100, 1/75, 1/50, 1/33, and 1/20 until the strength deterioration occurred, or until the stroke of

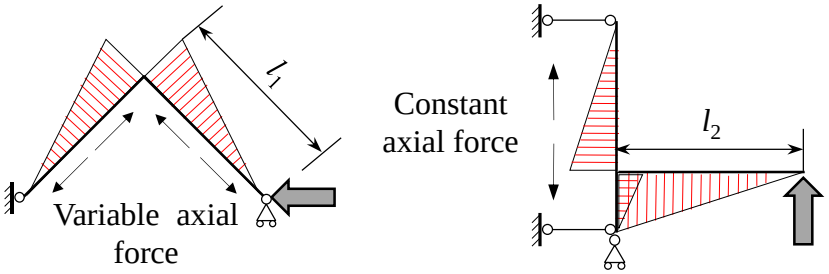

(a) A-series specimens (b) B&C-series specimens

Figure 2-6 Axial force and moment distribution of specimens

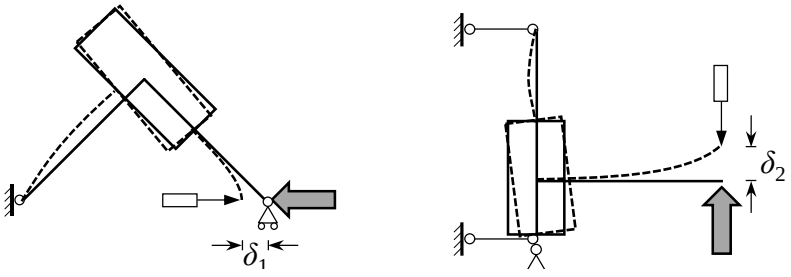

(a) A-series specimens (b) B&C-series specimens

Figure 2-7 Measurement plan to calculate story drift ratio R

the hydraulic jack reached its limitation, as shown in Figure 2-8. To calculate the story drift R controlled in the loading, displacement transducers were set to measure the deformation of steel column, column base, and foundation beam, which are the components of the story drift R. As illustrated in Figure 2-6 and Figure 2-7, the story drift R was calculated by Eqs. 1 and 2 for the A, B, and C series specimens, respectively.

$$R = \frac{\delta_1}{\sqrt{2} \times l_1} \tag{1}$$

$$R = \frac{\delta_2}{l_2} \tag{2}$$

To investigate the mechanism of concrete breakout failure, the tensile strain of anchor rods and column rebar also needed to be measured. Thus, the strain gauges were glued on the anchor rods and the column rebar. Additionally, strain gauges were glued on hoops that were close to anchor plates to clarify the horizontal component of concrete breakout failure strength. The position of strain gauges will be illustrated in the corresponding experiment result parts.

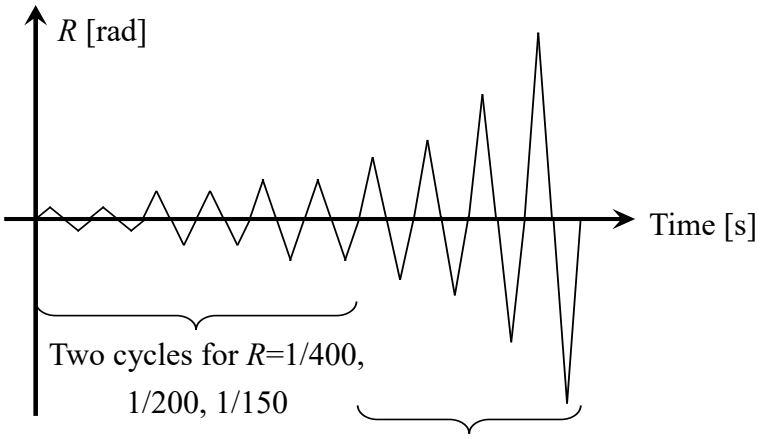

Figure 2-8 Loading protocol

2.1.3 Material test results

As listed in Table 2-3, the material properties of steel rebar arranged in concrete column and foundation beam and anchor rods were obtained based on coupon tests according to the Japanese industrial standard (JIS) Z 2201 [2-3]. The coupon tests were separately performed for the rebars as column rebar, beam rebar, hoops, and anchor rods. Table 2-4 lists the material properties of concrete and base mortar according to JIS A 1108 [2-4], JIS A 1142 [2-5] for the compression strength of concrete and base mortar, respectively.

Table 2-3 Material test results for steel

Position	Specimen	Steel grade	σ_y [N/mm^2]	σ_u [N/mm^2]	YR [%]
Column main bar	A-series	D13-390	431	623	69.1
	B-series	D13-295	335	480	69.7
Beam transverse bar	A-series	D16-390	464	639	72.6
	B19-390-20d	D19-390	382	544	70.2
	B16-490-20d	D16-490	529	692	76.4
	B16-590-20d B16H-590-20d C-series	D16-590	621	766	81.0
Hoops[a]	A-series	D6-295	418	539	77.5
	B and C-series	D6-295	429	623	68.9
Anchor rods	A-series	M24-ABR490	332	490	67.7
	B-series	Φ19 PC Grade C	1185	1280	92.5
	C-series	M20-ABR490[b]	343	551	62.2

Note: E: Young`s modulus; σ_y: yield strength; σ_u: tensile strength; YR: yield ratio.

[a]Yield strength of hoops is the 0.2% offset strength.

[b]Material property based on the mill test report.

Table 2-4 Material test results of concrete and base mortar

Specimen	Concrete		Base mortar	
	Age [days]	σ_c [N/mm^2]	Age [days]	σ_c [N/mm^2]
A16-390-20d	44	23.2	37	74.2
A16S-390-20d	56	23.6	49	78.2
B19-390-20d	68	24.8	65	74.5
B16-490-20d	70	25.0	67	74.6
B16-590-20d	88	25.8	85	74.8
B16H-590-20d	94	45.9	91	74.9
C16-590-20d	95	23.9	75	63.7
C16-590-30d	97	24.0	77	63.9
C16-590-39d	90	23.7	70	63.3
C16-590-39db	82	23.3	62	62.5

Note: σ_c: Compression strength.

2.2 Experiment results

2.2.1 Ultimate strength and failure modes

The maximum strength of specimens in both loading directions and the calculation strength of different possible failure modes were listed in Table 2-5. The failure modes for different series of specimens were different. In A-series, the major failure mode was the concrete breakout failure in the closing loading direction. However, it was found that the ultimate strength of A-series specimens was greatly smaller than the calculation value of concrete breakout failure strength following the current design recommendation. Such that the recommendation might overestimate the concrete breakout failure strength. In B-series, the failure mode was beam bending failure due to the yielding of beam transverse rebar. From the relation between the calculation value and experiment results, the ultimate strength could be evaluated accurately. On the other hand, as the maximum strength is lower than the concrete breakout failure strength, the concrete breakout failure cracks were also observed in the specimens. In C-series, the failure mode is the concrete compression and bending failure due to the insufficient column longitudinal rebar. On the other hand, the maximum strength is greatly higher than the calculation value of concrete breakout failure strength. The detailed behavior of specimens and strength evaluation will be discussed separately by the series of specimens in the following sections.

Table 2-5 Strength of specimens, failure mode, and comparison with the calculated results

No.	$+Q$ [kN]	$-Q$ [kN]	${}_{cal}{}^{a}F_y$ [kN]	${}_{cal}{}^{b2}F_y$ [kN]	${}_{cal}{}^{c}F_y$ [kN]	$\frac{+Q}{\min\{F_y\}}$	$\frac{-Q}{\min\{F_y\}}$	Failure mode
A16-390-20d[a]	323.9	219.2	612.9 (234.5)	588.4 (434.8)	270.5 (208.4)	1.20	1.05	CBF
A16S-390-20d[a]	322.4	210.9	613.7 (234.6)	589.3 (435.6)	270.5 (208.4)	1.19	1.01	CBF
B19-390-20d	243.3	206.0	182.7	650.0	316.0	1.33	1.13	BBF
B16-490-20d	219.3	189.9	179.4	650.5	316.0	1.22	1.06	BBF
B16-590-20d	236.7	205.5	210.6	653.0	316.0	1.12	0.98	BBF
B16H-590-20d	240.3	221.2	210.6	706.1	431.8	1.14	1.05	BBF
C16-590-20d	174.4	173.2	202.7	104.0	162.0	1.68	1.67	CCBF
C16-590-30d	187.9	176.6	202.7	117.0	162.0	1.61	1.51	CCBF
C16-590-39d	194.3	173.2	202.7	127.0	162.0	1.53	1.36	CCBF
C16-590-39db	189.4	185.9	202.7	127.0	162.0	1.49	1.46	CCBF

Note: $+Q$, $-Q$: Maximum strength in closing and opening side.

${}_{cal}{}^{a}F_y$: bending failure of beam by the yielding of beam rebar.

${}_{cal}{}^{b2}F_y$: concrete breakout failure strength calculated by considering all column rebars. [2-6]

${}_{cal}{}^{c}F_y$: full plastic strength of column base by considering the yield of the anchor rod.

Failure mode: CBF: concrete breakout failure; BBF: beam bending failure; CCBF: column compression bending failure.

[a]: Strength marked in the parentheses is the calculated value in the opening side.

2.2.2 A-series specimens

Hysteresis relation between shear force on the column base Q and story drift R is presented in Figure 2-9. The sketch showing the parameters of A-series specimens (embedded length of beam transverse rebar) is also indicated next to its hysteretic curve. The envelope curve for both loading directions is indicated with a thicker line. The timing of anchor rods and hoop yielding judged by strain gauge results are marked in the hysteretic curve with round marks. For both specimens, on the closing side, the strength deteriorated owing to the concrete breakout failure. As illustrated in Figure 2-10, concrete breakout failure cracks occurred in specimen A16-390-20d when R = +1/400. In the ultimate state, severe conical cracks could be observed from specimens, crack distribution of specimen A16-390-20d was taken as an example, which will be illustrated in the following pages with the increment of loading amplitude. The maximum strengths of both specimens were similar and approximately equal to 322 kN on the closing side and 210 kN on the opening side. The considerable difference in the maximum strength in different loading directions was attributed to the varying axial force applied on the foundation beam as the specimen was set as 45° at an inclined orientation. Specifically, for the opening side, the tension applied on the column base caused the strength to be smaller than the closing side. Owing to this reason, in Table 2-5, both the calculated values of the failure strength are listed separately. The strength in the opening side was marked within

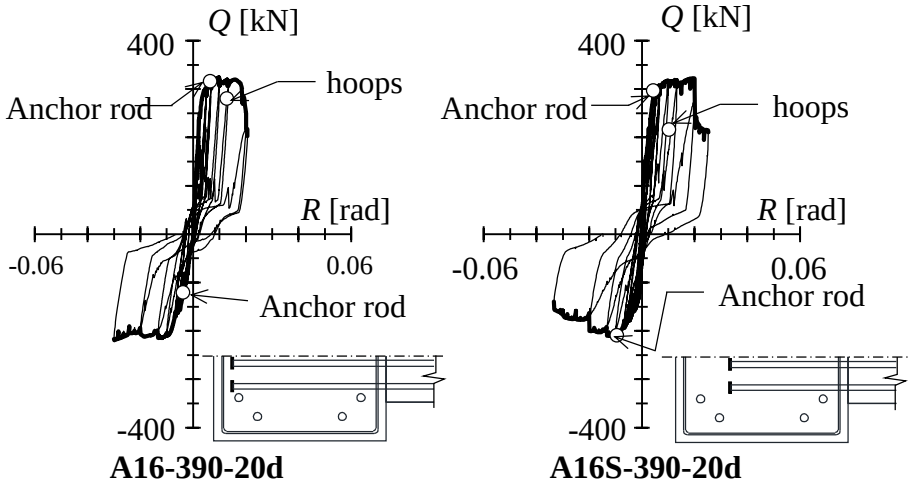

Figure 2-9 Hysteresis curve of A-series specimens

parentheses. Regarding the experimental results, in the closing side, anchor rods yielded at a loading amplitude of $R = 0.5\%$ for both specimens, and the hoop closing to the anchor plate also yielded in a subsequent loading process. However, the difference in the embedded length of the beam rebar did not influence the structural behavior in the closing side. The maximum strength and failure mode were similar.

Conversely, in the opening side in the case of specimen A16-390-20d, the strength was stable until the ultimate state; however, for specimen A16S-390-20d, the strength deteriorated by approximately 20% owing to the insufficient anchorage strength because of the short-embedded length of the beam rebar. Regarding the effect of the anchorage length of the beam rebar on the concrete breakout failure, there was no considerable difference between the two specimens. The increment of cracks of specimen A16-390-20d with the corresponding Q - R hysteresis curve was illustrated in the following pages. Furthermore, the increment of critical crack width of specimen A16-390-20d was also summarized and discussed.

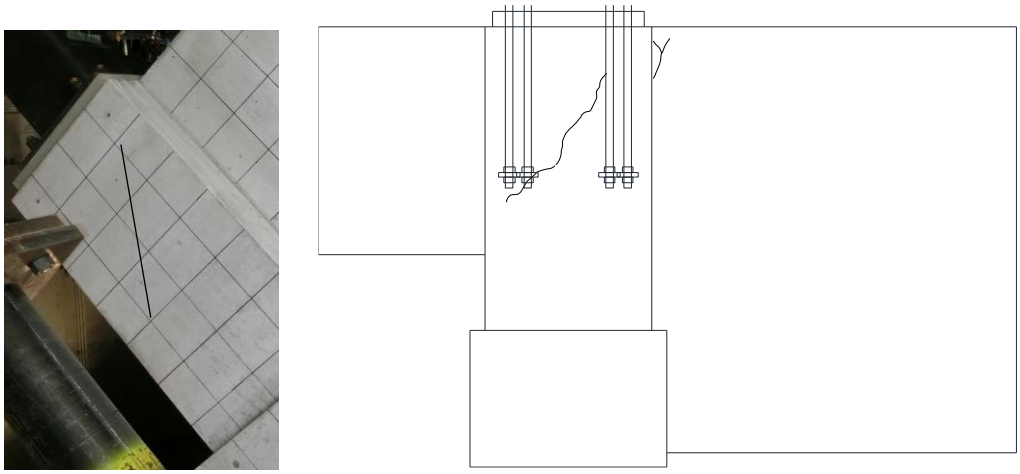

Figure 2-10 Concrete breakout failure cracks occurred in specimen A16-390-20d when $R = +1/400$

- **Crack distribution of specimen A16-390-20d**

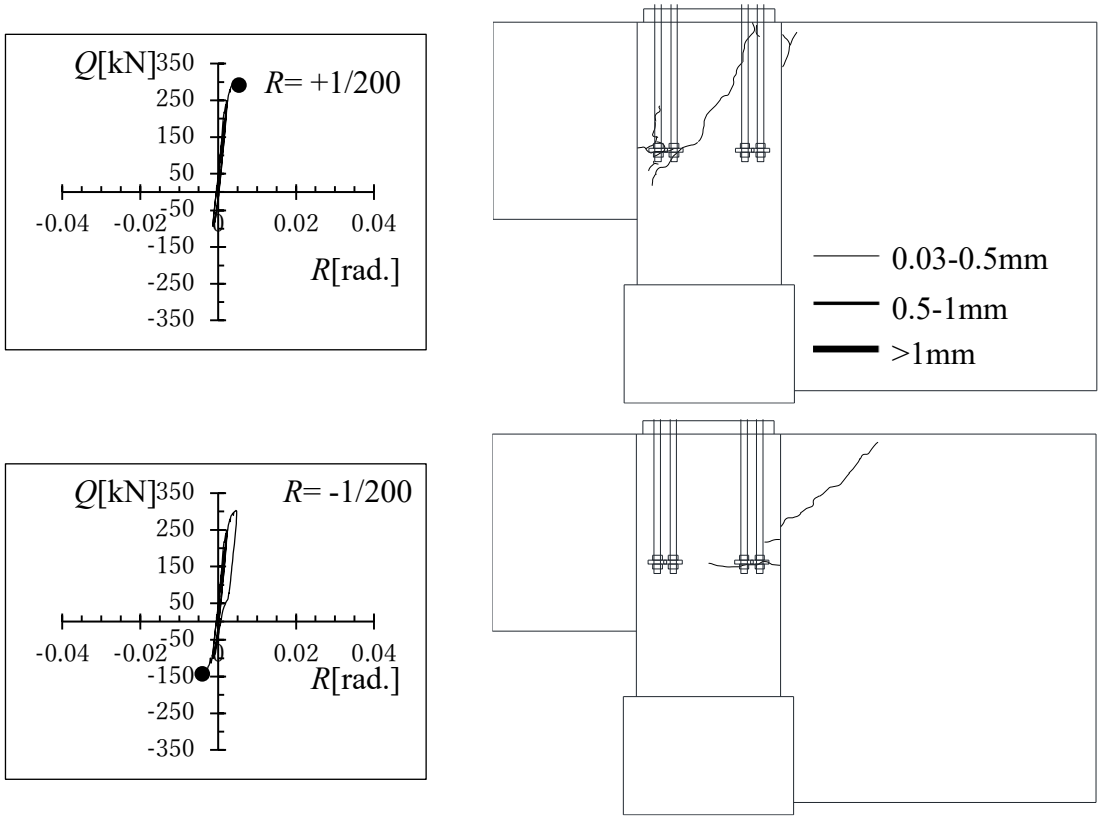

Hysteresis curve of *Q*-*R* and crack distribution when *R* = ±1/200

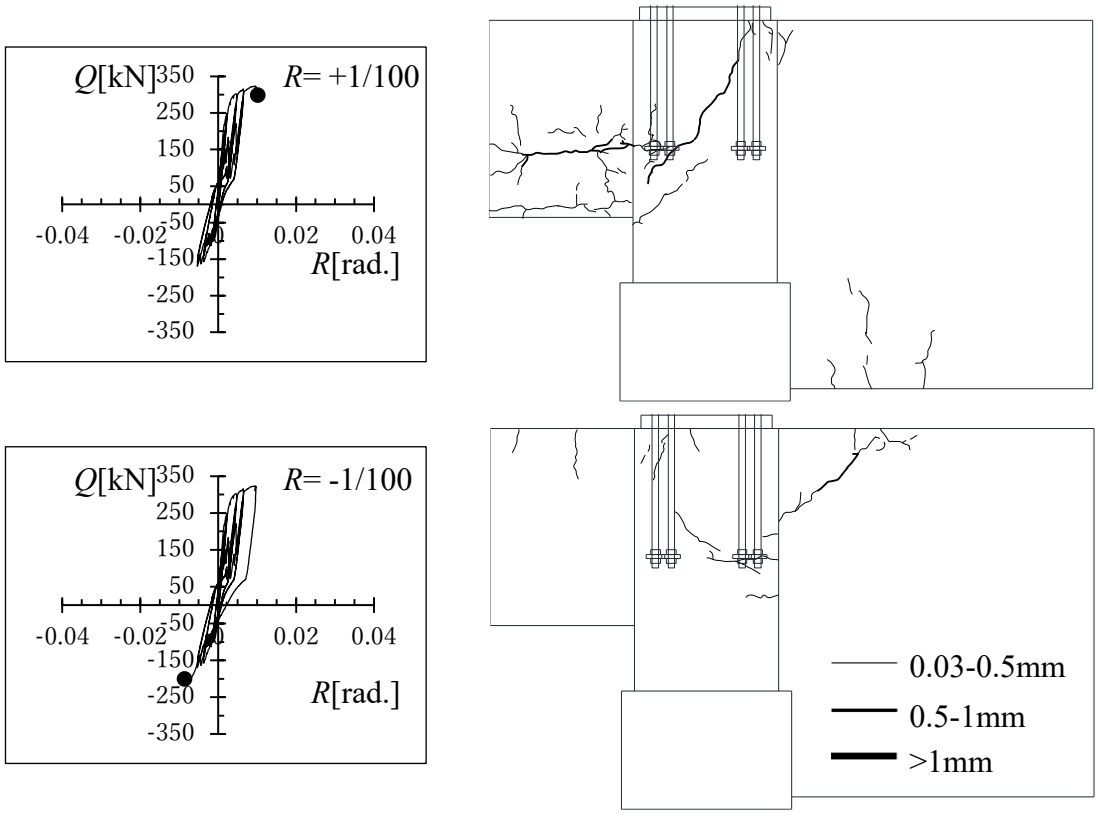

Hysteresis curve of *Q*-*R* and crack distribution when *R* = ±1/100

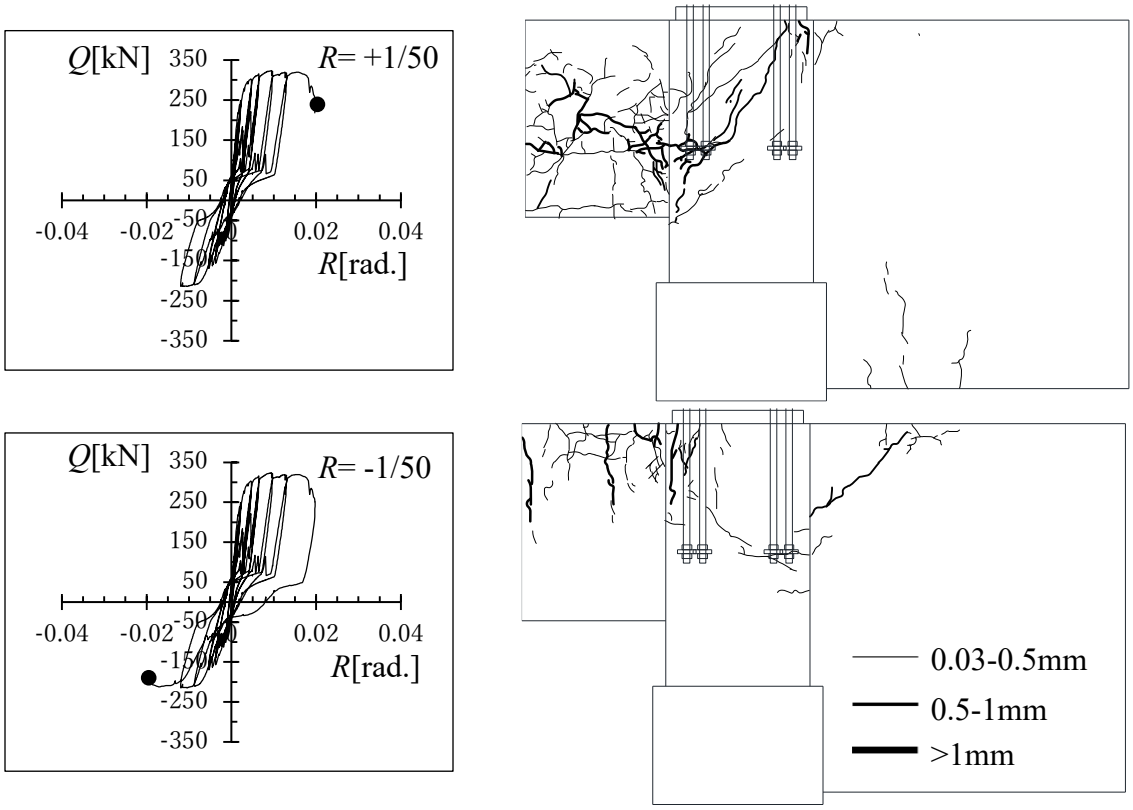

Hysteresis curve of *Q*-*R* and crack distribution when *R* = ±1/50

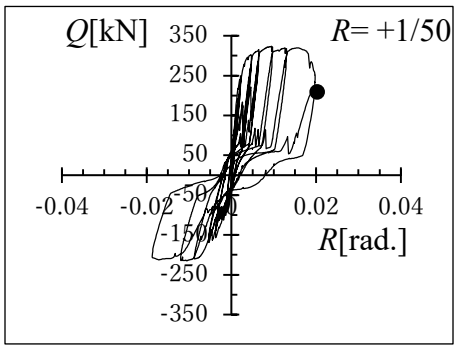

The cracks were not measured in the second cycle loading of *R* = +1/50

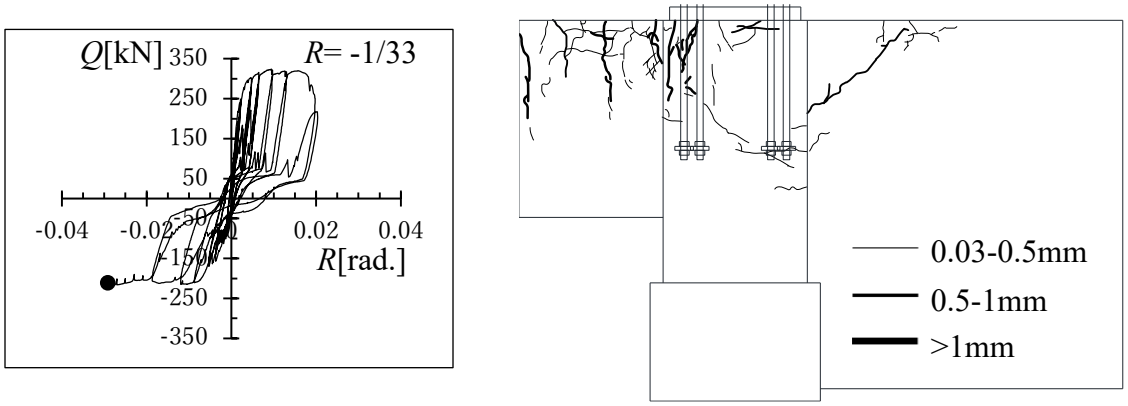

Hysteresis curve of *Q*-*R* and crack distribution when *R* = -1/33

- **Crack width increment of specimen A16-390-20d**

The crack width in every loading amplitude was measured and summarized. The most severe crack for concrete breakout failure was picked up as marked in a circle or triangle corresponding to different positions.

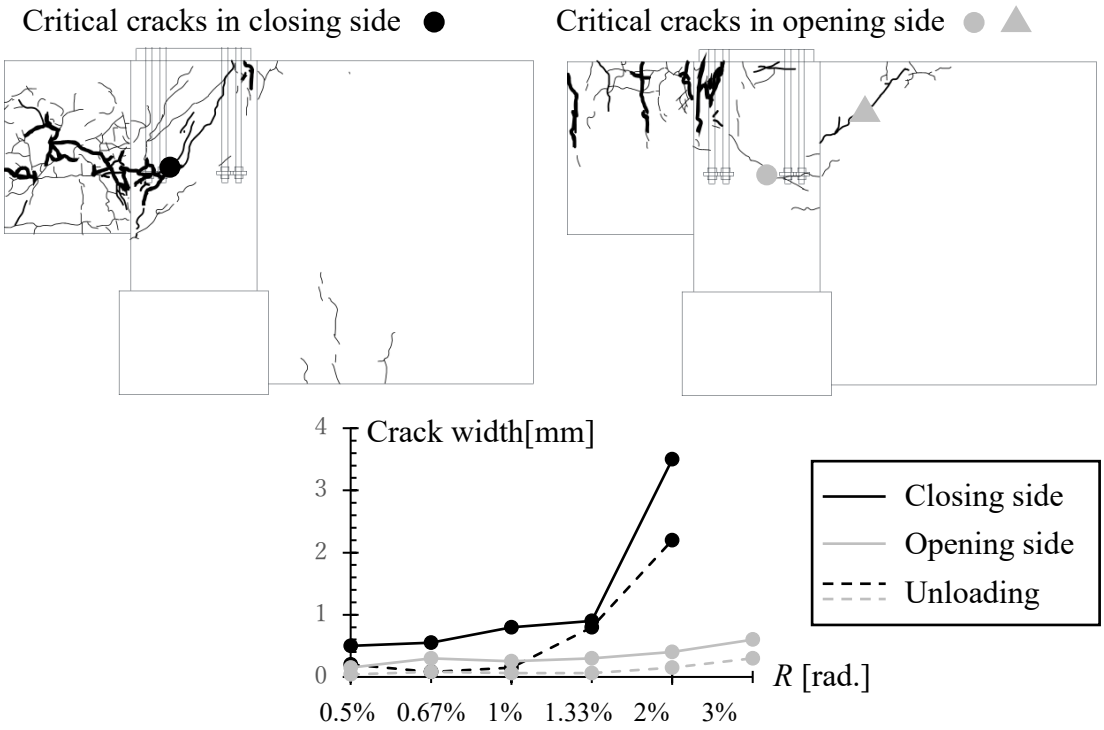

Increment of width of concrete breakout failure cracks

As could be observed from the figure above, the width in the closing side increased significantly when $R = 2\%$, reaching around 4 mm, as it was also the trigger of the strength deterioration in the loading of closing side. Comparingly, on the opening side, the width of cracks is relatively small, around 0.5 mm in the ultimate state.

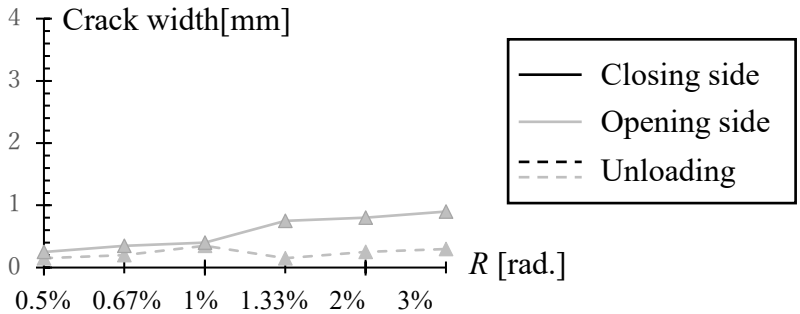

Increment of width of concrete breakout failure cracks in foundation beam

The crack in the foundation beam showed similar behavior with the cracks in the concrete column in the opening side.

2.2.3 B-series specimens

Hysteresis relation between shear force on the column base Q and story drift R is presented in Figure 2-11. The sketch showing the parameters of B-series specimens (strength and diameter of beam transverse rebar and concrete strength) is also indicated next to its hysteretic curve. In the sketch of the specimens next to their hysteretic curve, darker colors on the beam rebar and concrete body represent higher strength. The envelope curve for both loading directions is indicated with a thicker line. The timing of anchor rods and hoop yielding judged by strain gauge results are marked in the hysteretic curve with round marks. The failure mode of specimens was beam bending failure that occurred following the yielding of beam rebar. Different beam rebar grades caused the changing of maximum strength. Severe bending cracks can also be observed in the

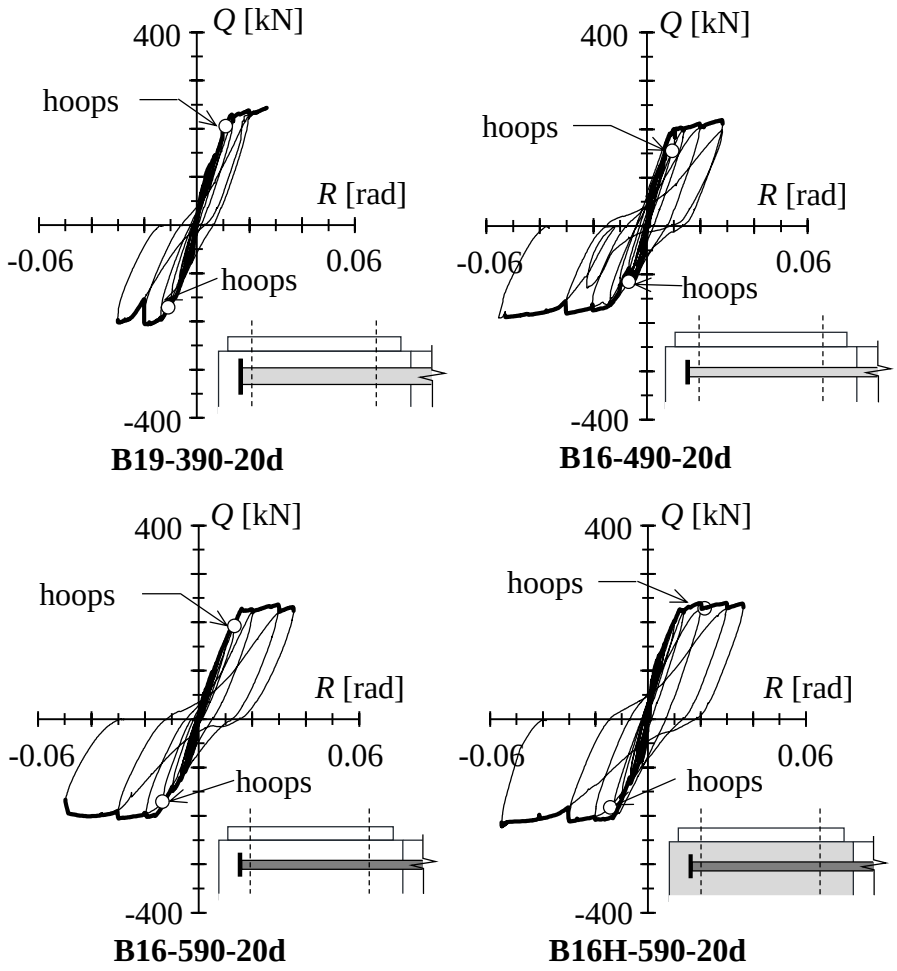

Figure 2-11 Hysteresis curve of B-series specimens

specimens in the ultimate state. The crack distribution of specimen B16-590-20d was taken as an example, which will be illustrated in the following pages with the increment of loading amplitude. The maximum strengths of the specimens were approximately 1.12 to 1.33 times the calculated value on the closing side and 0.98 to 1.13 times on the opening side. In respect of the concrete breakout failure, conical cracks could be observed from the surface of specimens displayed in Figure 2-12 and Figure 2-13, despite the fact that the maximum strength did not reach the calculated value ${}_{cal}{}^{b2}F_y$. Regarding the influences of the beam rebar on the concrete breakout failure, no considerable differences were found in both loading directions. The increment of cracks of specimen B16-590-20d with the corresponding Q-R hysteresis curve was illustrated in the following pages. Furthermore, the increment of critical crack width of specimen B16-590-20d was also summarized and discussed.

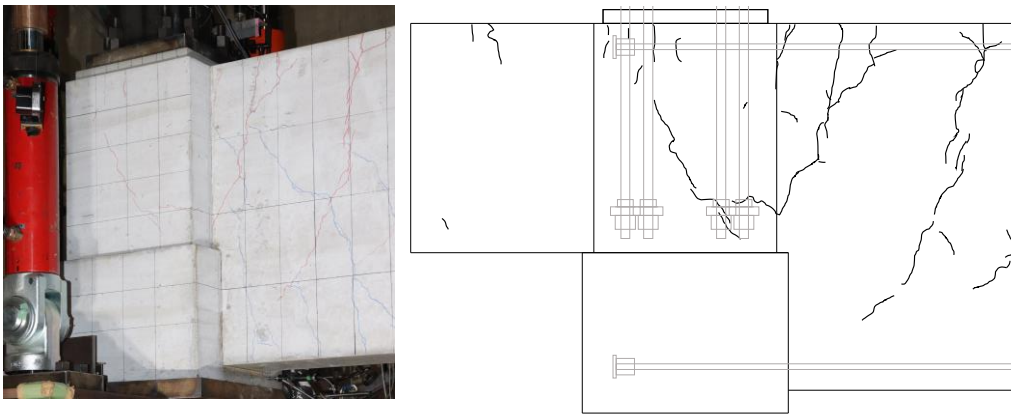

Figure 2-12 Concrete breakout failure cracks occurred in specimen B16-590-20d when R = -1/100

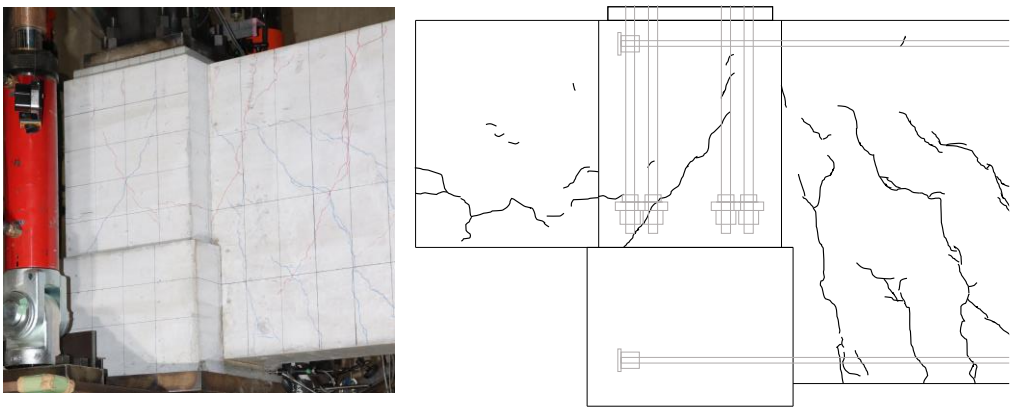

Figure 2-13 Concrete breakout failure cracks occurred in specimen B16-590-20d when R = +1/75

- **Crack distribution of specimen B16-590-20d**

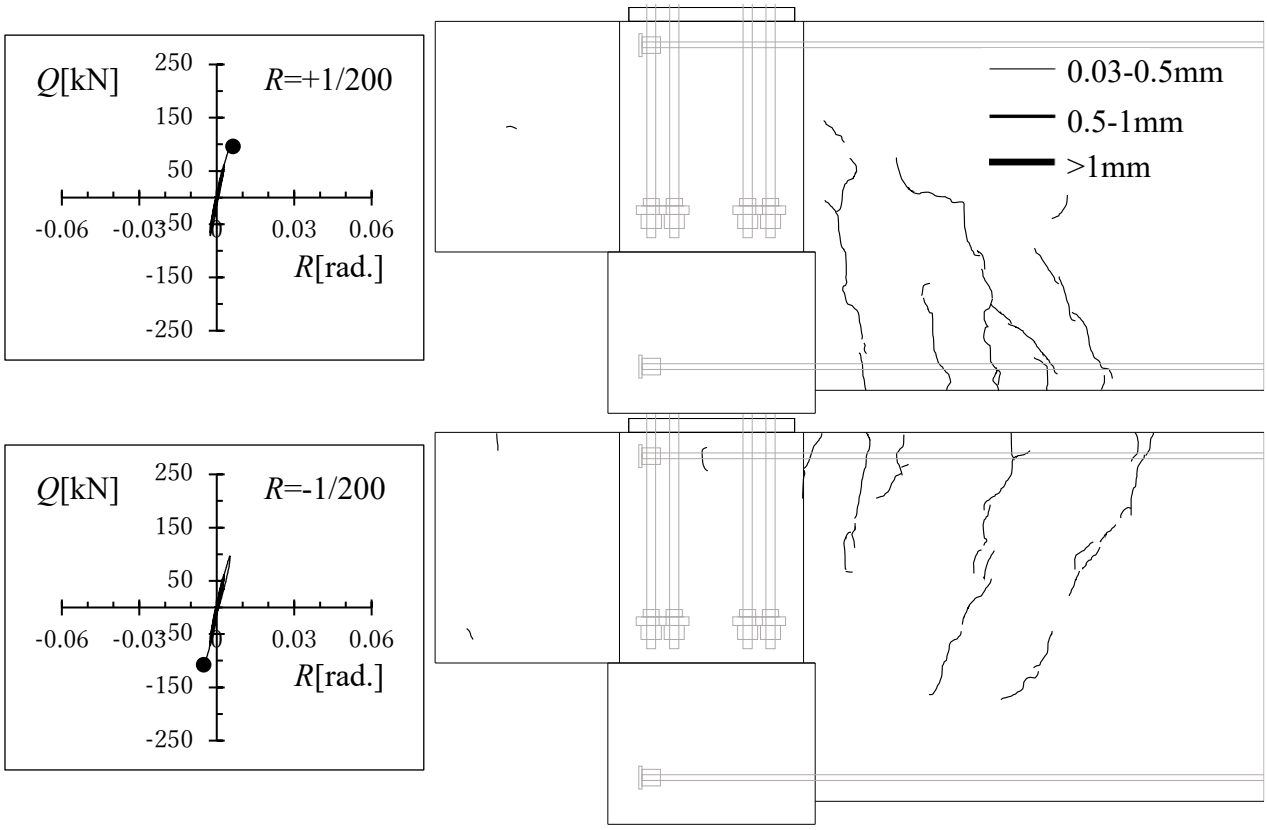

Hysteresis curve of Q-R and crack distribution when $R = \pm 1/200$

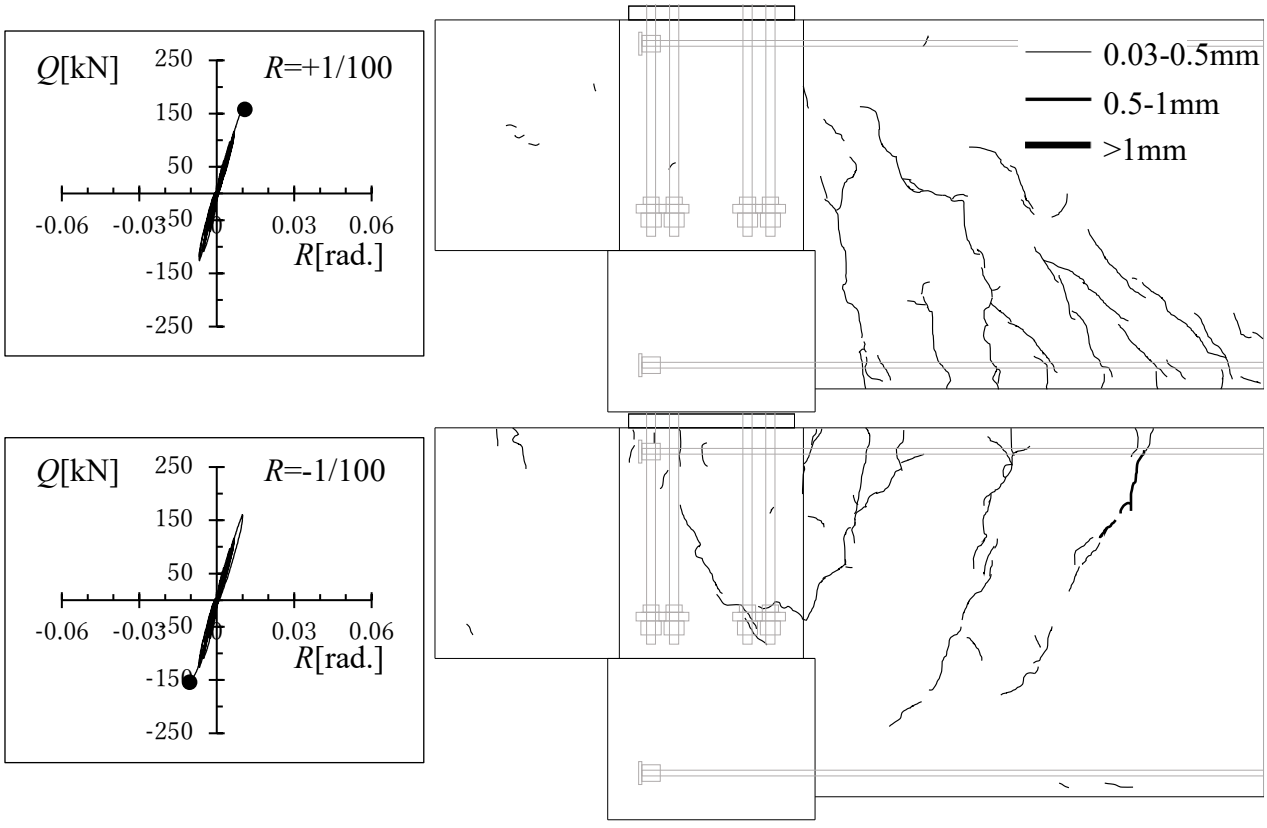

Hysteresis curve of Q-R and crack distribution when $R = \pm 1/100$

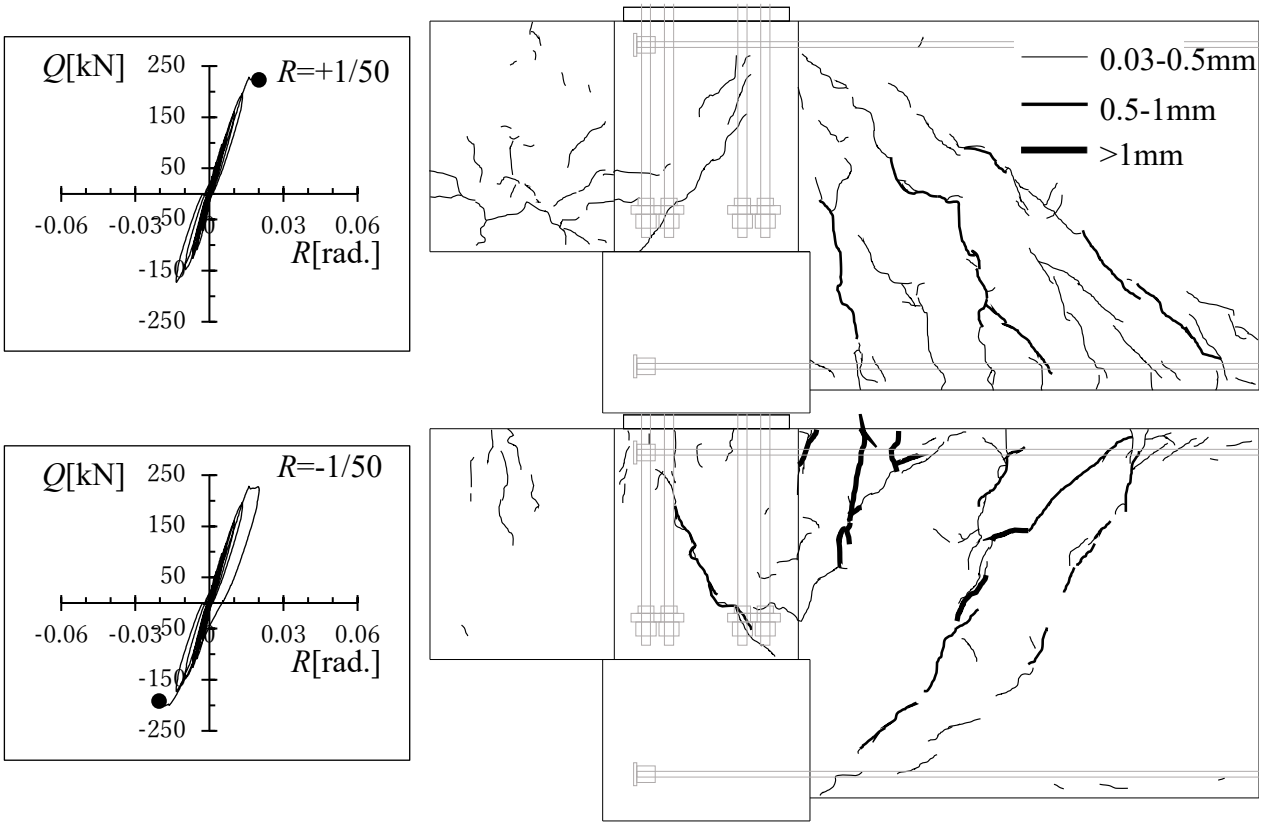

Hysteresis curve of *Q*-*R* and crack distribution when $R = \pm 1/50$

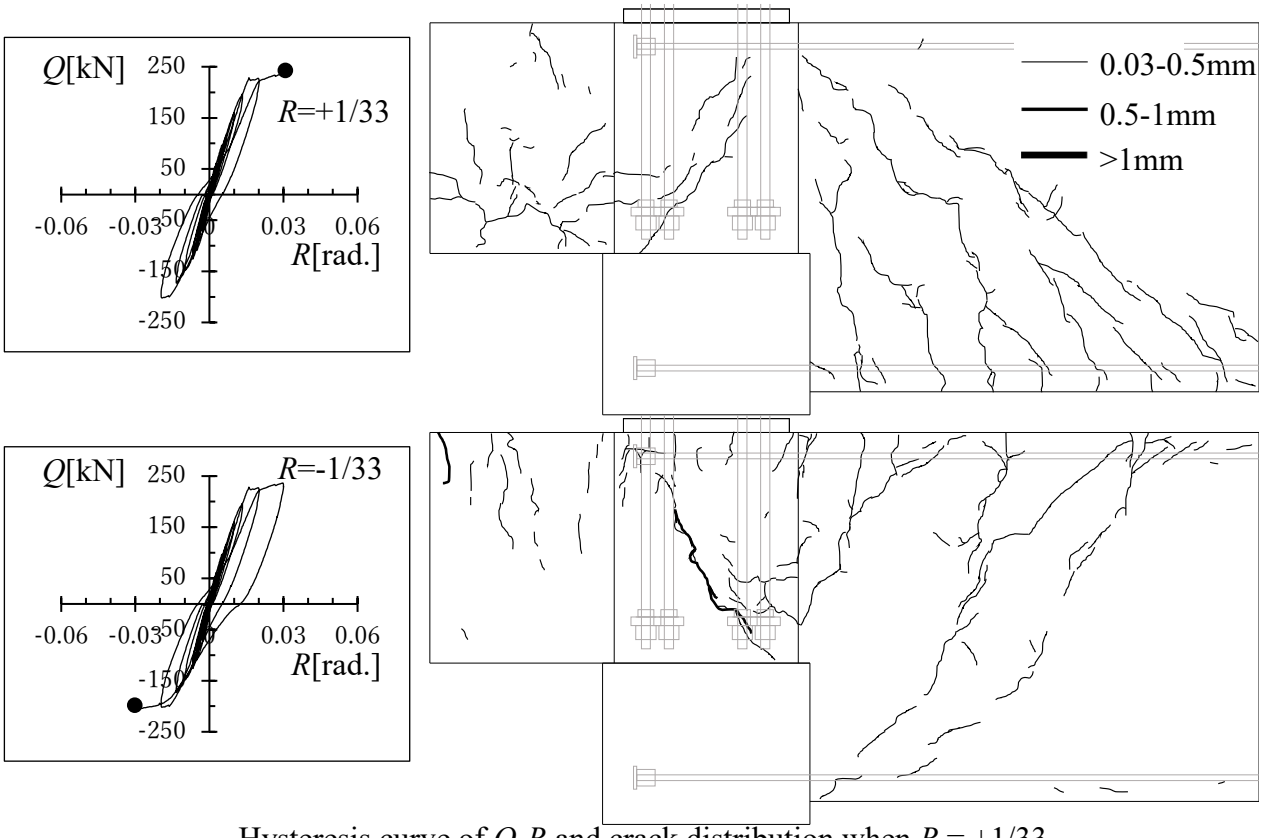

Hysteresis curve of *Q*-*R* and crack distribution when $R = \pm 1/33$

(width of beam cracks was not measured)

- **Crack width increment of specimen B16-590-20d**

The crack width in every loading amplitude was measured and summarized. The most severe crack for concrete breakout failure and foundation beam was picked up as marked in circle, square, and triangle, respectively.

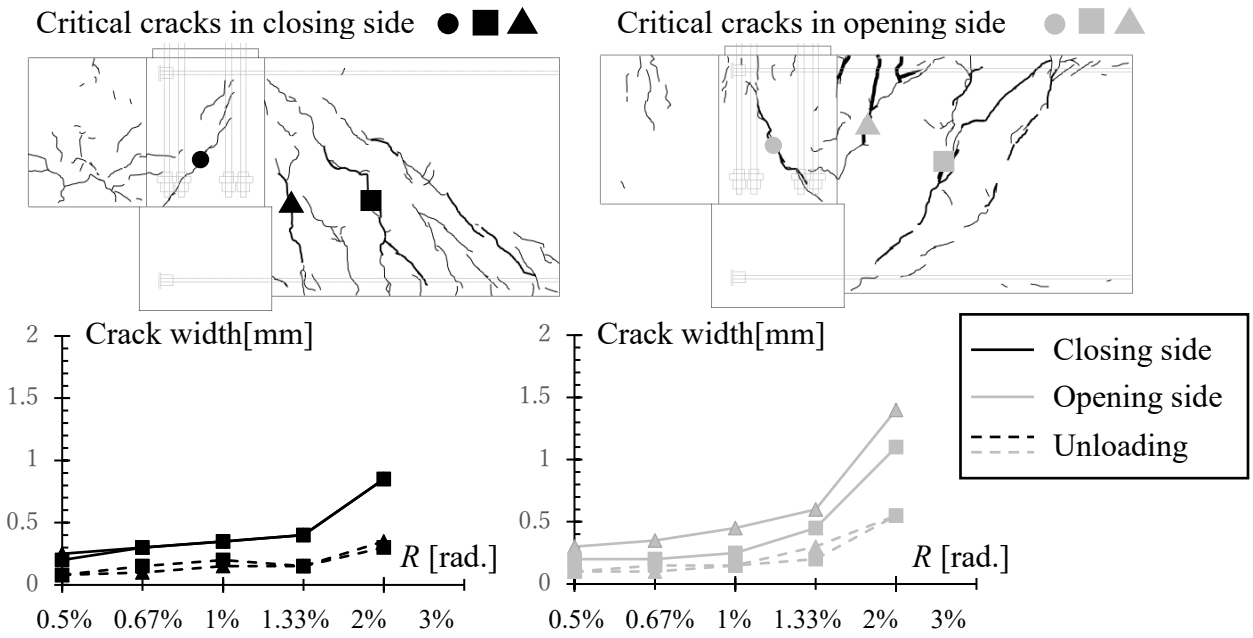

Increment of width of cracks on the foundation beam

As could be observed from the figure above, the width of cracks on the foundation beam kept increasing slowly until R = 1.33% and increased suddenly at the loading amplitude of R = 2%.

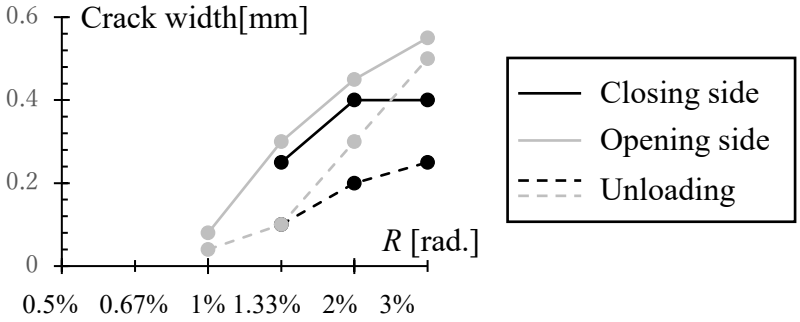

Increment of width of concrete breakout failure cracks

As could be observed from the figure above, the width of concrete breakout failure cracks was relatively small than the crack width in foundation beam, the crack width kept increasing until the ultimate state.

2.2.4 C-series specimens

Hysteresis relation between shear force on the column base Q and story drift R is presented in Figure 2-14. The sketch showing the parameters of C-series specimens (embedded length of anchor rods and their type) is also indicated next to its hysteretic curve. The envelope curve for both loading directions is indicated with a thicker line. The timing of anchor rods and hoop yielding judged by strain gauge results are marked in the hysteretic curve with round marks. The failure mode of specimens was the column compression bending failure in the bottom of concrete column during the closing side loading following the considerable deterioration of strength. In the ultimate states, severe cracks are concentrated on the bottom of the column on the closing side. The reason was attributed to the inadequate column rebar in C-series specimens. Additionally, conical

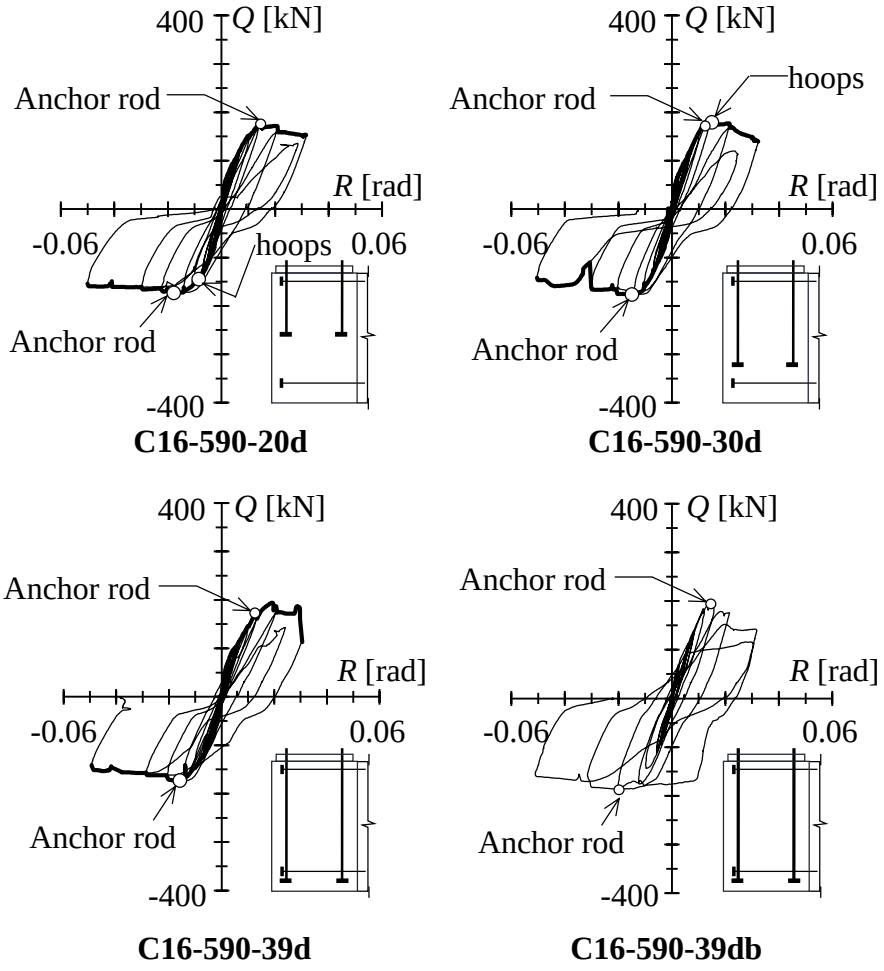

Figure 2-14 Hysteresis curve of C-series specimens

cracks were observed in the opening side loading of specimen C16-590-20d shown in Figure 2-15. For specimen C16-590-39d, with the exception of cracks on the foundation beam, the cracks accumulated on the bottom side of the concrete column. Regarding the maximum strength of C-series specimens, in the opening side, the strength was very similar to the yielding of anchor rods with a difference of approximately 3.4 kN. In the closing side, the strength increased as a function of the embedded length of anchor rods. Although the maximum strength of the specimen was approximately 1.36 to 1.68 times the calculated value of the concrete breakout failure strength ($_{cal.}{}^{b}F_y$), the pullout of anchor rods owing to concrete breakout failure did not occur. However, the anchorage failure on specimen C16-590-20d was observed. Although in the calculation in design, the anchorage failure of foundation beam rebar was not expected to occur due to the strength being around 1.3 times the concrete breakout failure strength. While in the experiment result, the concrete breakout failure strength is greatly larger than the calculation value, thus the anchorage failure occurred on the closing side. A footing with more reinforcement might prevent anchorage failure.

Also, comparing specimen C16-590-39d and C16-590-39db, the difference in the type of anchor rods has no significant influence on the structural behavior in both loading directions. The maximum strength and failure mode were similar. And the maximum strength all fit well with the calculated full-plastic strength. The increment of cracks of

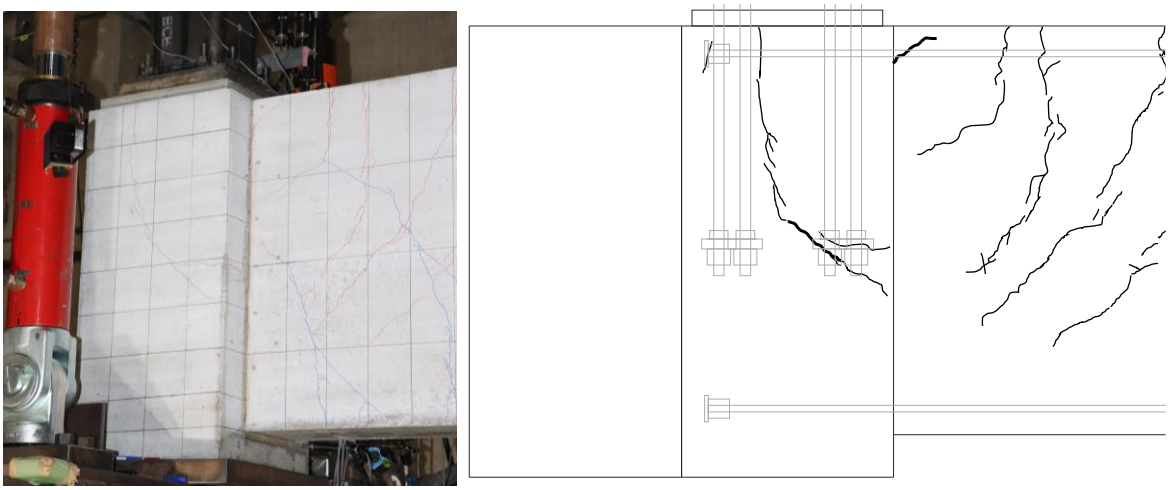

Figure 2-15 Concrete breakout failure cracks occurred in specimen C16-590-20d when R = -1/100

specimen C16-590-20d with the corresponding *Q*-*R* hysteresis curve were illustrated in the following pages. Furthermore, the increment of critical crack width of specimen C16-590-20d was also summarized and discussed.

- **Crack distribution of specimen C16-590-20d**

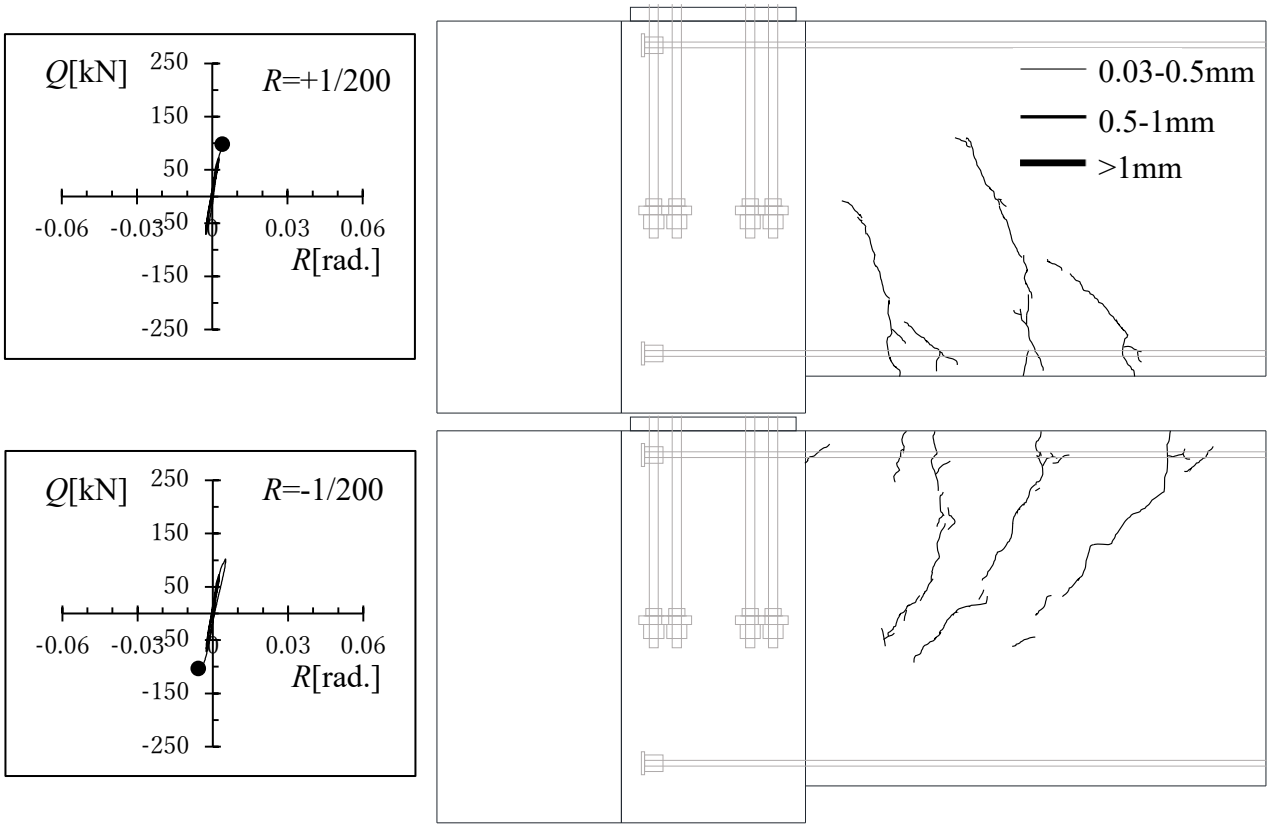

Hysteresis curve of Q-R and crack distribution when R = ±1/200

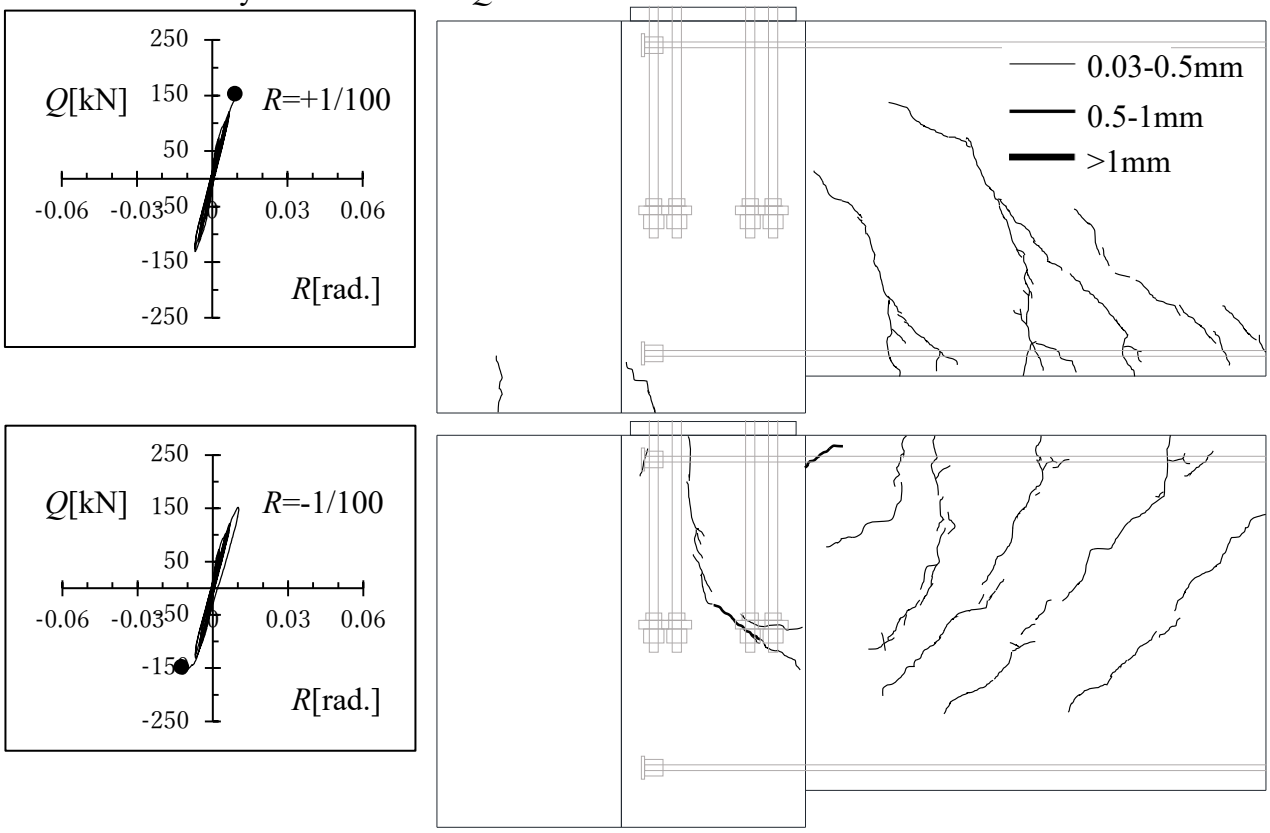

Hysteresis curve of Q-R and crack distribution when R = ±1/100

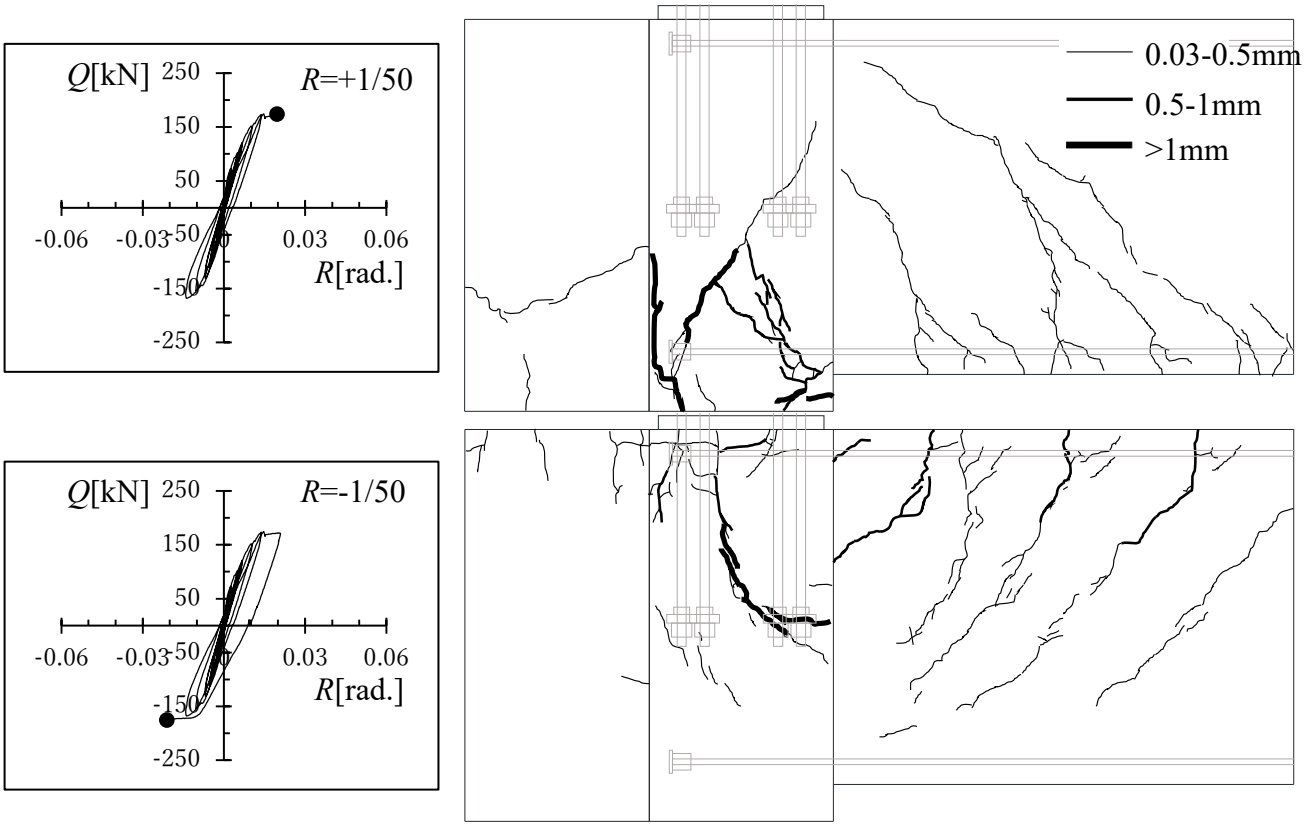

Hysteresis curve of Q-R and crack distribution when $R = \pm 1/50$

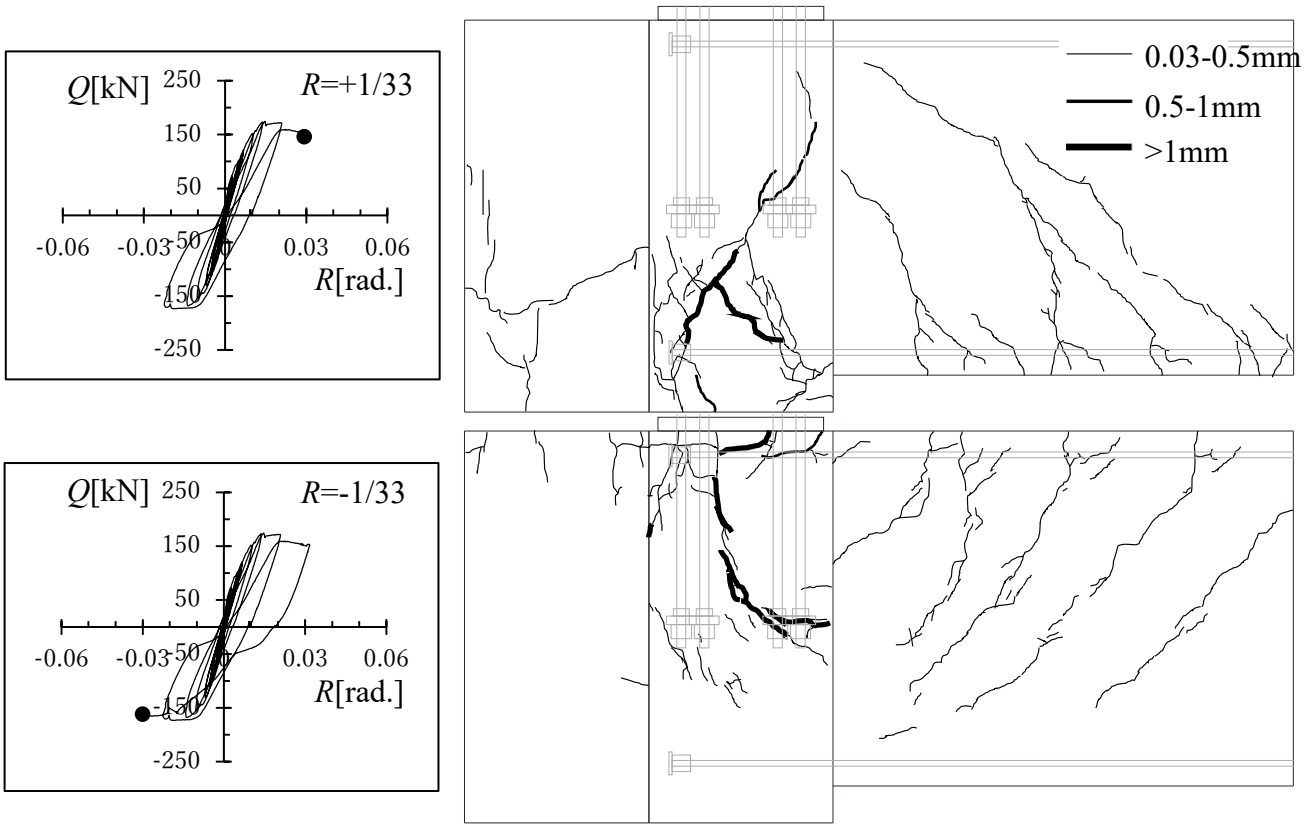

Hysteresis curve of Q-R and crack distribution when $R = \pm 1/33$

(width of beam cracks was not measured)

- **Crack width increment of specimen C16-590-20d**

The crack width in every loading amplitude was measured and summarized. The most severe crack for concrete breakout failure and foundation beam was picked up as marked in circle, square, and triangle, respectively.

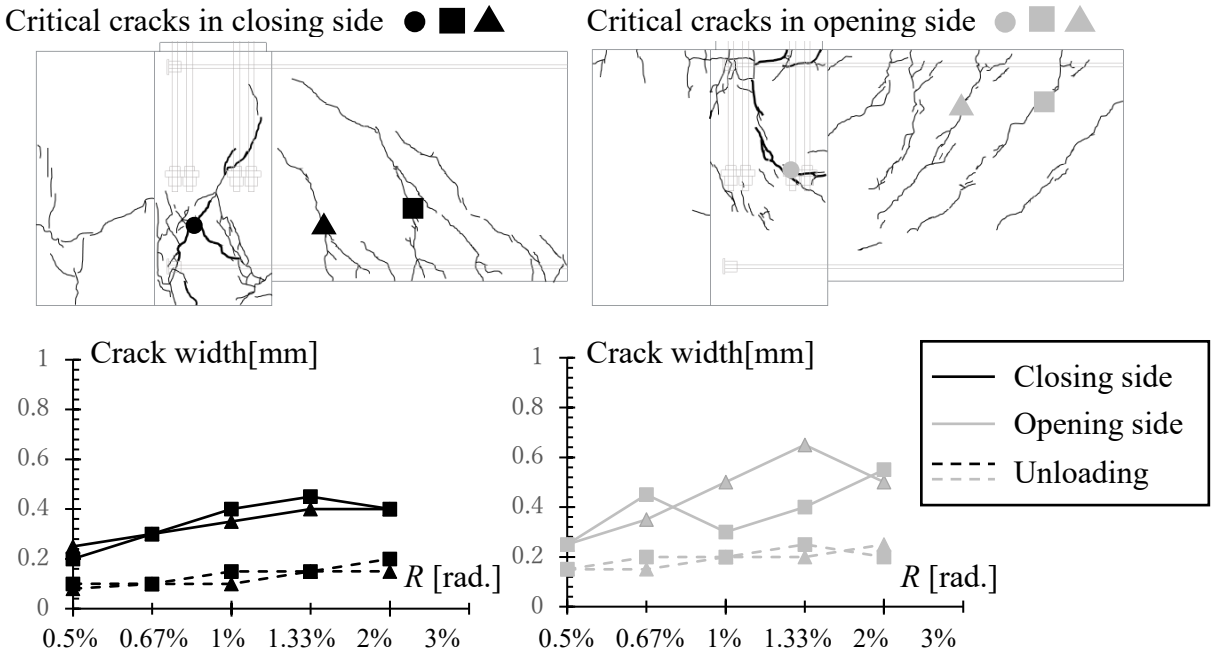

Increment of width of cracks on the foundation beam

As could be observed from the figure above, the width of cracks on the foundation beam kept increasing slowly until R = 1.33% and decreased until the ultimate loading amplitude.

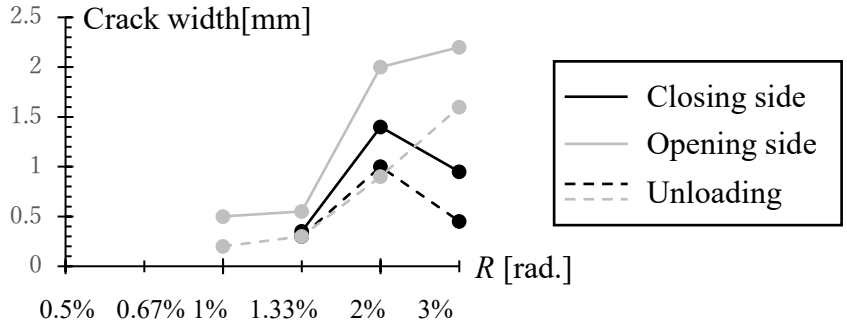

Increment of width of concrete breakout failure cracks

As could be observed from the figure above, the width of concrete breakout failure cracks was significantly larger than the crack width in foundation beam, the width of concrete breakout failure cracks kept increasing until the ultimate state.

2.3 Summary

In this chapter, ten exterior column type specimens were specially designed and tested to clarify the concrete breakout failure mechanism and bearing stress in the case of exposed column bases. Experiment parameters contained the number of column rebars, embedded depth of anchor rods, compression strength of concrete, and strength of beam transverse rebar. The following conclusion is inferred based on the experiment results.

In A-series, the major failure mode was the concrete breakout failure in the closing loading direction. However, it was found that the ultimate strength of A-series specimens was greatly smaller than the calculation value of concrete breakout failure strength following the current design recommendation. Also, the difference in the embedded length of the beam rebar did not influence the structural behavior in the closing side.

In B-series, the failure mode was beam bending failure due to the yielding of beam transverse rebar. From the relation between the calculation value and experiment results, the ultimate strength could be evaluated accurately. However, although the maximum strength is lower than the calculated concrete breakout failure strength, the concrete breakout failure cracks were also observed in the specimens.

In C-series, the failure mode is the concrete compression and bending failure due to the insufficient column longitudinal rebar. On the other hand, the maximum strength is greatly higher than the calculation value of concrete breakout failure strength. It is also found that the difference in the type of anchor rods has no significant influence on the structural behavior in both loading directions.

In all, from the experiment results, it could be concluded that the current design recommendation could not evaluate the concrete breakout failure strength accurately. Thus, the detailed analysis and discussion on the concrete breakout failure will be introduced in Chapter 3. On the other hand, as the experiment results showed great relevance of the maximum strength of the exposed column base, the discussion on bearing failure in conducted in Chapter 4 based on this result.

References

[2-1] Instruction manual of building structures' technical standards affiliated with the Building Standards Law, 2015 (in Japanese).

[2-2] JIS G 3109: 2008, Steel bars for prestressed concrete, 2008.

[2-3] JIS Z 2201: 1998, Test pieces for tensile test for metallic materials, 1998.

[2-4] JIS A 1108: 2018, Method of test for compressive strength of concrete, 2018.

[2-5] JIS A 1142: 2018, Method of test for fine aggregate containing organic impurities by compressive strength of mortar, 2018.

[2-6] Architectural Institute of Japan: 2017, AIJ Guidebook on Design and Fabrication of Column Base in Steel Structure, Maruzen, Tokyo, 2017 (in Japanese).

Chapter 3.
Design approach of concrete breakout failure

3. Design approach of concrete breakout failure

To ensure the anchor rods yielding in the exposed column base, the pull-out of anchor rods should be prevented. One of the failure modes related to the pull-out of anchor rods is the concrete breakout failure. In this chapter, by analyzing the data from the experiment, the concrete breakout failure mechanism was clarified. It was found that the current design recommendation in Japan overestimated the number of effective column rebar. The design approach of concrete breakout failure was proposed based on this finding. A database that contained the previous concrete breakout failure experiments was established and it was proved that the proposed design approach could evaluate the concrete breakout failure strength conservatively.

3.1 Introduction and background

3.1.1 Introduction

Concrete breakout failure is a brittle failure that must be prevented in the exposed column base. However, there is no specific method regarding the concrete breakout failure strength in the case of the exposed column base. In Japan, in the Recommendation for Design of Connections in Steel Structures (Connections Recommendation) [3-1], the equation used to calculate pull-out strength was based on the RC beam-to-column connections outlined in the Design Guidelines for Earthquake Resistant Reinforced Concrete Buildings Based on Inelastic Displacement Concept [3-2].

In the Connections Recommendation [3-1], the pull-out strength of anchor rods was considered as indicated in Figure 3-1. Eqs. (1–2) showed the calculation of the pull-out strength of the anchor rods due to the concrete breakout failure.

$$ {}_cT_u = \varphi_1 T_a + 0.7T_r \tag{1} $$

$$ T_a = 0.31\sqrt{F_C} \cdot A_c \tag{2} $$

Where ${}_cT_u$ is the pull-out strength of the anchor rods, φ_1 is the reduction factor considered to be equal to 2/3, T_a is the concrete breakout failure strength, T_r is the yield strength of the effective column rebar in the range of failure surface, F_c is the nominal compression strength of concrete, and A_c is the projected area of concrete breakout failure.

There are two components in the calculation of pull-out strength, namely, concrete and the column longitudinal rebar (column rebar). As shown in Figure 3-1, in the case of the experiment specimens of this study, which is an exposed column base with one side foundation beam, the loading tends to close or open the knee-joint-shaped specimen is defined as the closing side and opening side, respectively. The embedded length of anchor rods E_{ar} is required to be at least 20 times its nominal diameter [3-3]. In the concrete column, from the anchored position, a 45° concrete breakout failure surface is assumed.

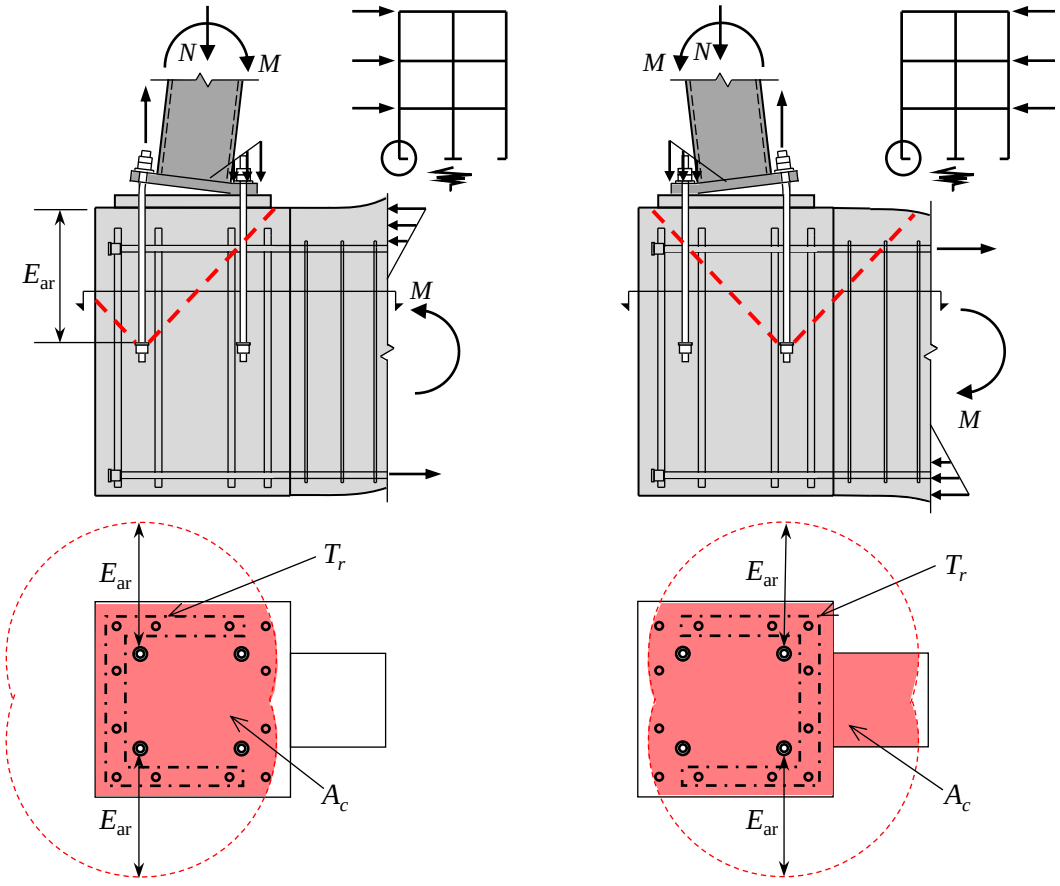

(a) Closing side (b) Opening side

Figure 3-1 Calculation method of pull-out strength of anchor rods owing to the concrete breakout failure [3-1]

Projection area on the top surface of concrete is defined as effective concrete breakout failure area A_c, which could be observed from the red area in Figure 3-1. A method used to determine A_c involves drawing circles from the center of anchor rods (exposed to tension) with a radius of E_{ar} plus the radius of anchor plate r, then subtracting the area of the anchor plate and anchor rods (πr^2) from the circle. In the case of opening side, A_c contains part of the foundation beam as illustrated in Figure 3-1 (b). Regarding the effect of rebar, all the column rebar in the failure area are considered as effective rebar (as marked in the dotted frame).

In the United States, the Building Code Requirements for Structural Concrete (ACI 318M-14) and Commentary (ACI 318RM-14) [3-4] refers to a calculation method of the concrete breakout failure strength N_{cbg} for a group of anchors, as indicated by Eq. (3)

$$N_{cbg} = \frac{A_{Nc}}{A_{Nco}} \cdot \Psi_{ec,N} \cdot \Psi_{ed,N} \cdot \Psi_{c,N} \cdot \Psi_{cp,N} \cdot N_b \tag{3}$$

where A_{Nc} is the projected concrete failure area of a group of anchors, A_{Nco} is the projected concrete failure area of a single anchor with an edge distance equal to or greater than $1.5E_{ar}$, $\Psi_{ec,N}$ is the modification factor for anchor groups loaded eccentrically in tension, $\Psi_{ed,N}$ is the modification factor for edge effects, $\Psi_{c,N}$ is the modification factor for anchors located in a region of a concrete member where the analysis indicates no cracking at service load levels, $\Psi_{cp,N}$ is the modification factor for post-installed anchors, and N_b is the basic concrete breakout strength of a single anchor in tension in cracked concrete

However, when the column rebar is developed, the design strength of the column rebar can be used instead of the concrete breakout strength for the determination of the tension of anchor rods with a 0.75 strength reduction factor from the conservative point-of-view [3-5]. It is a quite different design conception compared with Japan. In this chapter, both the contribution of concrete and column rebar was discussed and clarified.

3.1.2 Previous researches

A very limited number of existing studies focused on the concrete breakout failure

strength in structures with RC foundations based on consideration of the effect of column rebar. Masuda et al. [3-6][3-7] conducted stud column experiments with parameters of the embedded length of anchor rods and the number of column rebar. The results indicated that the column rebar contributed to the concrete breakout failure strength. Koya et al. [3-8][3-9] investigated the influence of column rebar's anchorage method and its contribution to an inner column type specimen. A stress transfer mechanism was proposed. Kadoya et al. [3-10] conducted an inner column type experiment, whereby the adhesion length of column rebar should be ensured if its contribution to the concrete breakout failure strength is assumed.

However, there were a few research studies that focused on the concrete breakout failure behavior of the corner column, and the effect of beam longitudinal rebar (beam rebar) on the concrete breakout failure. Furthermore, these research studies did not clarify the precise number of effective column rebars. Additionally, the timing at which the column rebar started to strengthen and concrete breakout failure crack occurred was not clear either.

Thus, by analyzing the experiment results, the following points were clarified: a) the concrete breakout failure strength, b) precise contribution of column rebar to the strength of the exposed column base with one-sided foundation beam, and c) effect of beam rebar on the pull-out strength of anchor rods owing to concrete breakout failure.

3.2 Experiment results related to concrete breakout failure

3.2.1 Failure modes and hysteretic curve

The hysteresis relation between shear force on the column base Q and story drift R is presented. The sketch showing the parameters of each series specimen is also indicated next to its hysteretic curve. The envelope curve for both loading directions is indicated with a thicker line. The timing of anchor rods and hoop yielding judged by strain gauge results are marked in the hysteretic curve with round marks. Additionally, concrete breakout failure strength T_{cone} and the residual concrete breakout failure strength $T_{cone,res}$ were marked with square marks. The definitions and discussion on T_{cone} and $T_{cone,res}$ are listed in section 3.2.2. The experimental results consist of failure modes and maximum strength are listed in Table 3-1. Additionally, Table 3-1 shows the calculated strength of several failure modes following the Column Base Recommendation and its comparison with experiment results. The strengths of every failure mode were converted to the shear force applied on column bases for the convenience of comparison. The failure modes involved concrete breakout failure, bending failure of the beam, and hinged column base caused by the yielding of anchor rods. The behavior of every specimen will be explained by the order of their series.

- **A-Series specimens**

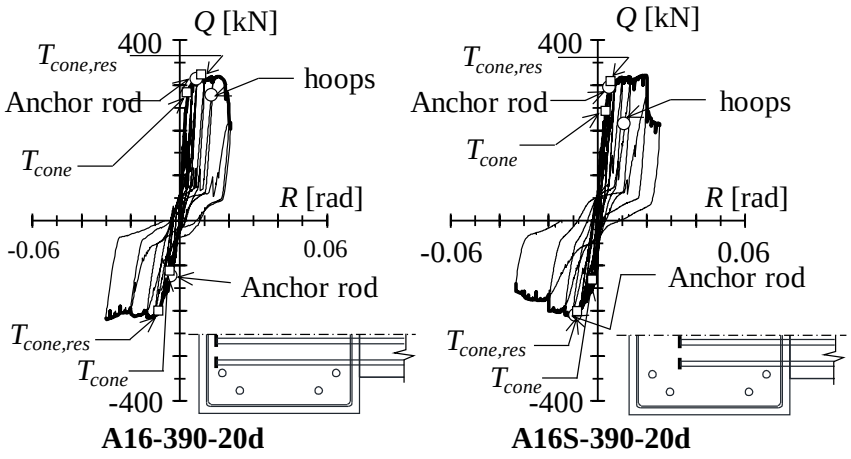

Figure 3-2 Hysteresis curve of A-series specimens

For specimens in A-series, the hysteresis relation between shear force on the column base Q and story drift R is presented in Figure 3-2. On the closing side, the strength deteriorated owing to the concrete breakout failure. Severe conical cracks could be observed from specimens, crack distribution of specimen A16-390-20d was taken as an example as illustrated in Figure 3-5(a). The maximum strengths of both specimens were similar and approximately equal to 322 kN on the closing side and 210 kN on the opening side. The considerable difference in the maximum strength in different loading directions was attributed to the varying axial force applied on the foundation beam as the specimen was set as 45° at an inclined orientation. Specifically, for the opening side, the tension applied on the column base caused the strength to be smaller than the closing side. Owing to this reason, in Table 3-1, both the calculated values of the failure strength are listed separately. The strength in the opening side was marked within parentheses. Regarding the experimental results, on the closing side, anchor rods yielded at a loading amplitude of R = 0.5% for both specimens, and the hoop closing to the anchor plate also yielded in a subsequent loading process. The strength deteriorated owing to the concrete breakout failure on the closing side. Severe conical cracks could be observed from the specimen, the crack distribution of specimen A16-390-20d was taken as an example as observed in Figure 3-5(a). However, the difference in the embedded length of the beam rebar did not influence the structural behavior in the closing side. The maximum strength and failure mode were similar.

Conversely, in the opening side in the case of specimen A16-390-20d, the strength was stable until the ultimate state; however, for specimen A16S-390-20d, the strength deteriorated by approximately 20% owing to the insufficient anchorage strength because of the short-embedded length of the beam rebar. Regarding the effect of the anchorage length of the beam rebar on the concrete breakout failure, there was no considerable difference between the two specimens. Regarding the position of $T_{cone,res}$, because the strain gauge glued on the anchor rods failed at the amplitude of R = 1%, the $T_{cone,res}$ was taken from the last available value in that loading cycle.

- **B-series specimens**

For specimens in A-series, the hysteresis relation between shear force on the column base Q and story drift R is presented in Figure 3-3. In the sketch of the specimens next to their hysteretic curve, darker color on the beam rebar and concrete body represent higher strength. The failure mode of specimens was beam bending failure that occurred following the yielding of beam rebar. Different beam rebar grades caused the changing of maximum strength. Severe bending cracks can also be observed in Figure 3-5(c) and (d). The maximum strengths of the specimens were approximately 1.12 to 1.33 times the calculated value on the closing side and 0.98 to 1.13 times on the opening side. In respect of the concrete breakout failure, conical cracks could be observed from the surface of specimens displayed in Figure 3-5(c) and (d), although the maximum strength did not reach the calculated value ${}_{cal}{}^{b2}F_y$. Regarding the influences of the beam rebar on the

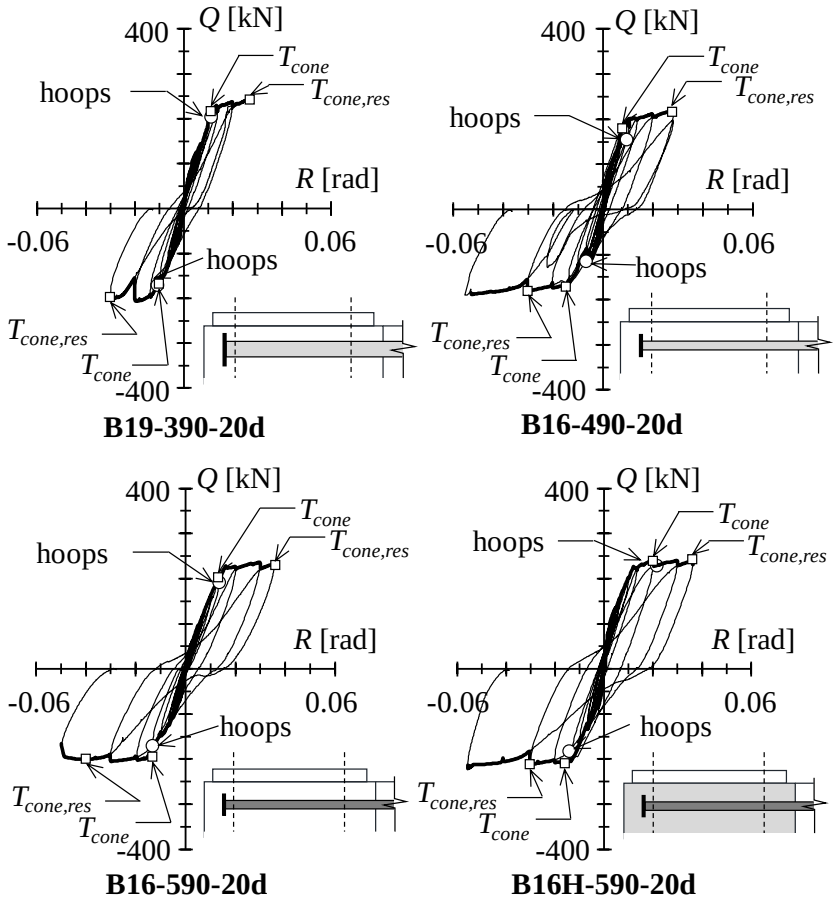

Figure 3-3 Hysteresis curve of B-series specimens

concrete breakout failure, no considerable differences were found in both loading directions.

- **C-series specimens**

For specimens in A-series, the hysteresis relation between shear force on the column base Q and story drift R is presented in Figure 3-4. The failure mode of specimens was the column compression bending failure in the bottom of concrete column during the closing side loading following the considerable deterioration of strength. As shown in Figure 3-5(e), severe cracks are concentrated on the bottom of the column on the closing side. The reason was attributed to the inadequate column rebar in C-series specimens. Additionally, conical cracks were observed in the closing side loading of specimen C16-590-30d and the opening side loading of specimen C16-590-20d shown in Figure 3-5(f). For specimens C16-590-39d and C16-590-39db, except cracks on the foundation beam,

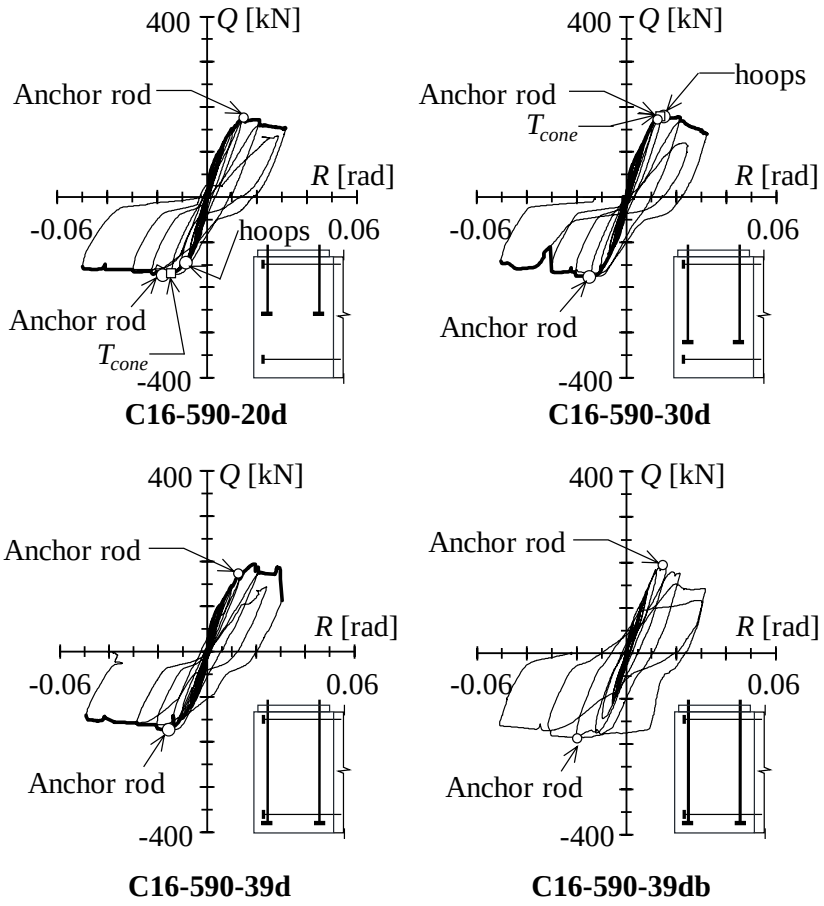

Figure 3-4 Hysteresis curve of C-series specimens

the cracks accumulated on the bottom side of the concrete column. Regarding the maximum strength of C-series specimens, in the opening side, the strength was very similar to the yielding of anchor rods with a difference of approximately 3.4 kN. On the closing side, the strength increased as a function of the embedded length of anchor rods. Although the maximum strength of the specimen was approximately 1.36 to 1.68 times the calculated value of the concrete breakout failure strength ($_{cal.}{}^{b}F_{y}$), the pullout of anchor rods owing to concrete breakout failure did not occur.

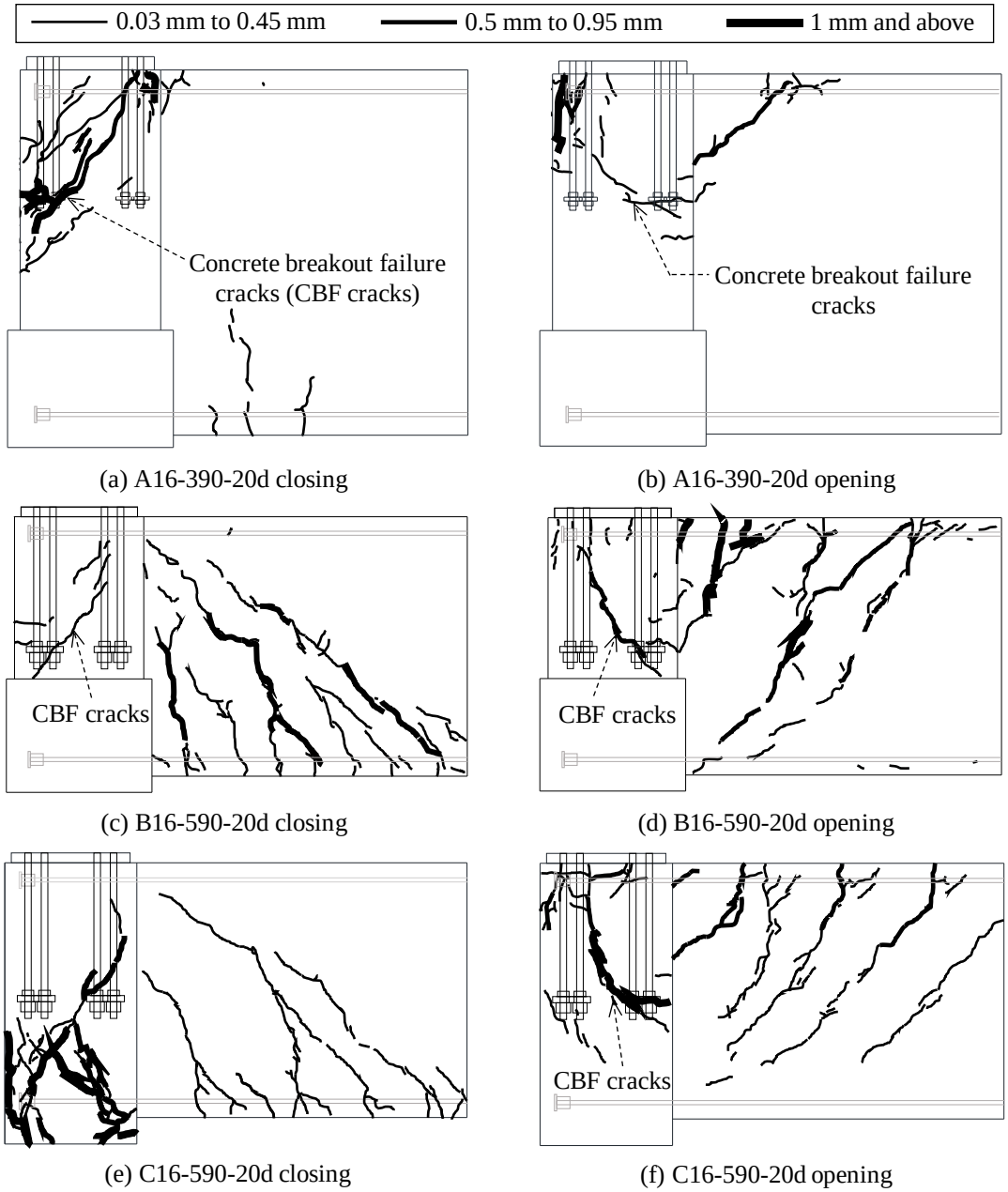

(a) A16-390-20d closing

(b) A16-390-20d opening

(c) B16-590-20d closing

(d) B16-590-20d opening

(e) C16-590-20d closing

(f) C16-590-20d opening

Figure 3-5 Crack distributions on the specimens in the ultimate states

Table 3-1 Strength of specimens, failure mode, and comparison with the calculated results

No.	$+Q$ [kN]	$-Q$ [kN]	${}_{cal}{}^{a}F_y$ [kN]	${}_{cal}{}^{b1}F_y$ [kN]	${}_{cal}{}^{b2}F_y$ [kN]	${}_{cal}{}^{c}F_y$ [kN]	$\frac{+Q}{\min\{F_y\}}$	$\frac{-Q}{\min\{F_y\}}$	Failure mode
A16-390-20d[a]	323.9	219.2	612.9 (234.5)	291.7 (215.6)	588.4 (434.8)	270.5 (208.4)	1.20	1.05	CBF
A16S-390-20d[a]	322.4	210.9	613.7 (234.6)	292.6 (216.3)	589.3 (435.6)	270.5 (208.4)	1.19	1.01	CBF
B19-390-20d	243.3	206.0	182.7	302.5	650.0	316.0	1.33	1.13	BBF
B16-490-20d	219.3	189.9	179.4	302.8	650.5	316.0	1.22	1.06	BBF
B16-590-20d	236.7	205.5	210.6	303.7	653.0	316.0	1.12	0.98	BBF
B16H-590-20d	240.3	221.2	210.6	323.9	706.1	431.8	1.14	1.05	BBF
C16-590-20d	174.4	173.2	202.7	104.0		162.0	1.68	1.67	CCBF
C16-590-30d	187.9	176.6	202.7	117.0		162.0	1.61	1.51	CCBF
C16-590-39d	194.3	173.2	202.7	127.0		162.0	1.53	1.36	CCBF
C16-590-39db	189.4	185.9	202.7	127.0		162.0	1.49	1.46	CCBF

Note: $+Q$, $-Q$: Maximum strength in closing and opening side.

${}_{cal}{}^{a}F_y$: bending failure of beam by the yielding of beam rebar.

${}_{cal}{}^{b1}F_y$: concrete breakout failure strength calculated based on considerations of reduced numbers (6 or 8) of column rebars.

${}_{cal}{}^{b2}F_y$: concrete breakout failure strength calculated by considering all (20) column rebars.

${}_{cal}{}^{c}F_y$: full plastic strength of column base by considering the yield of the anchor rod.

Failure mode: CBF: concrete breakout failure; BBF: beam bending failure; CCBF: column compression bending failure.

[a]: Strength marked in the parentheses is the calculated value in the opening side.

3.2.2 Concrete breakout failure strength evaluation

From the behaviors of specimens in A and B-series, conical cracks were observed on the surface of the concrete column. Furthermore, the failure mode for the A-series specimen was concrete breakout failure. However, from the calculated results listed in Table 3-1, the concrete breakout failure strength calculated based on the Connections

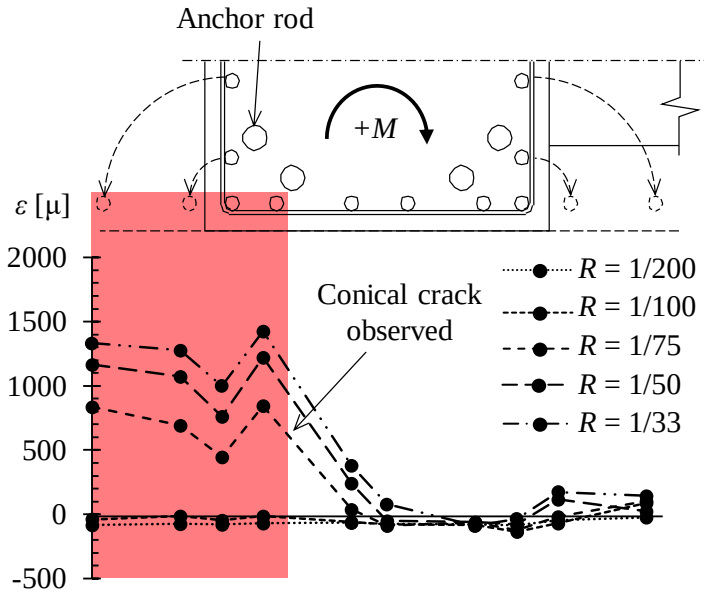

Figure 3-6 Strain distribution on the column rebar of specimen B16-590-20d in closing side

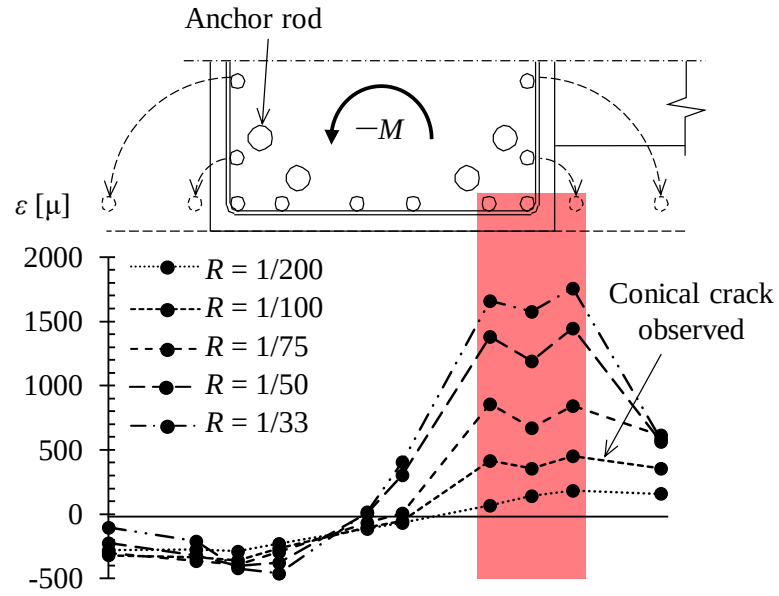

Figure 3-7 Strain distribution on the column rebar of specimen B16-590-20d in opening side

Recommendation [3-1] was approximately 1.82 to 2.06 times the maximum strength of the specimens ($_{cal.}{}^{b2}F_y/Q$). This means that the Connections Recommendation overestimated the concrete breakout failure strength. To clarify the efficiency of each component, the behavior of column rebar and anchor rods are discussed by the results of glued strain gauge.

As indicated in Figure 3-6, the strain values of strain gauge glued on the column rebar are summarized by peak values of every loading amplitude on the closing side. The experimental result of specimen B16-590-20d was illustrated as an example. On the closing side, the strain increased significantly and attained the same amplitude as that attained by the conical crack that was observed initially. In the half section of the column, four column rebars were counted as effective in the concrete breakout failure strength (marked in color). On the opening side, as illustrated in Figure 3-7, the strain amplitude also increased when the conical crack was also observed. However, the effective number of column rebars was three. Compared with the closing side, the different one existed in the area close to the foundation beam. It was considered that the foundation beam also contributed to the concrete breakout failure area. Thus, the rebar in that region required a smaller strength than the others. In conclusion, the effective number of column rebar was far less than the number mentioned in the Connections Recommendation [3-1]. Additionally, for the corner column, the effective number of column rebar in the side

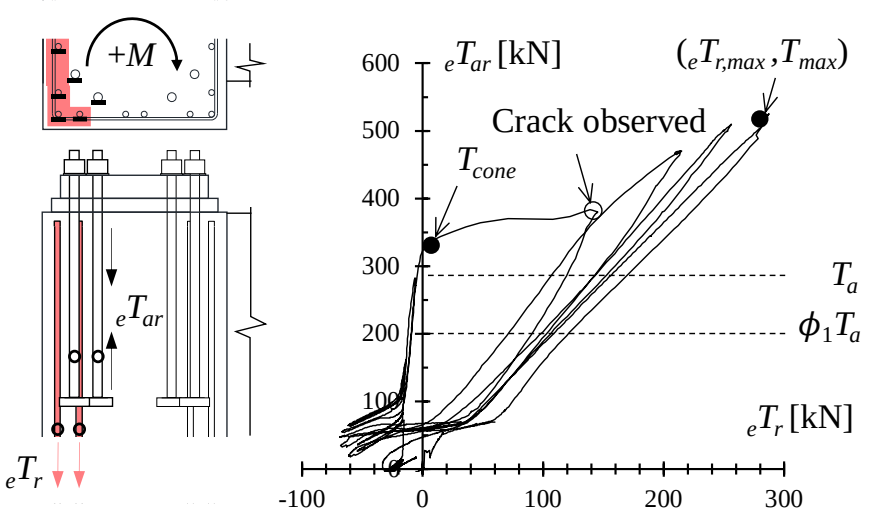

Figure 3-8 Strength relation of anchor rod and column rebar of specimen B16-590-20d

without the foundation beam was higher than that in the side with the foundation beam.

The strength relation of the anchor rod and column rebar is displayed in Figure 3-8. Only the effective ones were picked up to consider the strength relation. The experimental result of specimen B16-590-20d in the closing side was chosen as an example. The strengths of the column rebar and anchor rods were represented as ${}_eT_r$ and ${}_eT_{ar}$, and were calculated from the strain gauge data. In Figure 3-8, the ${}_eT_r$ value started to increase considerably when the ${}_eT_{ar}$ reach the value of T_{cone}, which refers to the column rebar starting to take strength when the conical crack occurred inside the concrete. T_{cone} was the peak value in the vertical axis in Figure 3-9, which represents the experiment value of concrete failure strength ${}_eT_a$ which was defined as the difference between ${}_eT_{ar}$ and ${}_eT_r$ as the concrete proportion could not be measured directly. The timing of strength reached T_{cone} was considered as concrete breakout failure occurred. Additionally, conical cracks were also observed from the surface of specimens in peak value of the same loading cycle as marked in a hollow circle in Figure 3-8. The maximum value of ${}_eT_{ar}$ and ${}_eT_r$ was defined as T_{max} and ${}_eT_{r,max}$. As can be observed from Figure 3-9, after ${}_eT_a$ reached T_{cone}, ${}_eT_a$ started to decrease to the range between $\varphi_1 T_a$ and T_a (mentioned in Eq. 1), and maintained almost stable subsequently. The value of ${}_eT_a$ in the ultimate state was defined as $T_{cone,res}$, which indicated the residual concrete failure strength. Discussion about these defined strengths will be introduced in the following section.

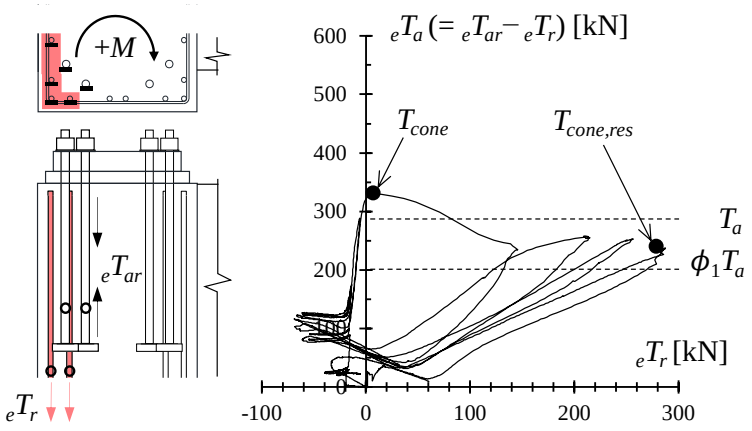

Figure 3-9 Strength relation of concrete and column rebar of specimen B16-590-20d

3.3 Discussion

3.3.1 Concrete breakout failure strength

The values of T_{cone}, $T_{cone,res}$, and T_a were plotted and compared in Figure 3-10 and Figure 3-11. T_a is a calculated value of concrete breakout failure strength according to Eq. (2). To discuss the concrete breakout failure strength T_{cone}, as mentioned in Connections Recommendation [3-1], $\varphi_1 T_a$ is also shown in a dashed boundary line. As illustrated in Figure 3-10, in the case of specimens of A-series, the results were around $\varphi_1 T_a$. The reason is attributed to the fact that the strain gauge on the anchor rod failed in the early stage

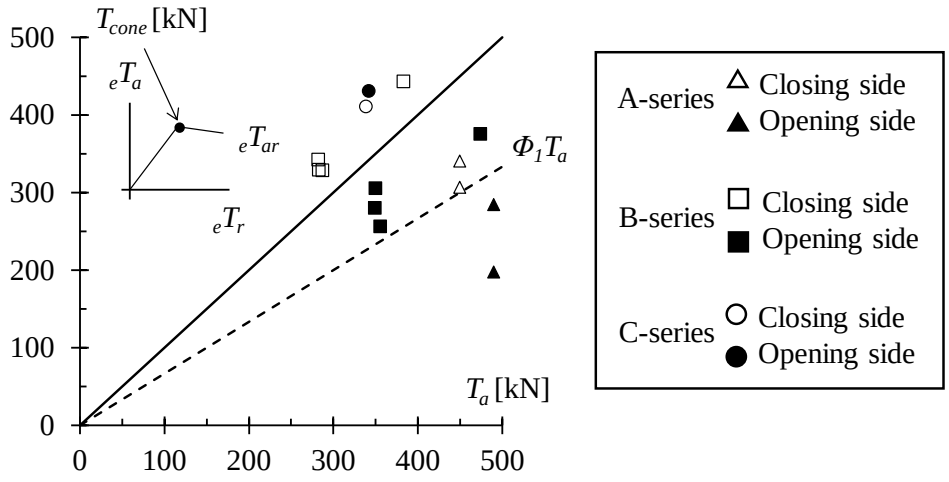

Figure 3-10 Comparison of experiment result T_{cone} with calculated result T_a

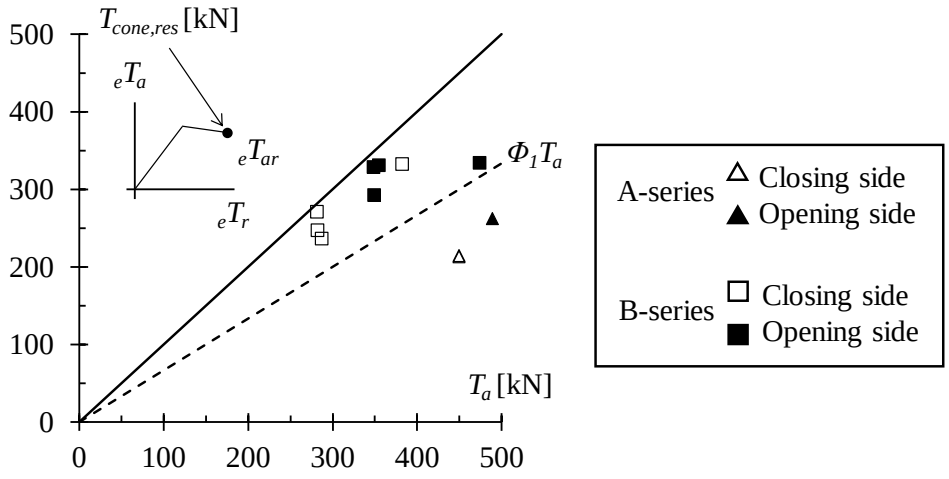

(b) Residual concrete breakout failure strength

Figure 3-11 Comparison of experiment result $T_{cone,res}$ with calculated result T_a

such that the maximum value of ${}_eT_a$ could not be achieved. For the B-series, the T_{cone} showed different results owing to the different loading direction, in the closing side, and the T_{cone} was over T_a. However, in the opening side, the T_{cone} value was in the range between T_a and $\varphi_1 T_a$. Regarding the C-series, since there was no column rebar in the specimen, only T_{cone} was used in the comparison. When the two specimens with conical crack occurred, T_{cone} was higher than T_a. This outcome matched the experimental result. In the design procedure, $\varphi_1 T_a$ was proposed as the concrete breakout failure strength to control the conical crack.

Conversely, in Figure 3-11, all of the experimental results in the B-series were in the range of T_a and $\varphi_1 T_a$. Regarding the A-series specimens, because the strain gauge attached on the anchor rods failed before the ultimate state, the maximum value from the strain gauge was used in the calculation, such that the $T_{cone,res}$ for A-series specimens was lower than $\varphi_1 T_a$.

3.3.2 Effectiveness of column rebar

As mentioned in section 3.2.2, the effective number of column rebar was less than the number mentioned in the Connections Recommendation [3-1]. Moreover, the effective number was different in the closing and opening sides (i.e., the side without or with foundation beams), as illustrated in Figure 3-12. The difference was in the column rebar close to the centerline of the foundation beam. Based on this result, in the ultimate state, the tension of the effective column rebar ${}_eT_{r,max}$ (calculated by the strain gauge data) was compared with its yield strength T_r, as shown in Figure 3-14 and Figure 3-13. In the Connections Recommendation [3-1], the effective strength of column rebar is considered as 70% of its yield strength in the ultimate state. As it can be observed in Figure 3-14, when all the column rebars were considered as effective in the concrete breakout failure, there was a considerable overestimation of the effect of the column rebars. However, in the case in which only the counting effective column rebars were considered, as shown in Figure 3-13, the tension of column rebar was approximately equal to 70% of its yield strength. Thus, it is rational to reduce the number of effective column rebars without

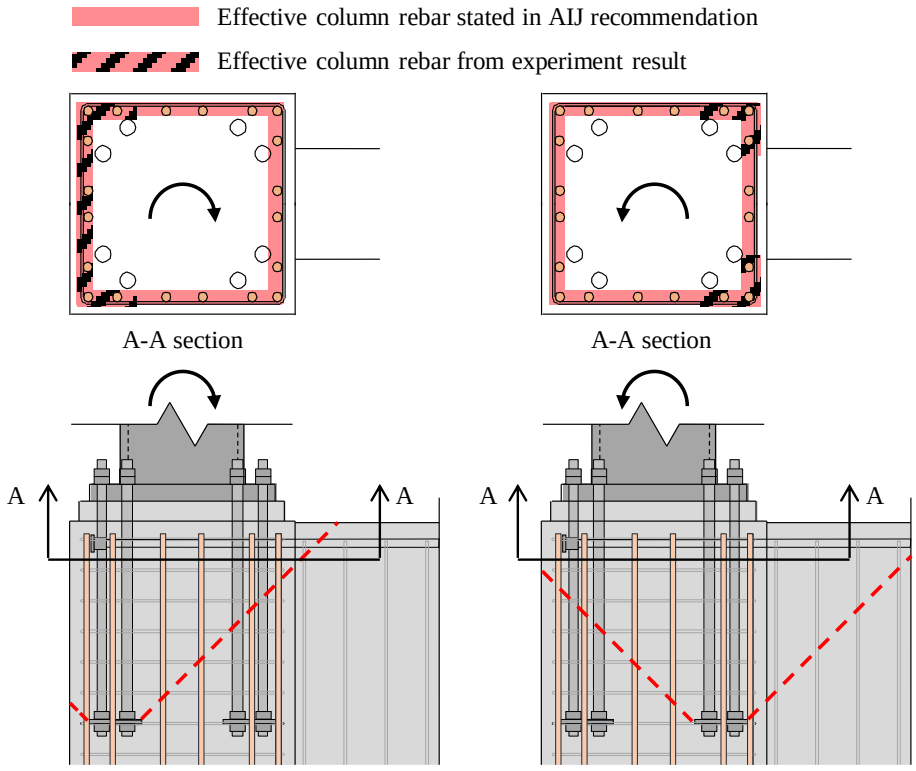

Figure 3-12 Effective column rebar for the specimens in different loading directions

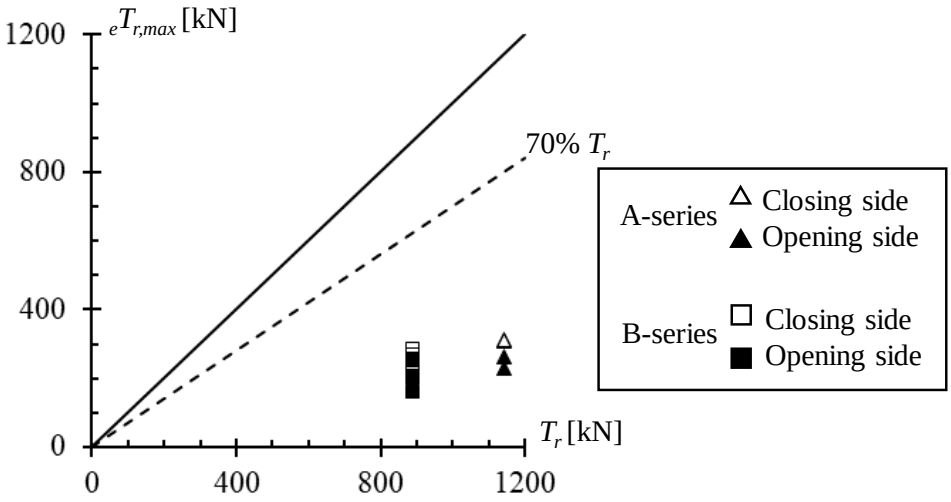

Figure 3-14 Comparison of experiment result $_eT_{r,max}$ with calculated results T_r by the definition of AIJ Recommendation

revising the reduction factor when considering the contribution to the concrete breakout failure strength.

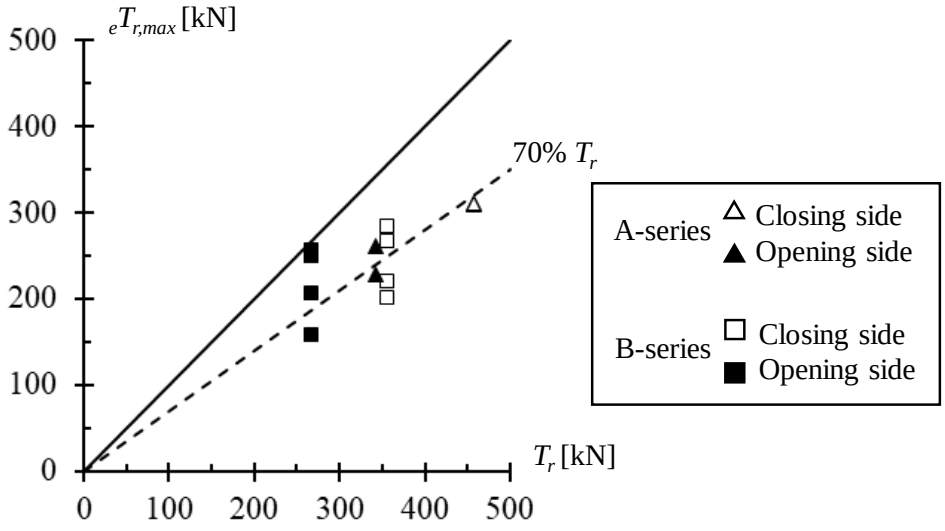

Figure 3-13 Comparison of experiment result $_eT_{r,max}$ with calculated results T_r by proposed number of effective column rebar

3.3.3 Evaluation of pullout failure strength

As shown in Figure 3-15, the maximum strength of anchor rods T_{max} is summarized and compared with the calculated value of pull-out strength of anchor rods ${}_cT_u$ according to Eq. (1). Based on considerations in section 3.2.2, the reduced number of effective column rebar was considered in the equation with a reduction factor of 0.7. The proposed evaluation method of the pull-out strength of anchor rods owing to the concrete breakout failure fits well with the experimental results (approximately equal to 0.8 to 1.2 times

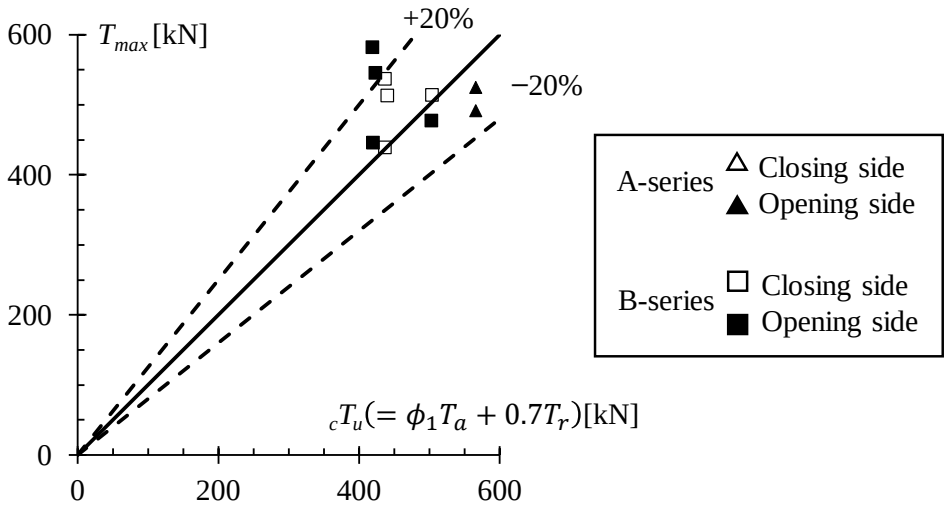

Figure 3-15 Comparison of experiment results T_{max} with the calculated results ${}_cT_u$ by AIJ recommendation

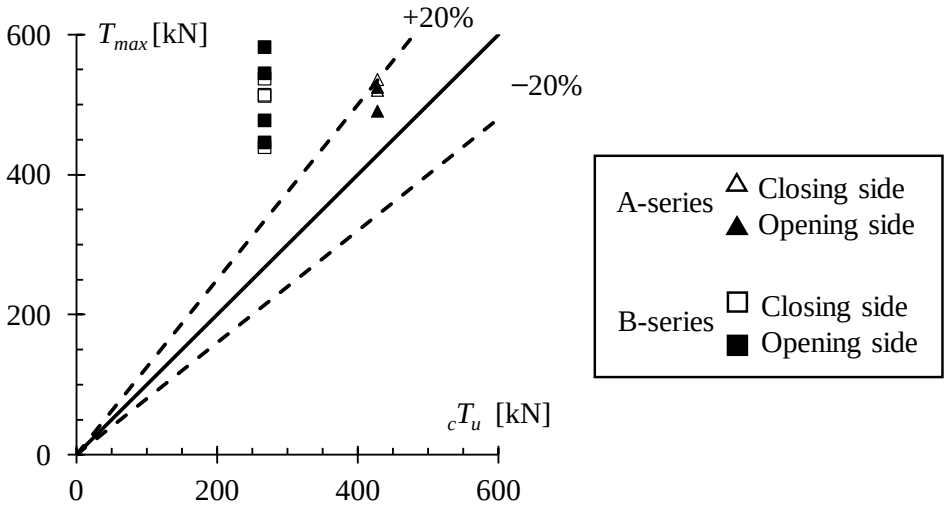

Figure 3-16 Comparison of experiment results T_{max} with the calculated results ${}_cT_u$ by ACI recommendation

calculated results). Correspondingly, considering reducing the number of effective column rebar is rational. On the other hand, as illustrated in Figure 3-16, maximum strength was underestimated following the ACI recommendation. In each series, calculation results were the same because the concrete breakout failure strength was replaced by the strength of effective column rebar with a strength reduction factor of 0.75.

3.3.4 Proposed concrete breakout failure mechanism

As concluded based on sections 3.3.1 to 3.3.3, a stage-wise approach is proposed to quantify the contributions of both the concrete and column reinforcement of concrete breakout failure, as illustrated in Figure 3-17. In the relation of tensile force of anchor rods T and rotation angle θ, concrete withstood all the force owing to the anchor rods with no support from column rebar, up to the point at which the tension of anchor rods reached T_{cone}. Subsequently, the effective column rebar started to withstand the exerted force when the conical cracks occurred but became stable (approximately $0.7T_r$) afterward. Meanwhile, the proportion of concrete decreased to $T_{cone,res}$. Both T_{cone} and $T_{cone,res}$ were considered to be above $\varphi_1 T_a$ in a conservative design. It is proposed that conical cracks can be controlled when the tension of anchor rods is less than T_{cone}. The tension of anchor rods will continue increasing then reach the maximum value when the tension of column rebar reaches $0.7T_r$. The maximum tension of anchor rods T_{max} is approximately equal to 0.8 to 1.2 times the calculated value of ${}_cT_u$.

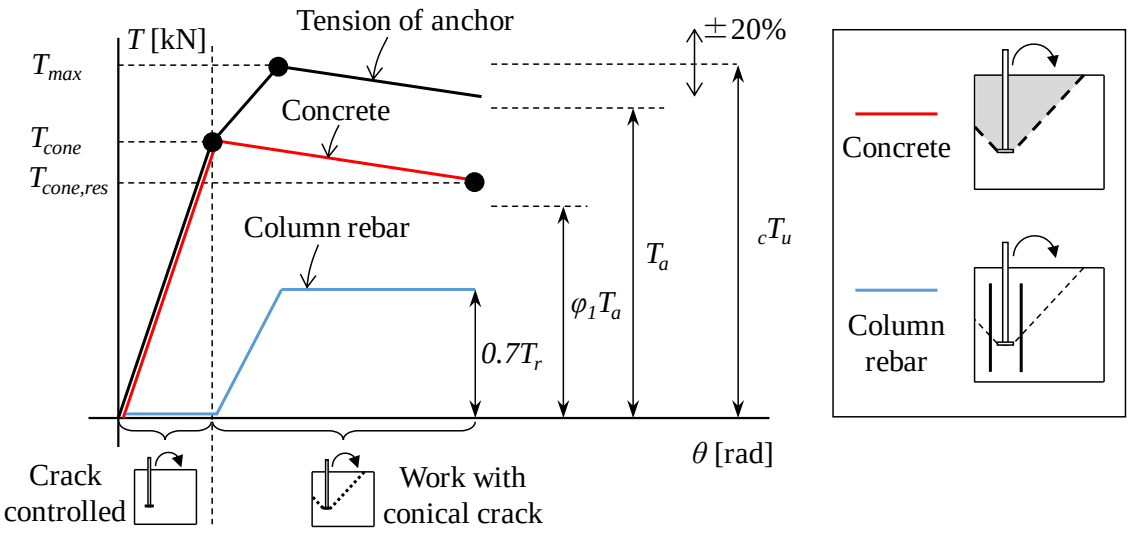

Figure 3-17 Proposed stage-wise approach of concrete breakout failure

3.4 Database and confirmation of proposed mechanism

Based on the review of literature, several research studies focused on the concrete breakout failure. Their specimen types contained the internal column (with both sides of the foundation beam) and the stud column (without a foundation beam). To nominalize the experimental data, tension of anchor rods was calculated based on an assumption that the center of resultant compressive force of foundation concrete was in the compressed flange of steel columns, as shown in Eq. (4).

$$ {}_{e,cal}T_{ar} = \frac{{}_{e}M_{max} - {}_{e}N \times d_c}{d_t + d_c} \tag{4} $$

In this case, ${}_{e}M_{max}$ is the maximum moment from experimental results, ${}_{e}N$ is the axial force applied on column bases, d_c is the distance from the center of a column to the compressed flange of the column, and d_t is the distance from the center of a column to the center of tensile anchor rods.

To confirm the accuracy of this assumption, experimental results of B-series specimens were collected to compare with the calculated value, as displayed in Figure 3-18. As can be seen from the figure, calculated values fit well experimental results, such that the assumption is rational in the calculation of anchor rods' tension.

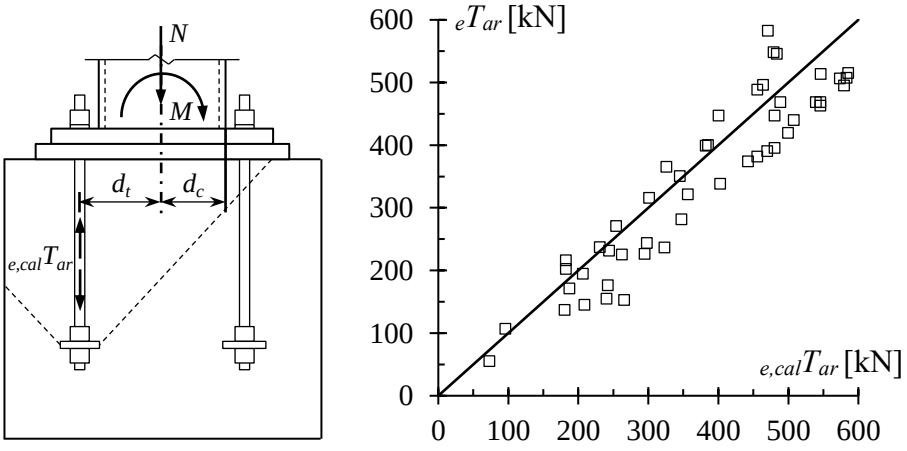

Figure 3-18 Assumption of anchor rod tension ${}_{e,cal}T_{ar}$ and comparison with experimental results

In the database, there were 11 specimens of interior column and nine specimens of stud column. The configuration of specimens and arrangement of anchor rods are listed in the bottom part of Table 3-2. The embedded length of anchor rods varied from 4 to 20 times its diameter and the compression strength of concrete varied from 20.5 to 43.7 N/mm^2. The concrete breakout failure strength T_a could be calculated with F_c and A_c. The arrangement of the column rebar is also listed in the table. The method used to determine effective column rebar was the same as that shown in Figure 3-12. The pull-out strength of anchor rods is expressed by Eq. (4) and complies with the form of Eq. (5) which is formulated based on a transformation from Eq. (1).

$$\frac{{}_cT_u - \phi_1 T_a}{\phi_1 T_a} = 0.7 \times \frac{{}_{cal}T_r}{\phi_1 T_a} \tag{5}$$

Several types of exposed column base specimens, internal column, stud column, and (in the case of our experiment) corner column (with one side of the foundation beam), were discussed separately as plotted in Figure 3-19 and Figure 3-20. The left and right sides of Eq. (5) were set as the vertical and horizontal axes, respectively, with a coefficient of 0.7 as a boundary dashed line. In the case of interior columns, it shows conservative results compared with the coefficient of 0.7. It was considered that for interior columns, in addition to column rebar, the beam stirrups are also covered in the concrete breakout failure area. In current formulas, the effect of beam hoops is not considered. Thus, there

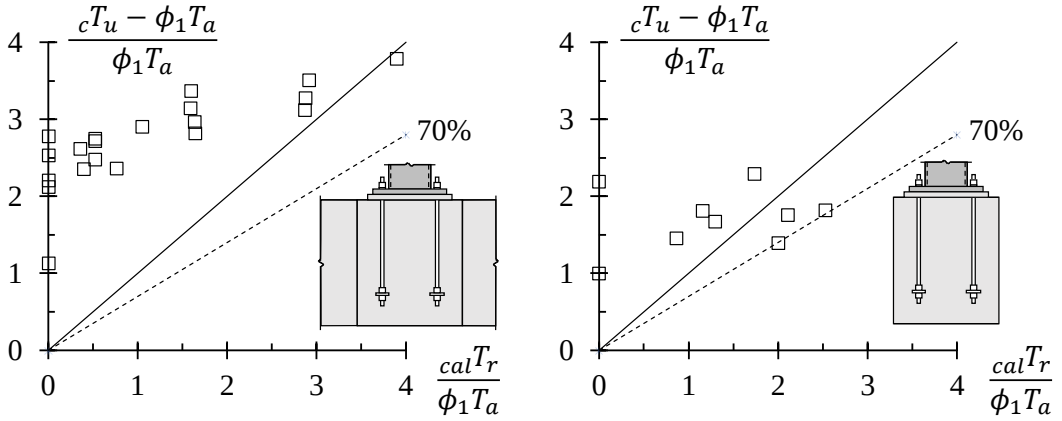

(a) Internal column[3-8]−[3-10] (b) Stud column [3-6][3-7]

Figure 3-19 Concrete breakout failure strength evaluations of specimens in data base

will be a conservative result in the case of interior columns. In conclusion, the current equation could evaluate the experimental results in a conservative range when only effective column rebar was considered.

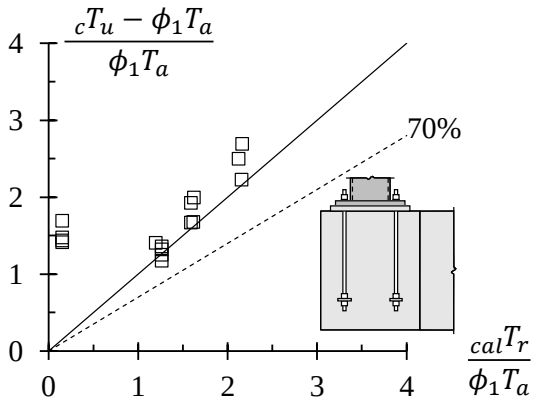

Figure 3-20 Concrete breakout failure strength evaluations of exposed column base with one side foundation beam

Table 3-2 Database focusing on concrete breakout failure

Identity (ID)				Anchor rod	Concrete			Column rebar		Pull-out strength
Paper ID	Specimen	Column type	Arrangement	E_{ar}/R_{ar}	F_c [N/ mm^2]	A_c [×10^4 mm^2]	$\varphi_1 T_a$ [kN]	Arrangement	$_{cal}T_r$ [kN]	$_{e,cal}T_{ar}$ [kN]
[3-8]	CB-4D	(I)	(i)	4	27.2	16.6	178.5	-	0	340.5
	CB-8D			8	27.2	27.4	295.4	-	0	725.5
	CB-12D			12	27.2	38.4	413.5	-	0	975.2
[3-9]	IB-C0	(I)	(i)	10	26.8	32.8	350.9	-	0	940.4
	IB-CC-2			10	26.8	32.8	350.9	(a)	138.7	999.2
	IB-CC-4			10	26.8	32.8	350.9	(g)	277.5	1039.9
[3-10]	A8M36-T04	(I)	(ii)	15.3	33.6	88.7	1063.5	(a)	310.2	2663.4
	A8M36-T12			15.3	32.8	88.8	1050.7	(c)	930.6	3247.2
	A8M36-T20			15.3	30.7	88.8	1016.5	(e)	1240.8	3128.0
	A8M39-T04			15.4	29.2	97.1	1084.7	(a)	280.5	2884.5
	A8M39-T16			15.4	27.3	97.1	1048.9	(d)	981.9	2946.6
[3-6]	B-5D	(II)	(iii)	5	20.5	7.4	68.8	-	0	219.9
	B-10D			10	20.5	17.3	162.0	(b)	324.1	388.7
	B-15D			15	20.5	22.8	213.5	(b)	540.1	603.6
	B-20D			20	20.5	27.3	255.8	(b)	540.1	705.9

Identity (ID)				Anchor rod	Concrete			Column rebar		Pull-out strength
Paper ID	Specimen	Column type	Arrangement	E_{ar}/R_{ar}	F_c [N/ mm^2]	A_c [$\times 10^4$ mm^2]	$\varphi_1 T_a$ [kN]	Arrangement	$_{cal}T_r$ [kN]	$_{e,cal}T_{ar}$ [kN]
[3-8]	0-D19	(II)	(iii)	15	43.7	22.8	311.7	-	0	624.0
	3-D16			15	29.5	22.8	256.1	(f)	221.9	629.2
	4-D16			15	29.5	22.8	256.1	(g)	296.0	721.2
	3-D19			15	29.5	22.8	256.1	(f)	331.7	685.4
	6-D16			15	29.5	22.8	256.1	(c)	443.9	844.0

Column type

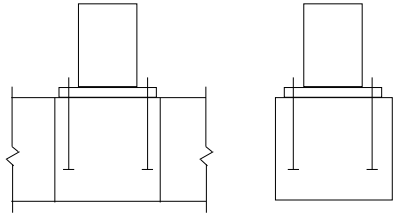

(I) (II)

Anchor rods arrangement

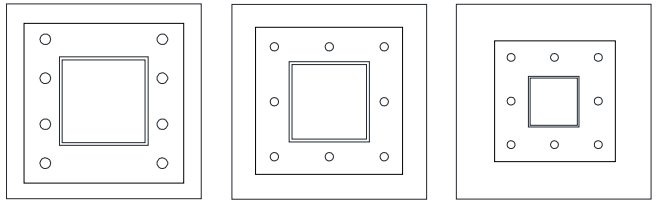

(i) (ii) (iii)

Column rebar arrangement

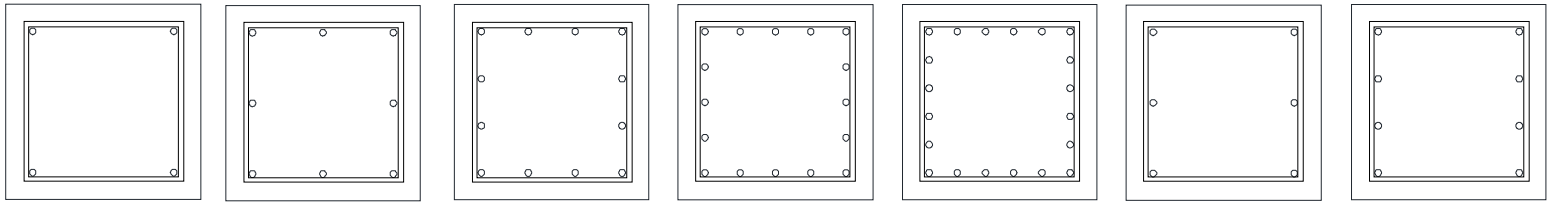

(a) (b) (c) (d) (e) (f) (g)

3.5 Summary

In this chapter, experiment results of exterior column type specimens were analyzed to clarify the contribution of column rebar and the timing of concrete breakout failure. Additionally, the effects of beam rebar were also considered. The following key conclusions are inferred based on the tests.

In the case of specimens without column rebar, the maximum strength of experimental results was approximately 1.36 to 1.68 times higher than calculated values of concrete breakout failure strength, while the strength deterioration caused by concrete breakout failure was not observed. Additionally, the effect of beam rebar on the pull-out strength was not observed.

The current Column Base Recommendation in Japan overestimates the number of effective column rebar in the evaluation of pull-out strength of anchor rods. Not all of the column rebar in the concrete breakout failure area were contributed. In the case of exterior column type specimens, the number of effective column rebar in the closing side was greater than that in the opening side. With the proposed reduction method of the number of effective column rebar, in the calculation of maximum strength, the current reduction factor applied to the column rebar could fit well the experiment results.

Regarding the concrete breakout failure strength, the experimental results confirmed its value at the instant at which conical cracks occurred and identified the ultimate state. In the design of the tension of anchor rods, in consideration of concrete breakout failure, it was proposed that a reduction factor should be applied for the calculation of concrete breakout failure strength to prevent the occurrence of conical cracks. In the ultimate state, the residual concrete strength and the strength of effective column rebar should also be considered based on the reduction factor. Overall, the experimental results fitted well the results obtained based on the proposed pull-out failure strength method. To confirm the applicability of proposed stage-wise approach, previous experimental results were also collected, which demonstrated good fitness outcomes to the proposed approach.

References

[3-1] Architectural Institute of Japan: 2012, Recommendation for design of connections in steel structures, Maruzen, Tokyo, 2012 (in Japanese).

[3-2] Architectural Institute of Japan: 1999, Design guidelines for earthquake resistant reinforced concrete buildings based on inelastic displacement concept, Maruzen, Tokyo, 1999 (in Japanese).

[3-3] Instruction manual of building structures' technical standards affiliated with the Building Standards Law, 2015 (in Japanese).

[3-4] American Concrete Institute (ACI), Building code requirements for structural concrete and commentary (318M-14, 318RM-14), Detroit.

[3-5] Eligehansen R. Anchorage in concrete construction. First ed. Berlin: Ernst & Sohn; 2012.

[3-6] Masuda H, Nakano T. Study on the static characteristics of exposed type column base of steel structure. Part 1: Bending test on cone-type fracture subjected to tension force by anchor bolt. Summaries of technical papers of annual meeting. AIJ 2000; 767–768 (in Japanese).

[3-7] Maruyama H, Nakano T, Masuda H. Study on static characteristics of exposed type column base of steel structure part3: Influence of footing columns longitudinal bars on cone shaped fracture. Summaries of technical papers of annual meeting. AIJ 2005; 661–662 (in Japanese).

[3-8] Koya Y, Tanaka T, Yoshimatsu R. Study on stress transferring mechanism of exposed column base to foundation beam connections. Part 1: Test plan and failure mode. Summaries of technical papers of annual meeting AIJ 2011; 941–942 (in Japanese).

[3-9] Yamamoto S, Tanaka T, Asada H, Tomotani Y. Study on stress transferring mechanism of exposed column base to foundation beam connections. Part 5: Test of

frames varying longitudinal bars in joint panels. Summaries of technical papers of annual meeting AIJ 2013; 885–886 (in Japanese).

[3-10] Kadoya H, Watanabe T, Takeuchi R, Hagino T, Morita K. Experimental study on anchorage strength of exposed-type column-base. J Struct Constr Eng AIJ 2013; 693: 1979–1988. 10.3130/aijs.78.1979 (in Japanese).

Chapter 4.
Design approach of concrete bearing stress

4. Design approach of concrete bearing stress

Besides the concrete breakout failure, to ensure the anchor rods yielding in the exposed column bases, the bearing failure of foundation concrete should also be prevented. In this chapter, the current evaluation methods of concrete breakout failure were summarized, by normalizing and analyzing the data of the previous experiments of exposed column bases, the most appropriate design method of concrete bearing stress was clarified. Furthermore, considering the design philosophy in Japan, a more conservative design approach of concrete bearing stress was proposed.

4.1 Introduction and background

4.1.1 Introduction

With a premise of the yielding of anchor rods, the ultimate strength (full plastic moment) of exposed column bases is calculated by the accumulating strength method [4-1] as illustrated in Figure 4-1. As the component of ultimate strength, on the compressive side, the strength is determined by the compression of concrete; on the tensile side, the strength is determined by the tension of anchor rods. By accumulating these two components, *M*-*N* interaction curve of the maximum strength of exposed column bases could be obtained. In different axial force states, the resisting mechanisms are also

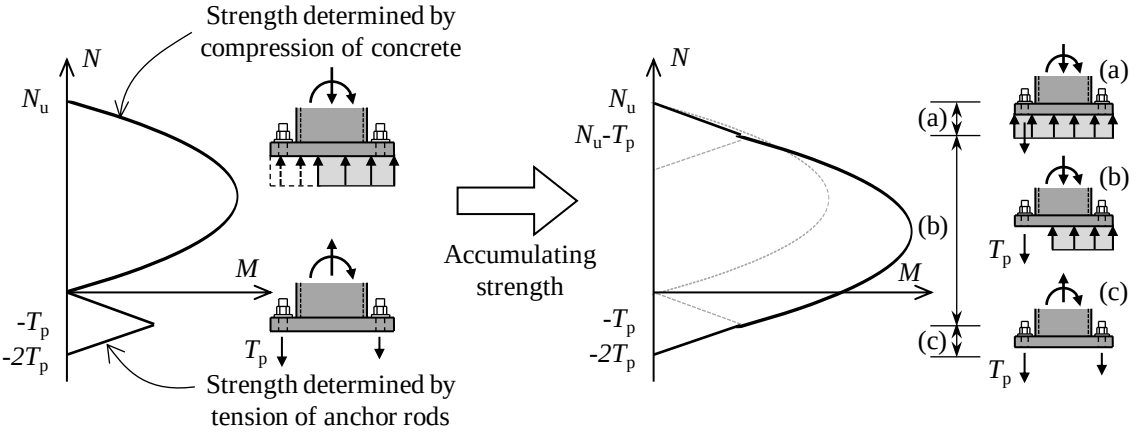

Figure 4-1 Accumulating strength method to calculate the ultimate strength of exposed column base

different as illustrated in Figure 4-1(a)-(c) with Eq. (1)-(3) to calculate the full plastic moment ${}_{cb}M_p$, respectively.

$$\text{When } N_u \geq N > N_u - T_p, \quad {}_{cb}M_p = (N_u - N)d_t \tag{1}$$

$$\text{When } N_u - T_p \geq N > -T_p, \quad {}_{cb}M_p = T_p \cdot d_t + \frac{(N + T_p)D}{2}\left(1 - \frac{N + T_p}{N_u}\right) \tag{2}$$

$$\text{When } -T_p \geq N > -2T_p, \quad {}_{cb}M_p = (N + 2T_p)d_t \tag{3}$$

Where, N_u is the maximum compression strength of concrete, $N_u = A_{bp} \cdot f_b$, A_{bp} is the section area of base plate, f_b is the bearing stress of concrete, $f_b = 0.85f_c$, f_c is the nominal compression stress of concrete, T_p is the yield strength of shaft part for the group of anchor rods in tension, $T_p = n_t \cdot p_{bp}$, n_t is the number of anchor rods in tension, p_{bp} is the yield strength of shaft part of one anchor rod, $p_{bp} = A_b \cdot F_{by}$, A_b is the section area of shaft part of anchor rod, F_{by} is the yield stress of anchor rod, d_t is the distance from the center of the steel column to the center of anchor rods in tension.

4.1.2 Previous researches

To ensure the yielding of anchor rods, the bearing failure of concrete must be prevented. In the calculation of bearing strength of concrete, bearing stress f_b is a significant factor. The bearing stress of concrete is very fundamental research that there were a great number of previous researches. Hawkins et al. [4-2] conducted experiments with a plate loaded on a concrete block considering the shape, size, and position of loading plate, concrete strength, and the size of concrete block. A conservative estimate equation of the ultimate bearing strength was proposed. Usami et al. [4-3] conducted small-scaled experiments with different shapes of steel column loaded on a concrete cylinder, considering the shape and dimension of steel column and the strength of concrete. An estimated equation of bearing stress and bearing area was proposed.

However, these researches only focused on the bearing stress in the case of plate or steel column loaded on a concrete column. In exposed column bases, the steel column is welded with the base plate, while a very limited number of studies considered the

influence of base plates on the bearing stress. Kutani et al. [4-4] conducted experiments with steel column welded with base plate loaded by compression force. The shape, size of steel column, shape and thickness of base plate, and size of footing were considered as parameters. Further, experiments with combined compression force and bending moment applied on the steel column were also conducted. Thickness of base plate, size of footing, and loading system were considered as parameters. The different stress distribution of concrete column was discussed and an estimate equation of bearing stress was proposed. Besides the equation proposed by Kutani, current design recommendation in Japan [4-1] and United States [4-6] also stated the calculation methods on the bearing stress of exposed column base. To clarify the accuracy and applicability of these methods, they are summarized and analyzed by the database containing previous experiment results of exposed column bases. Furthermore, considering the design philosophy in Japan, a relatively more conservative calculation method of the bearing stress was proposed and verified by the experiment results in the database.

4.2 Summarization of the bearing stress equations

In the AIJ recommendations [4-1], the bearing stress f_b of foundation concrete in exposed column base is formulated as shown in Eq. (4)

$$f_b = 0.85 f_c \tag{4}$$

Where, f_b is the bearing stress, f_c is the compression stress of concrete from the material test result.

Table 4-1 Calculation methods of bearing stress in exposed column base

Bearing stress f_b	Loading area A_1	Bearing area A_2
Kutani & Masuda (K & M method)	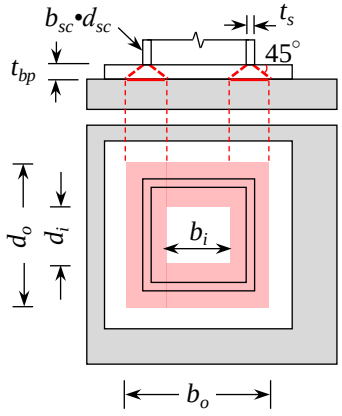	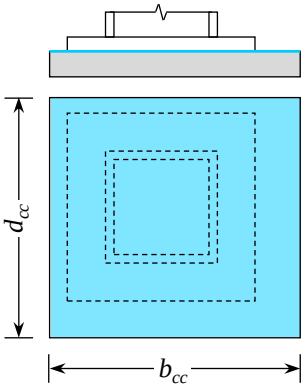
$f_b = 1.39 \times (\frac{A_2}{A_1})^{0.478} \times f_c$	$A_1 = d_o \times b_o - d_i \times b_i$ $= (d_{sc} + 2t_{bp})(b_{sc} + 2t_{bp}) -$ $(d_{sc} - 2t_s - 2t_{bp})(b_{sc} - 2t_s - 2t_{bp})$	$A_2 = d_{cc} \times b_{cc}$
ACI method	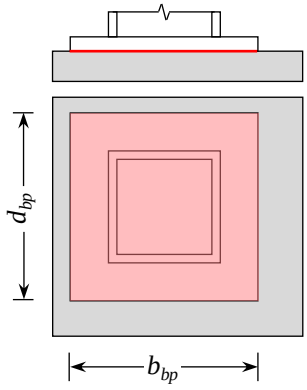	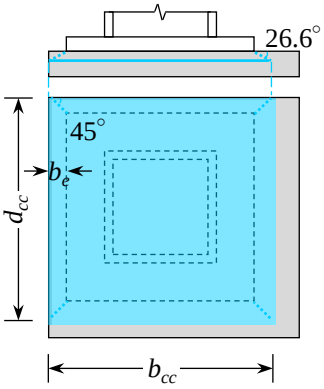
$f_b = 0.85 \times \min\{\sqrt{A_2/A_1}, 2\} \times f_c$	$A_1 = d_{bp} \times b_{bp}$	$A_2 = d_{cc} \times b_{cc}$ $= (d_{bp} + 2b_e) \times (b_{bp} + 2b_e)$

The coefficient 0.85 in Eq. (4) is taken as the lower limit from the previous experiment results [4-4]. Area effect (effect owing to the relation between the section area of base plate and concrete column) on the bearing stress was not considered. However, in the previous research, Kutani & Masuda [4-4] conducted the experiment and found the relation between the bearing stress and area effect. A calculation method (K & M method) was proposed. As shown in Table 4-1, loading area A_1 (effective area in base plate) was considered that to spread from the inner and outer edge of the steel column at a 45 degrees angle, and project an area in the bottom side of base plate (red area in Table 4-1). As for the bearing area A_2, it was considered the same as the section area of concrete column. The equations to calculate A_1 and A_2 were listed below the corresponding figure.

On the other hand, ACI Recommendation [4-6] also stated a method as shown in Table 4-1. Loading area A_1 was defined as the same area of base plate. Bearing area A_2 was considered to spread from the edge of base plate at a 26.6 degrees angle until it reached the edge of concrete column as shown in the blue area. The distance between the edge of base plate and concrete column b_e is used in the calculation of bearing area A_2. The equations to calculate A_1 and A_2 were listed below the corresponding figure. The equations to calculate bearing stress for both K & M method and ACI method were also shown in Table 4-1.

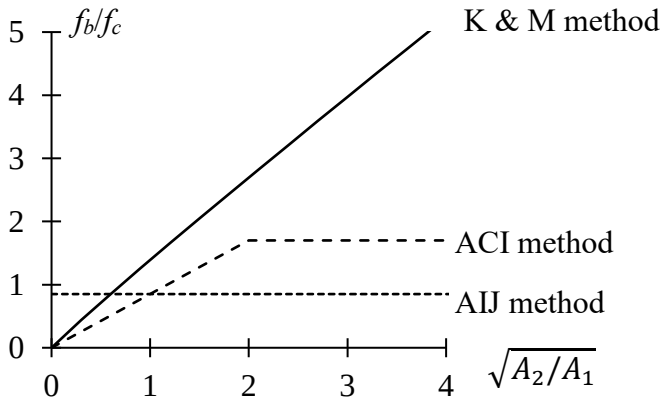

Figure 4-2 Relation of the loading and bearing area of all the evaluation methods

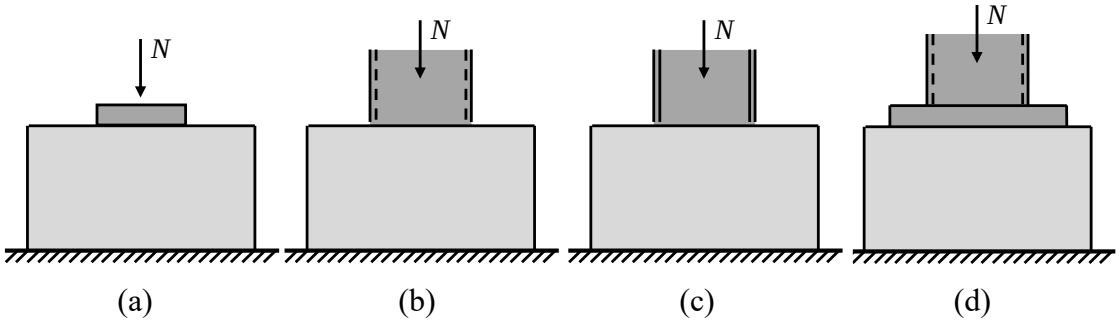

Figure 4-3 Simplified setup of previous experiments about bearing stress

Containing AIJ recommendation, all the methods are summarized in Figure 4-2. The horizontal axis is the relation of loading area A_1 and bearing area A_2, the vertical axis is the relation between bearing stress f_b and compression stress f_c. As three methods could evaluate the bearing stress f_b, their accuracy was confirmed by a great number of previous experiment studies.

From axial compression experiments and the loading specimens without base plate, loading was applied by square plate [4-2], square hollow section, h-shape steel [4-3], their brief experiment image summarized in Figure 4-3. Totally, 64 specimens were summarized. The detailed information of specimens and results in [4-2] and [4-3] were listed in the appendix, Table 4-3 and Table 4-4, respectively. Experiment parameters contained the size, position, and section area of square plate, section area of the steel column, and compression stress of the foundation concrete. As there was no base plate, for the definition of A_1 in K&M method, the t_{bp} was 0, A_1 was the section area of the

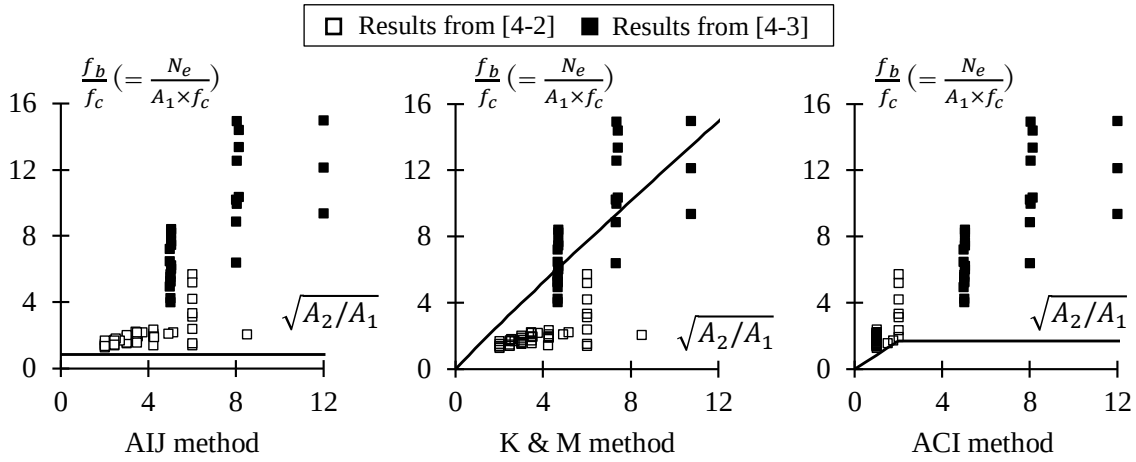

Figure 4-4 Evaluation results for previous bearing experiments

loading specimens which was the same as the definition in ACI equation. The difference between them was the bearing area A_2. The experiment results (axial force N_e, loading area A_1, bearing area A_2) were summarized and calculated by the three methods as shown in Figure 4-4. As can be found from Figure 4-4 (a) and (c), AIJ and ACI equations showed significantly conservative results for all the results. For K&M method, the evaluation results for specimens in [4-3] illustrated higher relevance comparing the results for specimens in [4-2]. However, in general, all the methods evaluated the results discretely.

As for the experiments conducted by Kutani & Masuda [4-4] shown in Figure 4-3 (d), the loading specimens were similar to the steel column of exposed column bases, and axial compression was applied on the specimens. Totally, 60 specimens were summarized. The detailed information of specimens and results in [4-4] were listed in the appendix, Table 4-5. Experiment parameters contained the size and shape of steel column, thickness of base plate, size of concrete column. As the summarization of experiment results shown in Figure 4-5, AIJ equation could conservatively evaluate the results with the least number of specimens overestimated. Comparingly, ACI equation evaluates the results closer to the average level. Compared with ACI and AIJ equations, K&M equation shows the best relevance with the results.

However, in practical cases, except the axial force, the exposed column base has to transfer shear force and bending moment from superstructures. Experiments for exposed column bases applied by eccentric compression or shear force were conducted in [4-4]. The image of experiment setup was summarized in Figure 4-6. Totally, 34 specimens were

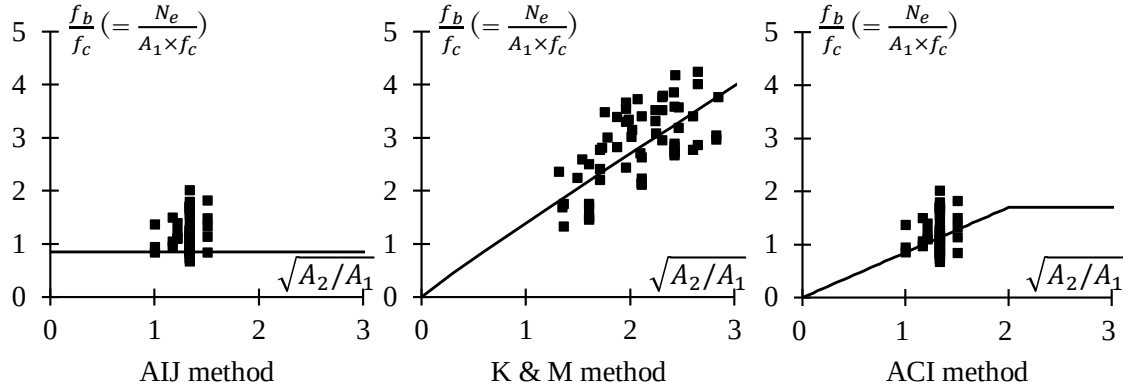

Figure 4-5 Evaluation results for bearing experiments with base plate [4-4]

loaded with parameters containing the size and thickness of baseplate, loading pattern, and eccentricity. The detailed information of specimens and results in [4-4] were listed in the appendix, Table 4-6. As a concrete column subjected to axial force and bending moment, the relation between the bending moment M and axial force N could be expressed by Eq. (5).

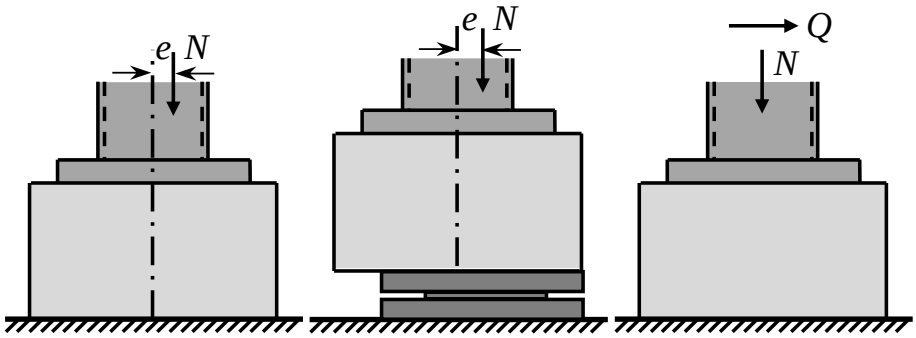

Figure 4-6 Simplified setup of bearing stress experiments of exposed column base

$$M = \frac{1}{2} \times N \times D \times \left(1 - \frac{N}{N_u}\right) \tag{5}$$

Where, D is the depth of base plate.

Owing to the dimension of specimens and compression stress of foundation concrete being different, these influences should be eliminated. The experiment results could be normalized by Eq. (6-7) for further discussion.

$$n = \frac{N}{N_u} \tag{6}$$

$$m = \frac{M}{D \times N_u} \tag{7}$$

Such that the Eq. (5) could be simplified to Eq. (8)

$$m = \frac{1}{2} \times n \times (1 - n) \tag{8}$$

m-n interaction curve following Eq. (8) is shown in Figure 4-7 with the plots representing the calculation results of three methods. The plots located outside of the

interaction curve represent that the experiment value is larger than the calculation value. In other words, the result is conservatively evaluated. As can be observed from the figure, AIJ method evaluates all the results in the conservative way, especially in the range of $n >$ 0.5. For K&M and ACI methods, the results fit well with the method when $n < 0.4$. When $n > 0.4$, ACI method tends to evaluate the results more conservatively compared with K & M method.

However, the above studies only considered the case of steel column with base plate, effect of anchor rods was not considered. Thus, the applicability of these equations on the evaluation of maximum strength of exposed column bases is still unclear. By analyzing the results of previous exposed column base experiments, the accuracy of these methods could be clarified.

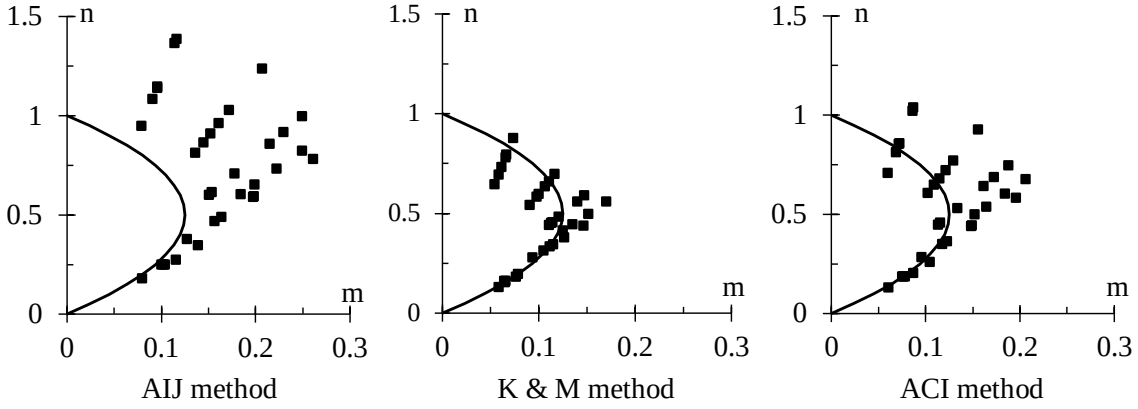

Figure 4-7 Evaluation results for bearing experiments for exposed column base

4.3 Experiment results related to bearing stress

To normalize and analyze the experiment results in previous studies, the method to get full plastic moment ${}_{cb}M_p$ of exposed column bases was proposed and confirmed available by our experiment results.

To define the full plastic moment ${}_{cb}M_p$ of exposed column bases, the strain behavior of anchor rods was focused. The relation between strain of anchor rods and column base rotation θ_{cb} is illustrated in Figure 4-8. The experiment result of specimen C16-590-20d is taken as an example. As the arrangement of anchor rods, the behavior of which in the inner side and outer side of column was different, thus strain gauges were glued on both anchor rods as the position shown in Figure 4-8. The timing when the strain of anchor rods reached the yield strain is marked by square with attached subscript y. The timing when strain gauge increased rapidly (represented that the anchor rod is completely yielded in that area) is marked by a triangle with attached subscript p, these points were defined as the full plastic strain points. When both the top and bottom of the strain in an anchor rod reached full plastic strain point, the anchor rod is considered as yielded and the bending moment of column base is considered as ${}_{cb}M_p$. To investigate ${}_{cb}M_p$, these yield points are replotted in the relation between the moment of column base M and column

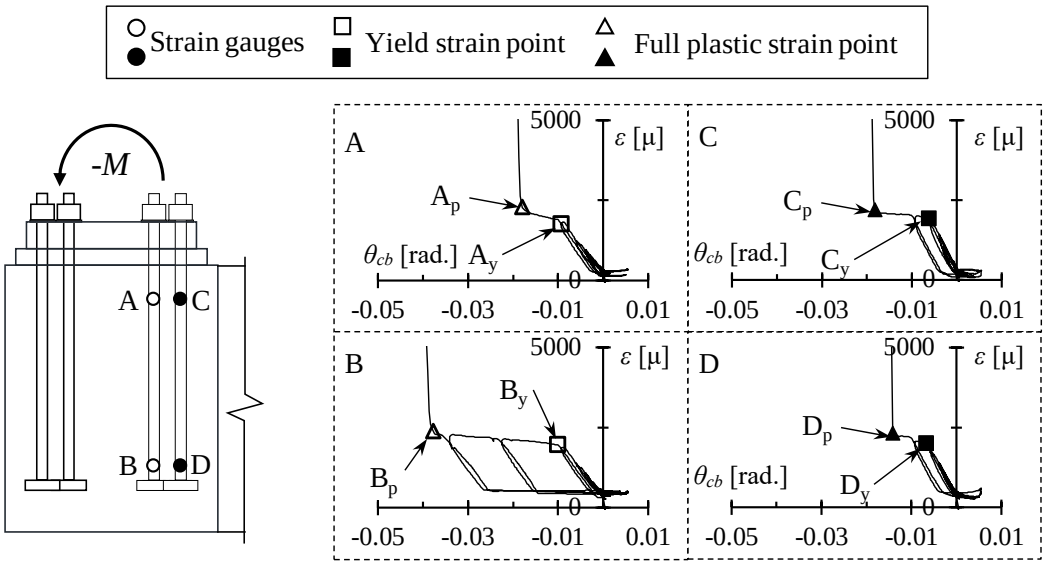

Figure 4-8 Relation between anchor rod strain and column base rotation of specimen C16-590-20d

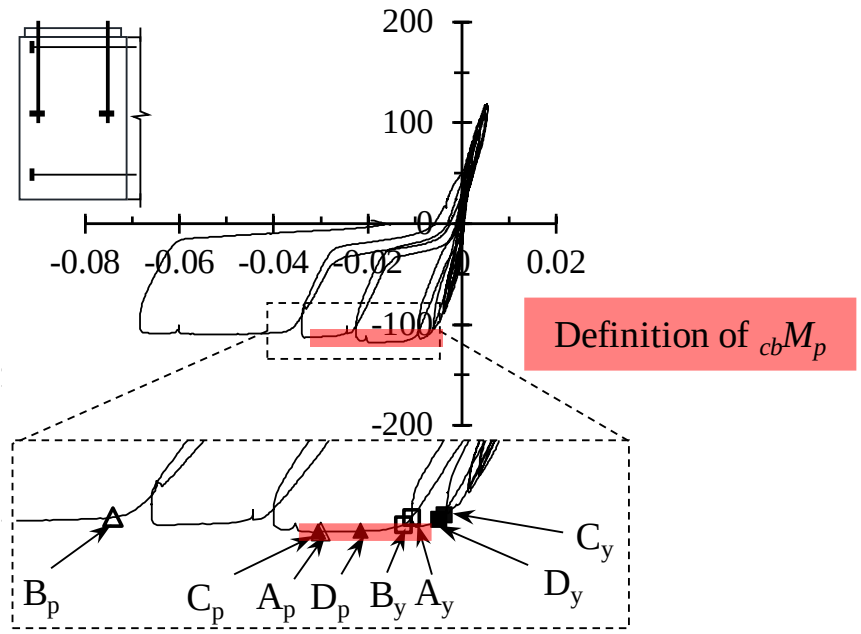

Figure 4-9 Definition of the full plastic strength cbMp

base rotation θ_{cb} as shown in Figure 4-9. Most of the yield points were distributed in the range when the moment kept stable for the first cycle, such that the maximum moment at that cycle is defined as $_{cb}M_p$ as illustrated in Figure 4-9.

To confirm the suitability of this definition, $_{cb}M_p$ got from the experiment results was compared with the *M*-*N* interaction curve calculated by Eq. (1-3). As shown in Figure 4-10, as the anchor rods had different yield stress, there are two *M*-*N* interaction curves. Blackline is for specimens 20d, 30d, and 39d, the blue line is for specimen 39db. The

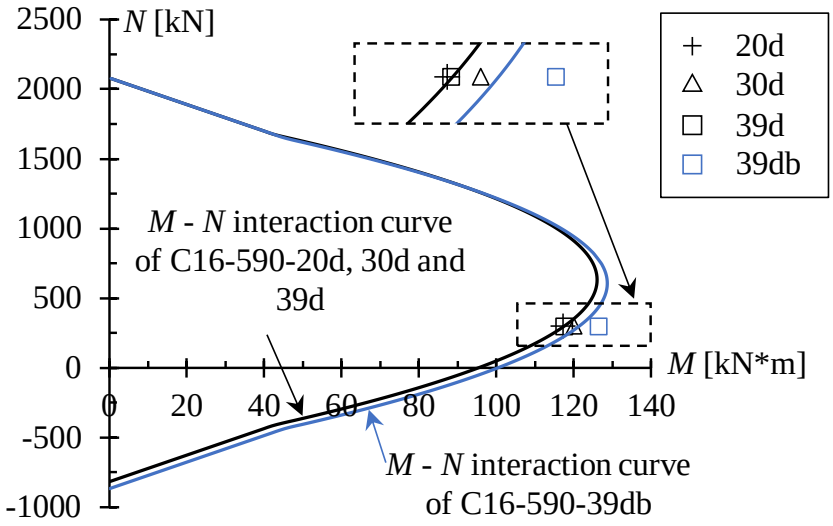

Figure 4-10 Comparison of the experiment results and calculation results

result of ${}_{cb}M_p$ got from the definition is plotted in Figure 4-10. It could be found that the embedded length and anchor rod type had no significant influence on the ultimate strength. The calculation results fit well with the *M*-*N* interaction curve, thus, it was proved reasonable to get the ultimate strength ${}_{cb}M_p$ from the M - θ_{cb} curve in experiment results. To this extent, a database containing previous exposed column base experiments was established and the experiment results were analyzed to discuss the accuracy of evaluation methods of bearing stress.

4.4 Database and confirmation of proposed mechanism

To normalize all the experiment results in the database, all of the specimens in database met the conditions that anchor rods were confirmed as yielded, and the M - θ_{cb} curves were also confirmed that fit the definition of ${}_{cb}M_p$ proposed in the last section.

4.4.1 Specimen properties

Totally, 129 specimens in 20 research papers [4-7]-[4-26] were collected in the database. Detailed properties of the specimens (contained section of steel column, base plate, concrete column, number and arrangement of anchor rods) and experiment results (axial force N and full plastic moment ${}_{cb}M_p$) were listed in Table 4-2. Specimen properties were summarized and had the following ranges: Shape of steel column section: H, steel tube and SHS; Size of steel column: from 125 mm to 450 mm; Size of base plates: from 210 mm to 800 mm; Size of concrete column: from 340 mm to 1300 mm; Compression strength of the concrete f_c: from 16.9 N/mm^2 to 50.0 N/mm^2; Number of anchor rods in tension n_t: from 1 to 4; Nominal diameter of anchor rods D_{ar}: from 16 mm to 56 mm

4.4.2 Normalizing method

To normalize the various experiment results in the database, the effect of tension of anchor rods and dimension of specimens should be eliminated. Based on the accumulating strength curve in Figure 4-1, as shown in Figure 4-11, by moving the axes of axial force N and bending moment M to N' and M', the effect of anchor rods was eliminated. N' and M' could be expressed as Eq. (11-12).

$$M' = M - T_p \times d_t \tag{11}$$

$$N' = N + T_p \tag{12}$$

Therefore, Eq. (2) could also be simplified as Eq. (13).

$$M' = \frac{1}{2} \times N' \times D \times \left(1 - \frac{N'}{N_u}\right) \tag{13}$$

Then, the effect of dimension and concrete compression stress could be eliminated following Eq. (14-15).

$$n = \frac{N'}{N_u} \tag{14}$$

$$m = \frac{M'}{N_u \times D} \tag{15}$$

Therefore, Eq. (13). could be further simplified as Eq. (16).

$$m = \frac{1}{2} \times n \times (1 - n) \tag{16}$$

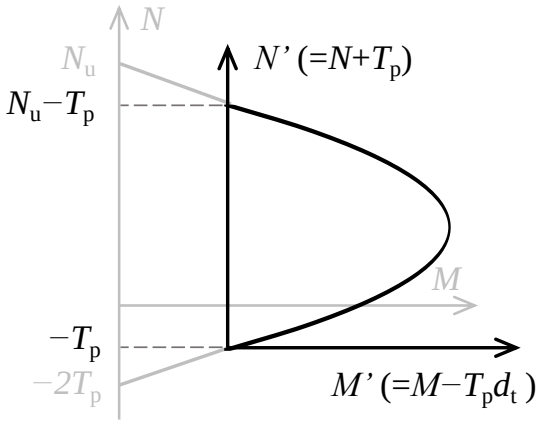

Figure 4-11 Method to eliminate the effect of anchor rods

The interaction curve of *m-n* following Eq. (16) will be the boundary curve for the evaluation. The axial force *N* and full plastic moment ${}_{cb}M_p$ in experiment results could also be normalized to n_{exp} and m_{exp} following Eq. (11-15). And for each n_{exp}, by Eq. (16), the value of *m* in the interaction curve could also be calculated and represented as m_{cal}. The ratio of m_{exp} and m_{cal} was considered as a criterion for evaluation and discussed in the following section.

Table 4-2 Parameter matrix and experiment results of specimens in the database

Paper ID	Specimen ID	Section of steel column[1] (all in mm)	Base plate	Concrete column		Anchor rods		Experiment results	
			b_{bp}*d_{bp}*t_{bp}	b_{rc}*d_{rc}	f_c	n_t-D_{ar}-d_t	f_y	N	$_{cb}M_p$
			All in mm	All in mm	[N/mm2]	All in mm	[N/mm2]	[kN]	[kN*m]
[4-7]	SH1	S-150*4.5	300*300*16	400*400	24.1	2-20-115	209.7	0.0	30.2
	SH25	S-150*25	300*300*75	400*400	24.1	2-22-115	309.7	0.0	58.8
	SF4	S-150*4.5	300*300*16	400*400	24.1	2-20-80	209.7	0.0	45.6
	SK1	C-165.2*4.5	300*300*16	400*400	24.1	3-20-115	209.7	0.0	41.9
	SC4	S-150*16	300*300*10	400*400	24.1	2-20-115	441.0	725.2	162.6
	SC9	S-150*25	300*300*75	400*400	23.8	2-22-115	307.7	613.5	126.4
	SC10	S-150*25	300*300*75	400*400	23.8	2-22-115	307.7	317.5	97.2
	SH14	S-150*25	300*300*75	400*400	24.1	2-22-115	309.7	0.0	57.1
	SV1	S-150*25	300*300*75	400*400	24.1	2-22-115	309.7	588.0	129.8
	SV2	S-150*25	300*300*75	400*400	23.7	2-22-115	309.7	980.0	164.7
	SV3	S-150*25	300*300*75	400*400	23.7	2-22-115	309.7	588.0	136.9
	SV4	S-150*25	300*300*75	400*400	23.7	2-22-115	309.7	196.0	90.7
	SV5	S-150*25	300*300*75	400*400	23.7	2-22-115	309.7	196.0	89.6
	SV6	S-150*25	300*300*75	400*400	23.7	2-22-115	309.7	-196.0	40.8
	SV7	S-150*25	300*300*75	400*400	23.7	2-22-115	309.7	980.0	153.3
	SV8	S-150*25	300*300*75	400*400	23.7	2-22-115	309.7	588.0	122.3
	SV9	S-150*25	300*300*75	400*400	23.7	2-22-115	309.7	196.0	82.6

	SV10	S-150*25	300*300*75	400*400	23.7	2-22-115	309.7	-196.0	33.7
	SV11	S-150*25	300*300*75	400*400	23.7	2-22-115	309.7	-196.0	33.8
	SV13	S-150*25	300*300*36	400*400	19.8	2-22-115	309.7	833.0	135.1
	SV14	S-150*25	300*300*25	400*400	19.8	2-22-115	309.7	656.6	107.6
	SV15	S-150*25	300*300*25	400*400	19.8	2-22-115	309.7	656.6	107.6
	SV16	S-150*25	300*300*50	400*400	19.8	2-22-115	309.7	833.0	130.6
	SV17	S-150*25	300*300*36	400*400	19.8	2-22-115	309.7	617.4	108.4
	SV18	S-150*25	300*300*25	400*400	19.8	2-22-115	309.7	441.0	93.0
	SV19	S-150*25	300*300*25	400*400	19.8	2-22-115	309.7	441.0	93.5
	SV21	S-150*25	300*300*50	400*400	26.1	2-22-115	309.7	588.0	124.1
	SV22	S-150*25	300*300*50	400*400	26.1	2-22-115	309.7	196.0	78.6
	SV23	S-150*25	300*300*50	400*400	26.1	2-22-115	309.7	-98.0	45.2
[4-8]	SH4	S-150*25	300*300*75	400*400	23.8	2-22-115	307.7	0.0	55.9
	SH5	S-150*25	300*300*75	400*400	23.8	2-22-115	307.7	0.0	54.9
	SH6	S-150*25	300*300*75	400*400	23.8	2-22-115	307.7	0.0	49.2
	SH7	S-150*25	300*300*25	400*400	23.8	2-22-115	307.7	0.0	54.9
	SH8	S-150*25	300*300*25	400*400	23.8	2-22-115	307.7	0.0	53.9
	SH9	S-150*25	300*300*75	400*400	20.8	2-22-115	304.8	0.0	53.9
	SH28	S-150*25	300*300*75	400*400	25.2	2-22-115	309.7	0.0	57.8
	SL4	S-150*25	300*300*50	400*400	26.8	2-22-115	305.8	0.0	47.8
	SL5	S-150*25	300*300*50	400*400	26.8	2-22-115	305.8	-98.0	35.8
	SL6	S-150*25	300*300*50	400*400	26.8	2-22-115	305.8	980.0	156.7

	SL7	S-150*25	300*300*50	400*400	26.8	2-22-115	305.8	980.0	156.1
	SL8	S-150*25	300*300*50	400*400	26.8	2-22-115	305.8	588.0	125.3
	SL9	S-150*25	300*300*50	400*400	26.8	2-22-115	305.8	196.0	82.5
	SL10	S-150*25	300*300*50	400*400	26.8	2-22-115	305.8	0.0	55.7
	SL11	S-150*25	300*300*50	400*400	26.8	2-22-115	305.8	-98.0	44.0
	SR3	S-150*25	300*300*50	400*400	28.5	2-22-115	309.7	0.0	51.1
	SR14	S-150*25	300*300*50	400*400	29.2	2-22-115	305.8	-98.0	40.7
	SR15	S-150*25	300*300*50	400*400	29.2	2-22-115	305.8	196.0	74.0
[4-9]	MA490	S-300*12	450*450*40	550*550	23.2	4-24-165	332.0	623.9	323.9
	MA370	S-300*12	450*450*40	550*550	23.6	4-24-165	332.0	622.4	322.4
	NA490	S-300*12	450*450*40	550*550	23.7	4-24-165	332.0	617.5	317.5
	MA490s	S-300*12	450*450*40	550*550	26.0	4-24-165	332.0	601.3	301.3
	MA490	S-300*12	450*450*40	550*550	23.2	4-24-165	332.0	80.8	219.2
	MA370	S-300*12	450*450*40	550*550	23.6	4-24-165	332.0	89.1	210.9
	NA490	S-300*12	450*450*40	550*550	23.7	4-24-165	332.0	94.0	206.0
[4-10]	A-1	H-200*200*8*12	380*300*25	500*500	18.7	2-19-150	240.1	0.0	63.7
	A-2	H-200*200*8*13	380*300*25	500*500	18.7	2-19-150	240.1	0.0	58.8
	C-2-1	H-200*200*8*14	380*300*19	350*350	16.9	2-19-150	243.3	0.0	49.0
	D-1-1	H-200*200*8*15	380*300*19	350*350	16.9	2-19-150	243.3	0.0	52.9
	D-1-2	H-200*200*8*16	380*300*19	350*350	16.9	2-19-150	243.3	0.0	44.1
[4-11]	35-8M33P50	S-350*25	630*630*50	850*850	33.9	3-33-256.3	622.0	0.0	812.0
	35-8M39-50	S-350*25	630*630*50	850*850	33.9	3-39-256.3	613.0	0.0	983.0

[4-12]	A38-C400	S-400*22	640*640*70	810*810	18.8	2-38-255	516.0	0.0	628.9
	A28-C300	S-300*16	470*470*55	680*680	19.5	2-28-185	618.0	0.0	242.5
	A25-C200	S-200*12	360*360*36	520*520	19.5	2-25-135	516.0	0.0	91.3
	A25-C200P	S-200*12	360*360*36	520*520	20.2	2-25-135	516.0	0.0	87.2
[4-13]	N-1	S-200*12	400*400*39	600*600	31.7	2-22-155	371.9	175.0	101.9
	N-2	S-200*12	400*400*39	600*600	31.7	2-22-155	371.9	275.0	113.8
	N-3-1	S-200*12	400*400*39	600*600	31.7	2-22-155	371.9	360.0	133.4
	N-3-2	S-200*12	400*400*39	600*600	31.7	2-22-155	371.9	360.0	122.4
	N-4	S-200*12	400*400*39	600*600	31.7	2-22-155	371.9	475.0	125.8
	C12-B40-N1	S-200*12	400*400*40	600*600	48.5	2-22-155	372.2	158.0	85.7
	C12-B40-N2	S-200*12	400*400*40	600*600	42.4	2-22-155	372.2	216.0	92.4
	C12-B40-N3	S-200*12	400*400*40	600*600	44.4	2-22-155	372.2	274.0	96.1
	C9-B40-N3	S-200*9	400*400*40	600*600	50.0	2-22-155	372.2	274.0	95.3
	C12-B36-N3	S-200*12	400*400*36	600*600	45.3	2-22-155	372.2	280.0	80.5
	C12-B45-N3	S-200*12	400*400*45	600*600	44.6	2-22-155	372.2	304.0	85.5
	N-1	S-200*12	400*400*39	600*600	31.7	2-22-155	371.9	-120.0	54.2
	N-2	S-200*12	400*400*39	600*600	31.7	2-22-155	371.9	-20.0	79.6
	N-3-1	S-200*12	400*400*39	600*600	31.7	2-22-155	371.9	80.0	99.6
	N-3-2	S-200*12	400*400*39	600*600	31.7	2-22-155	371.9	80.0	77.9
	N-4	S-200*12	400*400*39	600*600	31.7	2-22-155	371.9	130.0	106.6
	C12-B40-N1	S-200*12	400*400*40	600*600	48.5	2-22-155	372.2	20.0	78.0
	C12-B40-N2	S-200*12	400*400*40	600*600	42.4	2-22-155	372.2	-20.0	71.6

	C12-B40-N3	S-200*12	400*400*40	600*600	44.4	2-22-155	372.2	-44.0	62.1
	C9-B40-N3	S-200*9	400*400*40	600*600	50.0	2-22-155	372.2	-80.0	68.1
	C12-B36-N3	S-200*12	400*400*36	600*600	45.3	2-22-155	372.2	-68.0	61.8
	C12-B45-N3	S-200*12	400*400*45	600*600	44.6	2-22-155	372.2	-50.0	73.3
[4-14]	ECB0-22-1	S-125*12	260*260*22	340*340	24.6	2-16-103	319.3	0.0	26.0
	ECB0-22-2	S-125*12	260*260*22	340*340	24.6	3-16-103	319.3	0.0	39.0
	ECB0-22-3	S-125*12	260*260*22	340*340	24.6	3-16-103	319.3	0.0	46.0
[4-15]	30N12P	S-300*16	520*520*45	650*650	25.3	3-38-210	545.0	-621.5	612.3
	30N24P	S-300*16	520*520*45	650*650	25.3	3-38-210	545.0	-1243.0	586.3
[4-16]	267--26	C-267.4*9	400*400*32	540*540	29.0	2-36-135	386.0	-254.8	215.0
	355-93	C-355.6*12	580*580*40	720*720	29.0	4-36-165	386.0	921.2	454.0
	355--46	C-355.6*12	580*580*40	720*720	29.0	4-36-165	386.0	-460.6	480.0
[4-17]	250-2	S-250*12	400*400*28	450*450	28.1	2-22-155	711.0	0.0	273.0
	250-3	S-250*12	400*400*28	450*450	28.1	2-22-155	711.0	764.3	325.0
	250-4	S-250*12	400*400*28	500*500	28.1	2-22-155	711.0	764.3	364.0
[4-18]	BD-1	S-300*12	500*500*50	700*700	27.1	2-35-200	517.0	0.0	412.5
	BD-4	S-300*16	500*500*50	700*700	27.1	2-35-200	517.0	765.0	540.0
	BD-5	S-300*16	500*500*50	700*700	27.1	2-35-200	517.0	765.0	510.0
	BD-7	S-300*16	500*500*50	700*700	28.2	2-35-200	525.0	765.0	562.5
	LD-1	S-300*16	500*500*50	700*700	27.9	2-35-200	525.0	765.0	487.5
	LD-2	S-300*12	500*500*50	700*700	27.9	2-35-200	525.0	0.0	420.0
	LD-3	S-300*16	500*500*50	700*700	27.9	2-35-200	525.0	765.0	487.5

	LD-4	S-300*19	500*500*50	700*700	27.9	2-35-200	525.0	2295.0	610.0
	LD-5	S-300*12	500*500*50	700*700	30.6	2-35-200	525.0	-765.0	250.0
[4-19]	P-1	S-150*6	285*285*19	400*400	30.4	1-16-112.5	294.0	0.0	18.1
	P-2	S-150*6	210*210*19	400*400	30.4	1-16-75	294.0	0.0	16.8
	P-3	S-150*6	210*210*19	400*400	30.4	2-16-55	294.0	0.0	17.6
[4-20]	PL-1	S-150*6	285*285*16	400*400	33.6	1-16-112.5	340.1	0.0	16.7
[4-21]	S-1-N0	S-250*9	400*400*22	500*500	27.9	2-20-150	336.1	0.0	61.7
[4-22]	1	S-450*28	800*800*82	1000*1000	22.0	3-56-320	537.0	0.0	2600.0
	2	S-450*28	800*800*75	1000*1000	22.0	3-56-320	537.0	0.0	2550.0
	3	S-450*28	800*800*68	1000*1000	22.0	3-56-320	537.0	0.0	2400.0
[4-23]	NT-8M33	S-350*25	630*630*50	850*850	33.9	3-33-240	617.3	0.0	827.0
	NT-8M39	S-350*25	630*630*50	850*850	33.9	3-39-240	617.3	0.0	1123.6
	NT-8M45	S-350*25	630*630*50	850*850	33.9	3-45-240	617.3	0.0	1365.2
[4-24]	B2522As	S-250*12	400*400*22	1300*1300	46.0	2-16-175	342.0	0.0	51.9
	B2528As	S-250*12	400*400*28	1300*1300	39.1	2-16-175	342.0	0.0	51.9
	B2522A	S-250*12	400*400*22	1300*1300	41.8	2-20-200	323.4	0.0	67.6
	B2528A	S-250*12	400*400*28	1300*1300	46.6	2-20-200	323.4	0.0	69.6
[4-25]	S1S2	H-206*216*10.2*17.4	460*460*32	1267*1140	49.0	2-19-165	340.6	0.0	93.6
	S1S4	H-206*216*10.2*17.4	460*460*32	1267*1140	49.0	2-19-165	355.1	0.0	84.5
	S2S1	H-206*216*10.2*17.4	460*460*32	1267*1140	49.0	2-19-165	514.3	0.0	112.8
	S2S2	H-206*216*10.2*17.4	460*460*32	1267*1140	49.0	2-19-165	823.9	0.0	176.3
	S2S4	H-206*216*10.2*17.4	460*460*32	1267*1140	49.0	2-19-165	355.1	0.0	83.6

[4-26]	S3S2	H-206*216*10.2*17.4	460*460*32	1267*1140	49.0	2-19-165	355.1	0.0	78.8
	S4S4	H-206*216*10.2*17.4	460*460*32	1267*1140	49.0	2-19-165	355.1	0.0	77.3

Note: b_{bp}: Width of base plate, d_{bp}: Depth of base plate, t_{bp}: Thickness of base plate, b_{rc}: Width of concrete column, d_{rc}: Depth of concrete column, f_c: Compression stress of concrete, n_t: Number of anchor rods in tension, D_{ar}: Diameter of anchor rods, d_t: Distance from the center of anchor rods in tension to the center of steel column. f_y: Yield stress of anchor rods.

[1] In the section of steel column, S is SHS column, C is circular column, H is H-shaped steel. For example, H-200*200*8*12 refers to H shaped steel-width of flange-depth of beam-thickness of web-thickness of flange.

4.5 Evaluation results and discussion

4.5.1 Evaluation results

The normalized experiment results n_{exp} and m_{exp} were plotted with the m-n interaction curve as shown in Figure 4-12(a)-(c), corresponding to the AIJ, K&M, and ACI methods, respectively. As can be observed from Figure 4-12(a)-(c), when n > 0.4, all the methods tend to underestimate the experiment results. When n < 0.2, as the plots were gathered and hard to be clarified, that region was enlarged and shown in Figure 4-12(d)-(l).

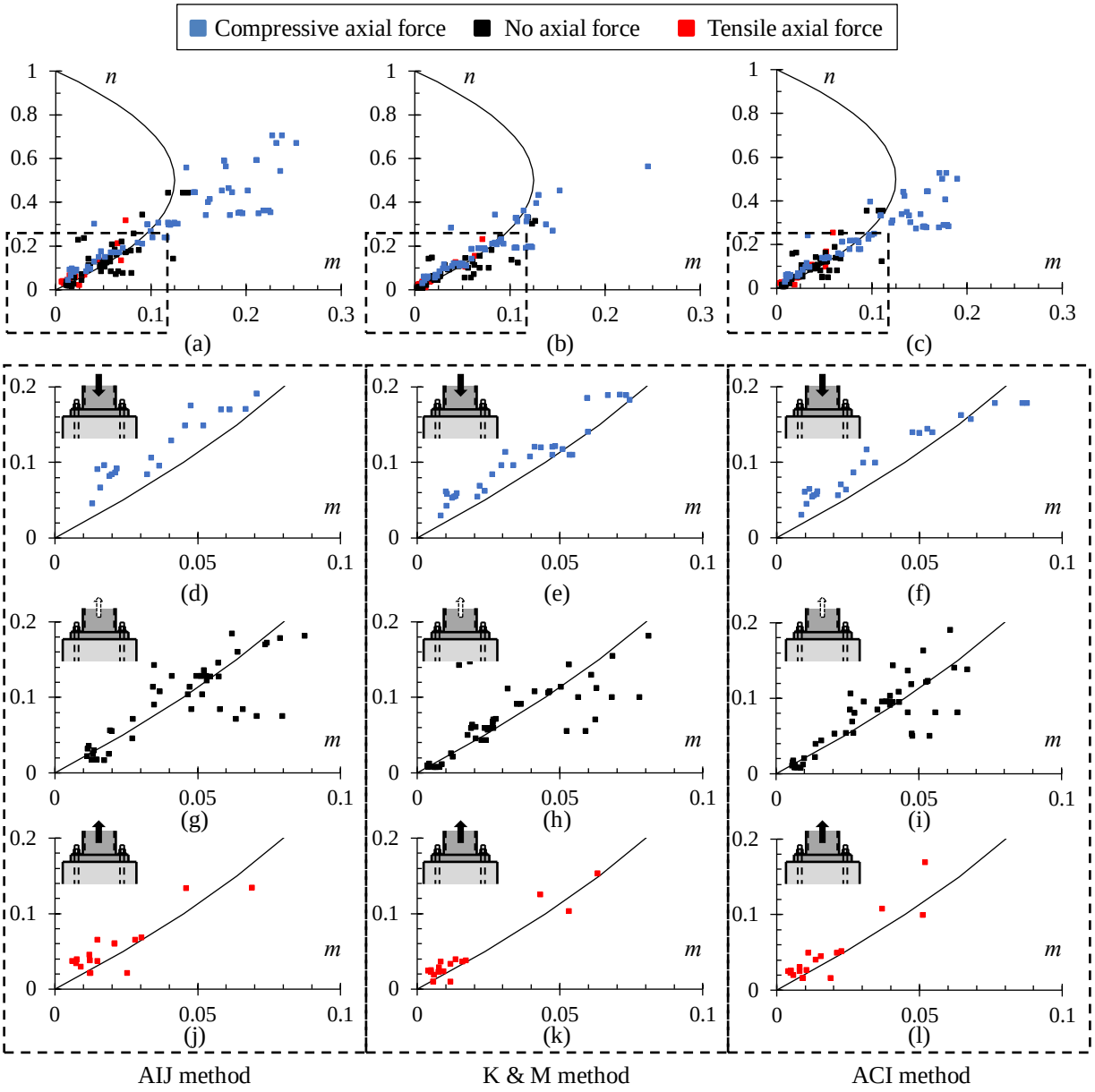

Figure 4-12 Evaluation result and comparison between three methods

Furthermore, the results were separated by the different axial force states applied on the exposed column bases. As shown in Figure 4-12(d)-(f), in the case of compressive axial force, for all the methods, most of the experiment results were overestimated. In the case of no axial force shown in Figure 4-12(g)-(i), significant differences in the results between three evaluation methods were not found. For the case of tensile axial force shown in Figure 4-12(j)-(l), most of the results were overestimated for all three methods. To discuss the effect of axial force state, concrete compression stress on the evaluation results, furthermore, to evaluate the accuracy and applicability of these evaluation methods, the ratio of m_{exp} and m_{cal} was considered as a criterion.

4.5.2 Influence of axial force and anchor rods strength

To clarify the effect of axial force N and strength of anchor rods T_p on evaluation results, the correlation of m_{exp}/m_{cal} and n was discussed. As stated in Eq. (13) and (15), the component of n contains the tensile strength of anchor rods T_p and axial force N. As the axial force state was different for specimens, the influences of N and T_p were discussed separately by different axial force state. For the specimens applied by compressive axial force, as shown in Figure 4-13, the vertical axis is m_{exp}/m_{cal}. The line of $m_{exp}/m_{cal} = 1$ was also illustrated in the figure as a boundary line. For the results below this line, they were

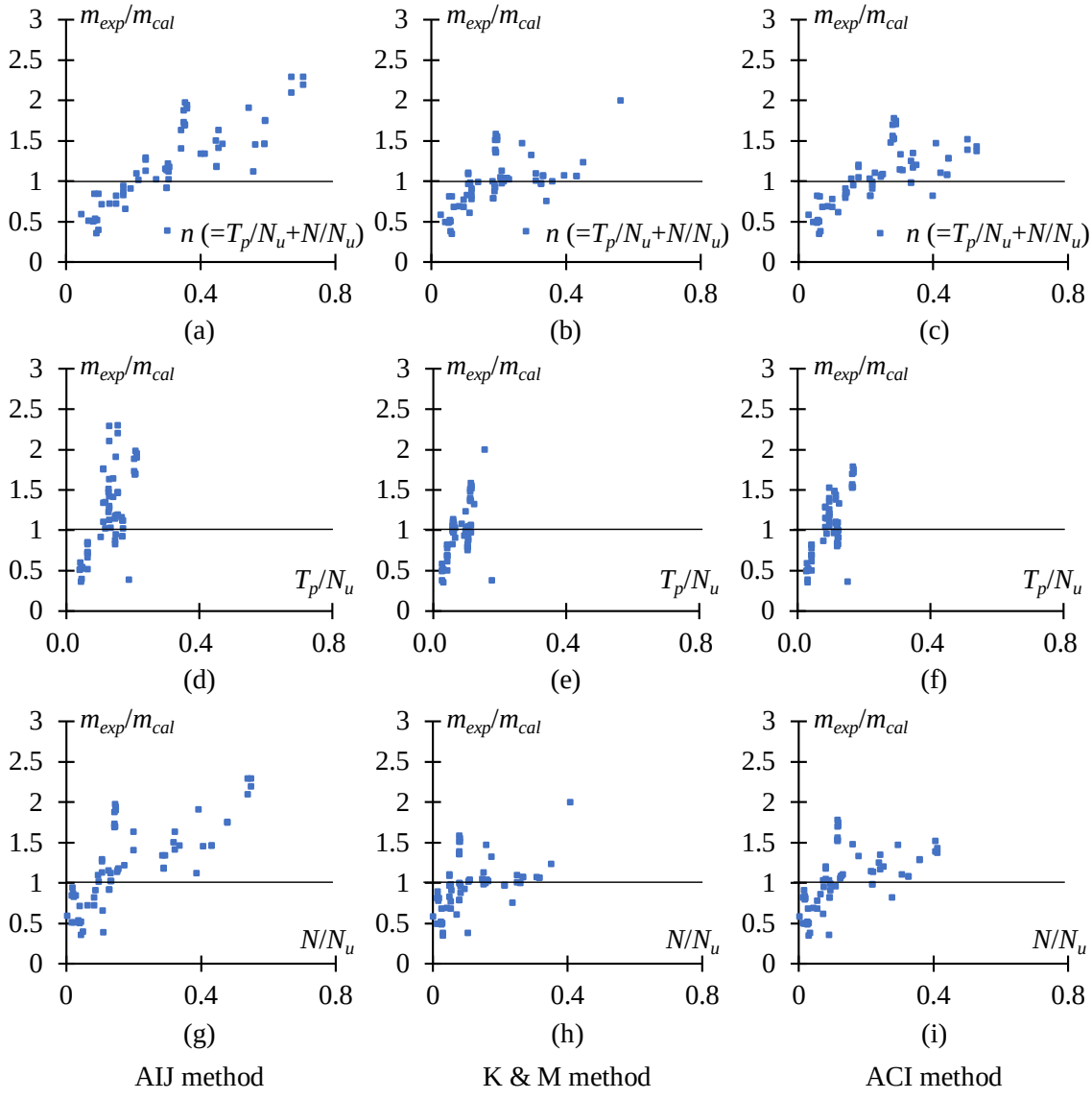

Figure 4-13 Influence of the component of n for specimens in compressive axial force

evaluated as overestimated. Figure 4-13 (a)-(c) illustrated the relation of m_{exp}/m_{cal} and n. It could be observed that m_{exp}/m_{cal} tends to increase with the increase of n. As for the components of n, strength of anchor rods T_p, T_p/N_u was set as the horizontal axis as shown in Figure 4-13 (d)-(f), for all the evaluation methods, it could be found that there is no significant relation between m_{exp}/m_{cal} and T_p/N_u. For the other component of n, axial force N, N/N_u was set as the horizontal axis as illustrated in Figure 4-13 (g)-(i), it could be found that the m_{exp}/m_{cal} increased with the increment of N/N_u, which is the same as the correlation between m_{exp}/m_{cal} and n. In consequence, the axial force N took a significant role in the evaluation result in the case of exposed column base applied by compressive axial force. With the increment of compression force N, the ultimate strength tended to be evaluated conservatively. In the case of zero axial force, the influence of T_p was discussed. The relation between m_{exp}/m_{cal} and n (= T_p/N_u as there was no axial force) is shown in Figure 4-14 for all three evaluation methods. The line of m_{exp}/m_{cal} = 1 was also illustrated in the figure as a boundary line. As can be observed from the figures, the correlation between m_{exp}/m_{cal} and T_p is not observed for all the evaluation methods.

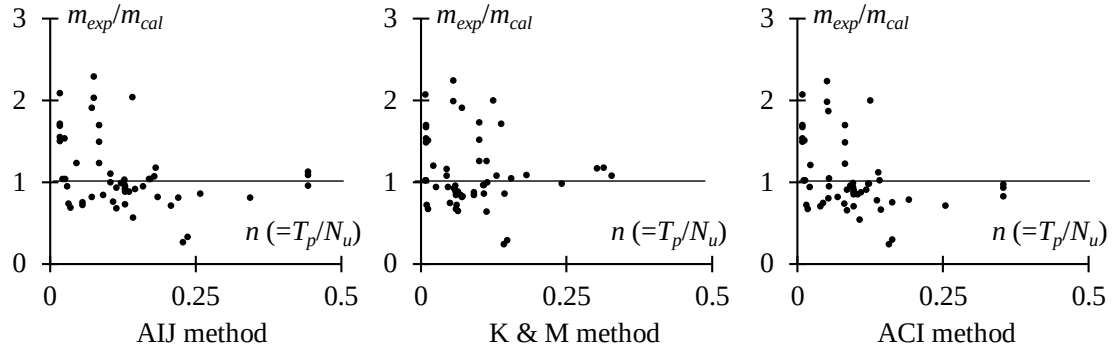

Figure 4-14 Influence of the component of n for specimens in no axial force

4.5.3 Influence of f_c on evaluation results

As shown in Figure 4-15, the relation between compression strength f_c and m_{exp}/m_{cal} is illustrated. Specimens in different axial force state is represented by different colors. The horizontal axis is f_c and the vertical axis is m_{exp}/m_{cal}. The dashed boundary line ($m_{exp}/m_{cal} = 1$) is also illustrated and the experiment results on the left side of the boundary line are defined as the overestimated specimens. As can be observed from the figure, most of the result were in the range of f_c =20 to 30 N/mm^2, and the evaluation results m_{exp}/m_{cal} showed a great difference. As a result, for all the evaluation methods, as the variance of f_c, the correlation between f_c and m_{exp}/m_{cal} was not observed.

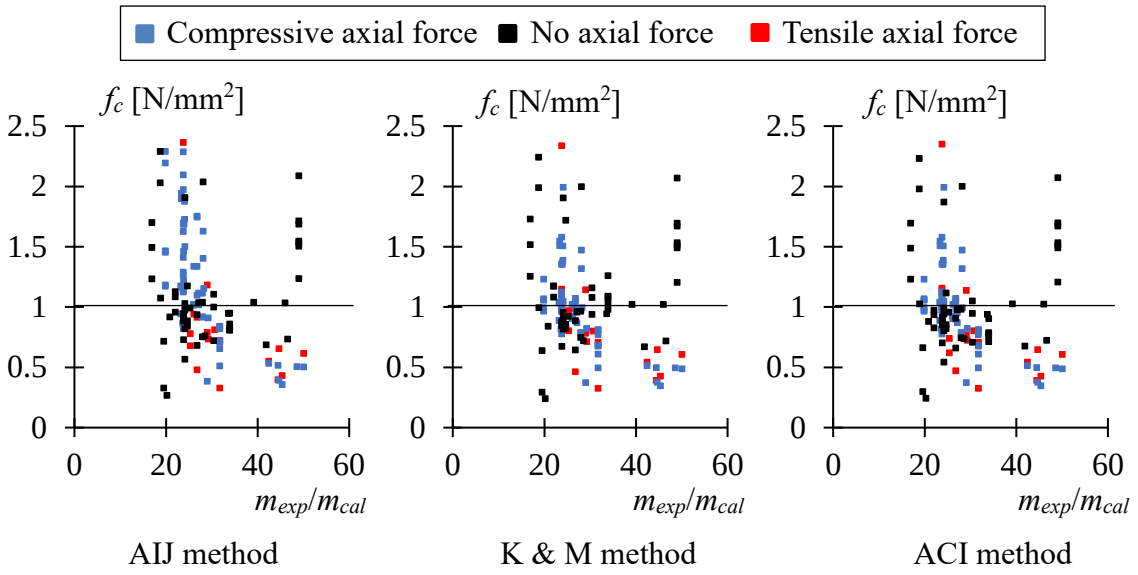

Figure 4-15 Evaluation results of m/m_{cal} - f_c

4.5.4 Accuracy and applicability of evaluation methods

To evaluate the accuracy of all the evaluation methods, the value of m_{exp}/m_{cal} is analyzed statistically. The result is illustrated in Figure 4-16. The horizontal axis is m_{exp}/m_{cal}. For the vertical axis, on the left side is the number of specimens, the right side is the probability density for the normal distribution. The dashed boundary line (m_{exp}/m_{cal} = 1) is presented and the experiment results on the left side of the boundary line are defined as the overestimated specimens. Also, the mean value and variance of the results are listed in the figure for three evaluation methods respectively. Further, the numbers of

overestimated specimens are also listed with number of all specimens in the database. Compared with the numbers of overestimated specimens, K&M and ACI methods have the same value, which is greater than the AIJ method. In consequence, the AIJ method could evaluate the result more conservatively. Compared with the K&M and ACI methods, as they have the same variance, the mean value of K&M method is closer to one. It is considered that the K&M method fit better when considering Load & Resistance Factor Design (LRFD) design philosophy.

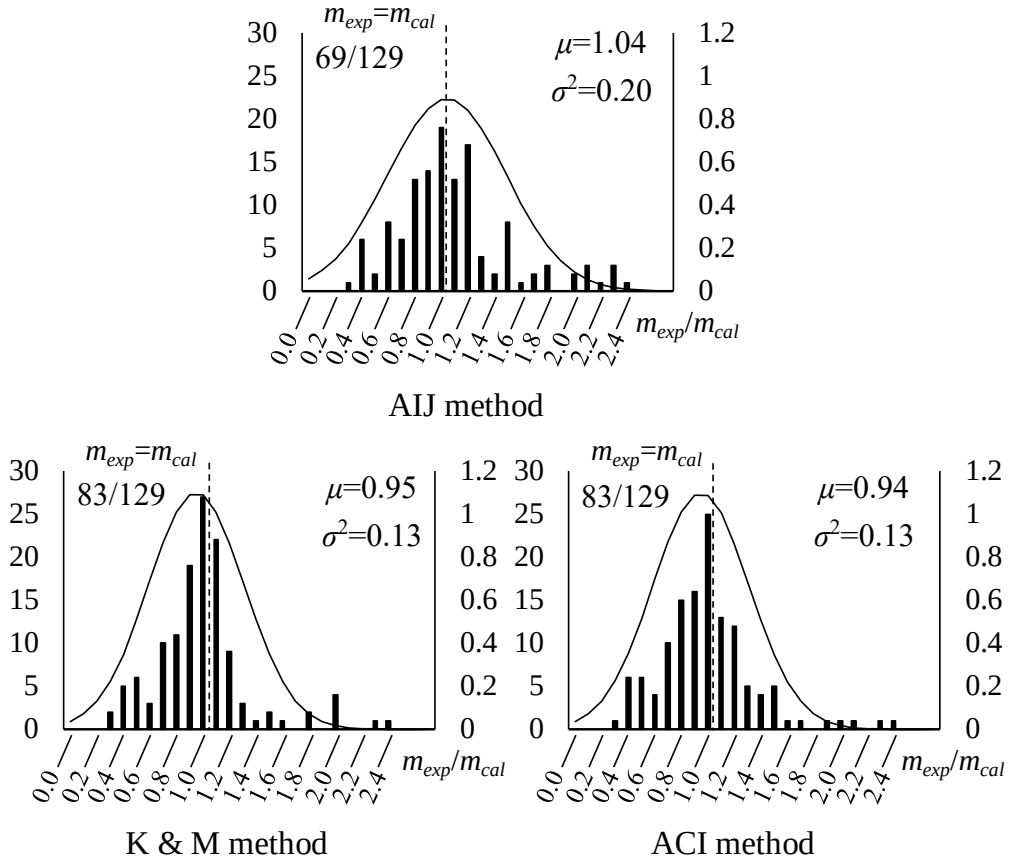

Figure 4-16 Statistical evaluation by existed calculation methods

4.5.5 Propose of the calculation method

Considering the prevalent design philosophy in Japan in terms of connection strength, the bearing strength of foundation concrete should be designed conservatively to ensure the yielding of anchor rods. As shown in Figure 4-16, for the most conservative method (AIJ method), the maximum strength was overestimated for 53.5% of the specimens. Thus, it is necessary to propose a more conservative calculation method. As illustrated in Figure 4-5, K & M method observed the correlation between f_b/f_c and A_2/A_1. Therefore, for the proposed calculation method, the definitions of loading area A_1 and bearing area A_2 are kept the same as in K & M method. Considering the simplicity of the equation, Eq. (17) is proposed. The statistical evaluation of m_{exp}/m_{cal} using Eq. (17) is shown in Figure 4-17. Compared with AIJ method, the proposed method reduces the number of overestimated specimens to approximately 19.3%, with a higher mean value in the evaluation result. With this proposal, exposed column bases could be designed more conservatively to prevent the bearing failure of foundation concrete.

$$f_b = \sqrt{A_2/A_1} \times f_c \tag{17}$$

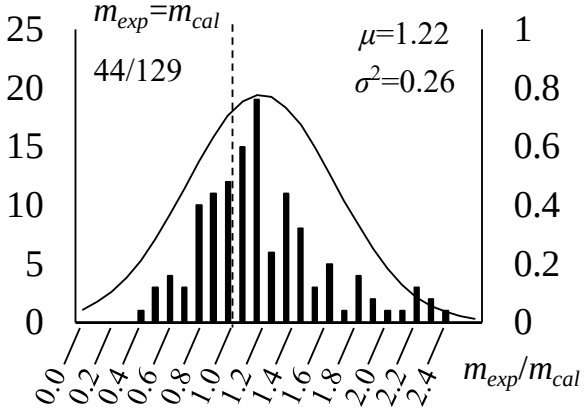

Figure 4-17 Statistical evaluation by proposed calculation methods

4.6 Summary

In this chapter, a method to get full plastic moment of exposed column bases from the moment-column base rotation hysteresis curve was proposed and confirmed by the results of a full-scale exposed column base experiment. With this proposed method, by summarizing and analyzing the previous experiment data, the accuracy and applicability of bearing stress calculation equations in the case of exposed column bases are evaluated. Key conclusions are listed below:

Previous experiment studies on the bearing stress were summarized and analyzed using three calculation methods (AIJ, K & M, and ACI methods). In the case of steel column without base plate loaded on concrete foundation, AIJ and ACI methods could evaluate the maximum strength very conservatively. For K & M method, the evaluation results showed a great discrepancy. In contrast, for exposed column bases, K & M method showed better agreement with the experimental results than AIJ and ACI methods. Thus, it was considered that a correlation exists between the bearing stress and the ratio of bearing area to loading area.

With the embedded length of anchor rods and type of anchor rods as parameters, a full-scale exposed column base experiment was conducted. The parameters were not observed to have a significant influence on the ultimate strength. From the strain behavior of anchor rods, a method to obtain the full plastic moment from the bending moment-column base rotation hysteresis curve was proposed and proved effective through a comparison between experimental and calculation results. Further, a database of the results of previous experiment studies on exposed column bases was established. Considering the yielding of anchor rods and the bending moment–column base rotation hysteresis curve, 129 specimens were summarized in total. These experiment results were normalized and analyzed.

The analysis results revealed that all the evaluation methods tend to underestimate the ultimate strength of specimens when $n > 0.4$. In contrast, for $n < 0.2$, all the methods tend to overestimate the maximum strength in the case of exposed column bases subjected to

compressive or tensile axial force. As components of *n*, the axial force played a significant role in the evaluation results and showed a positive correlation with the ratio of experimental to calculated results, while the tension of anchor rods was not observed to have an influence. Furthermore, there was no significant correlation between the compression stress of concrete and the evaluation results.

The evaluation results were statistically analyzed. A comparison of all the calculation methods revealed that AIJ method is the most conservative, with the least number of overestimated specimens. A comparison between K & M and ACI methods revealed that K & M method is better when considering the LRFD philosophy. Finally, considering the design philosophy prevalent in Japan, a more conservative calculation method is proposed based on the definition of loading area and bearing area in K & M method.

References

[4-1] Architectural Institute of Japan: 2017, AIJ Guidebook on Design and Fabrication of Column Base in Steel Structure, Maruzen, Tokyo, 2017 (in Japanese).

[4-2] Hawkins N. The bearing strength of concrete loaded through rigid plates. Magazine of Concrete Research 1968; Vol. 20, No. 62; 31-40.

[4-3] Usami T. Kei T. Aoki M. Bearing strength of concrete pile loaded by axial force from steel column. J Struct Constr Eng AIJ 2003; 572; 111-116. https://doi.org/10.3130/aijs.68.111_5 (in Japanese).

[4-4] Kutani K. Masuda K. Experimental studies on bearing strength on concrete footings at exposed type of steel column bases. J Struct Constr Eng AIJ 1991; 427; 59-68. https://doi.org/10.3130/aijsx.427.0_59 (in Japanese).

[4-5] Architectural Institute of Japan: 2021, Recommendation for design of connections in steel structures, Maruzen, Tokyo, 2021 (in Japanese).

[4-6] American Concrete Institute (ACI), Building code requirements for structural concrete and commentary (ACI 318-19), Detroit.

[4-7] Kutani K. Masuda K. Experimental studies on ultimate strength of exposed type of steel column bases. J Struct Constr Eng AIJ 1992; 433; 39-49. https://doi.org/10.3130/aijsx.433.0_39 (in Japanese).

[4-8] Kutani K. Masuda K. Experimental studies on load carrying mechanism of exposed type of steel column bases. J Struct Constr Eng AIJ 1992; 440; 113-124. https://doi.org/10.3130/aijsx.440.0_113 (in Japanese).

[4-9] Yang X. Tatsumi N. Ishida T. Kishiki S. Yamada S. Experimental study on structural behavior of exposed column base with concrete foundation. Proceedings of Constructional Steel 2018; 26; 666-671.

[4-10] Masuda K. Experimental studies on mechanical characteristics of the steel

column bases. J Struct Constr Eng AIJ 1980; 297: 11-23. https://doi.org/10.3130/aijsaxx.297.0_11 (in Japanese).

[4-11] Kadoya H. Kawaguchi J. Morino S. Experimental study on elastic-plastic behavior and ultimate strength of exposure fixed-type steel column-base subjected to bending moment. J Struct Constr Eng AIJ 2004; 583; 123-130. https://doi.org/10.3130/aijs.69.123_4 (in Japanese).

[4-12] Tanaka T., et, al. Elasto-plastic behaviour of exposed type of column bases with tensile force. Part1-2. Summaries of technical papers of annual meeting AIJ 1999, 633-636 (in Japanese).

[4-13] Somiya Y. Fukuchi Y. Chin B. Experimental study on elasto-plastic behavior and strength estimation of exposed-type column base with variable axial force. J Struct Constr Eng AIJ 2002; 562; 137-143. https://doi.org/10.3130/aijs.67.137_3 (in Japanese).

[4-14] Kajiyama H., et, al. Elasto-plastic behavior of exposed-type steel column basae with anchor bolt yielding. Part 1. Experimental program and results. Summaries of technical papers of annual meeting AIJ 2001, 949-950 (in Japanese).

[4-15] Yokoyama M., et, al. Experimental study on mechanical characteristic of steel column bases under fixed axial force part 1. Summaries of technical papers of annual meeting AIJ 2002, 789-790 (in Japanese).

[4-16] Yamakubo H., et, al. Experimental study on column bases under combined bending moment and shearing force. Technical papers of annual meeting AIJ (Kinki branch) 1995, 137-140 (in Japanese).

[4-17] Kawabata I., et, al. Structural behavior of exposed type of steel column base using screw re-bars. Part1-3. Summaries of technical papers of annual meeting AIJ 2006, 799-804 (in Japanese).

[4-18] Nishimura K., et, al. Experimental study on exposed type steel column bases using mechanical anchorages and screw re-bars. Part 1-3. Summaries of technical papers

of annual meeting AIJ 2004, 753-758 (in Japanese).

[4-19] Yoshimori K. Nakashima S. Mechanical behavior of steel column bases with small degree of fixity. Technical papers of annual meeting AIJ (Kinki branch) 1998, 345-348 (in Japanese).

[4-20] Yoshimori K. Nakashima S. Mechanical behavior of steel column bases with small degree of fixity (No.2). Technical papers of annual meeting AIJ (Kinki branch) 2001, 249-252 (in Japanese).

[4-21] Tanaka A. Masuda H. Motoda T. Experimental study on the exposed-type column base using anchor bolts with upset threaded parts. Kou kouzou rombunshuu 1999; Vol. 6 No. 24; 103-109. https://doi.org/10.11273/jssc1994.6.24_103 (in Japanese).

[4-22] Yamakubo H., et, al. Experimental study on mechanical characteristics of steel tubular column bases. Part 1. Full scale test of column bases using high strength anchor bolt. Summaries of technical papers of annual meeting AIJ 1998, 513-514 (in Japanese).

[4-23] Yamakubo H., et, al. Experimental study on mechanical characteristics of steel tubular column bases. Part 2. Full scale test of column bases using high strength anchor-bolts Summaries of technical papers of annual meeting AIJ 2000, 761-762 (in Japanese).

[4-24] Komatsu H., et, al. Structural behavior of column base for drive-in parking frame. Report-4. Column base bending test for column of depths 250mm and 300mm. Summaries of technical papers of annual meeting AIJ 1999, 685-686 (in Japanese).

[4-25] Trautner C, Hutchinson T, Grosser P, Silva J. Effects of detailing on the cyclic behavior of steel baseplate connections designed to promote anchor yielding. J Struc Eng 2015. DOI: 10.1061/(ASCE)ST.1943-541X.0001361

[4-26] Trautner C, Hutchinson T, Grosser P, Silva J. Investigation of steel column-baseplate connection details incorporating ductile anchors. J Struc Eng 2017. DOI: 10.1061/(ASCE)ST.1943-541X.0001759

Appendix

In the appendix, the parameter matrix experiment results related to bearing stress experiments were summarized and listed in the tables below.

Table 4-3 Parameter matrix and experiment results of [4-2]

Specimen ID	**Steel plate**		**Position of plate**	**Concrete block**	**Experiment results**
	$2b$	$2a$		f_c	f_b/f_c
	[mm]	[mm]		[MPa]	-
K1	25.4	25.4	corner	21.2	1.43
K2	25.4	25.4		30.1	1.55
K3	36.1	36.1		21.0	1.44
K4	50.8	50.8		21.0	1.54
K5	62.2	62.2		21.0	1.41
K6	76.2	76.2		24.6	1.29
L1	25.4	25.4	edge	44.1	2.42
L2	29.71	29.71		44.1	2.22
L3	36.06	36.06		47.2	2.01
L4	43.68	43.68		44.1	1.99
L5	61.46	61.46		47.4	1.75
L6	76.2	76.2		38.2	1.4
L7	43.68	43.68		30.1	1.95
L8	36.06	36.06		47.7	2.12
L9	50.8	50.8		47.7	1.77
L10	76.2	76.2		47.7	1.52
M1	50.8	50.8		26.5	1.91
M2	76.2	76.2		26.5	1.71
N1	50.8	50.8		35.0	1.68
N2	76.2	76.2		35.0	1.38
R1	29.21	57.15		46.8	2.2
R2	27.94	71.12		46.8	2.23
R7	50.8	72.39		47.2	1.84
S1	38.1	25.4		34.1	2.13

S2	50.8	25.4			34.1	1.92
S3	76.2	25.4			34.1	1.57
S4	50.8	76.2			34.1	1.71
S5	76.2	50.8			34.1	1.48
O1	25.4	25.4	28.194*	28.194*	29.8	3.14
O2	25.4	25.4	52.07*	52.07*	31.2	4.21
O3	25.4	25.4	76.2*	76.2*	29.1	5.73
P1	12.7	25.4	edge		33.1	2.09
P2	25.4	25.4	76.2*	33.782*	36.9	3.35
P3	25.4	25.4	76.2*	55.118*	31.9	5.22
Q1	36.06	36.06	38.1*	38.1*	36.8	2.37
Q2	43.94	43.94	38.1*	38.1*	33.7	1.76
Q3	50.8	50.8	38.1*	38.1*	35.0	1.59

Note: 2*b*: Length of the longer side of a rectangular plate or the side coincident with the edge for edge loading, 2*a*: Length of the shorter side of a rectangular plate or side of square plate

* Distance (mm) from the center of plate to the corner of block.

Table 4-4 Parameter matrix and experiment results of [4-3]

Specimen ID	**Shape of column**	**Section (all in mm)**	**Concrete cylinder**	**Experiment results**
			f_c	N_e
			[MPa]	[kN]
H5-2	H ($b*h*t_w*t_f$)	50*50*3*6	24.8	128
H5-4			44.1	205
H5-6			64.5	229
H8-2		35*35*2*3	24.8	95.9
H8-4			47.7	171
H8-6			64.5	179
DH5-2	King cross ($b*h*t_w*t_f$)	20*50*3*6	24.8	143
DH5-4			44.1	237
DH5-6			64.5	272
R5-2	Square	50*50*3.8	24.8	147

R5-4	hollow section (b*h*t)		44.1	232
R5-6			64.5	283
R8-2		26.6*26.6*2.9	24.8	102
R8-4			47.7	165
R8-6			64.5	177
S5-2	Square plate (a*a)	26.6*26.6	24.8	97.7
S5-4			44.1	165
S5-6			64.5	195
S8-2		16.6*16.6	24.8	70
S8-4			47.7	117
S8-6			64.5	114
S12-2		11.1*11.1	24.8	45.7
S12-4			47.7	71.3
S12-6			64.5	74.5
C5-2	Circular plate	Φ30	24.8	100
C5-4			44.1	164
C5-6			64.5	184

Note: b: Width of flange, h: Depth of beam, t_w: Thickness of web, t_f: Thickness of flange, t: Thickness of square hollow section, a: Side length of square plate.

Table 4-5 Parameter matrix and experiment results of [4-4]

Specimen ID	**Section of steel column[1] (all in mm)**	**Base plate**	**Concrete column**	**Compression strength**	**Experiment results**
		b_{bp}*d_{bp}*t_{bp}	b_{rc}*d_{rc}	f_c	N_e
		All in mm	All in mm	[N/mm^2]	[kN]
CC1	S-150*150*20	300*300*40	300*300	20.3	2501.9
CC2	S-150*150*20	300*300*19	300*300	20.3	1725.8
CC3	S-150*150*20	300*300*12	300*300	20.3	1552.3
CC4	S-150*150*20	300*300*40	350*350	20.3	2746.0
CC5	S-150*150*20	300*300*19	350*350	20.3	1929.6
CC6	S-150*150*20	300*300*12	350*350	20.3	1766.0
CC7	S-150*150*20	300*300*40	400*400	20.3	3677.9
CC8	S-150*150*20	300*300*19	400*400	20.3	2157.0

CC9	S-150*150*20	300*300*12	400*400	20.3	1865.9
CC11	S-150*150*20	300*300*19	400*400	24.1	2744.0
CC12	S-150*150*20	300*300*16	400*400	24.1	2726.4
CC13	S-150*150*20	300*300*12	400*400	24.1	2345.1
CC14	S-150*150*20	300*300*75	400*400	23.8	3579.0
CC15	S-150*150*20	300*300*25	400*400	23.8	2354.9
CC16	S-150*150*20	300*300*19	400*400	23.8	2124.6
CC17	S-150*150*20	300*300*12	400*400	23.8	1567.0
CC18	S-200*200*20	300*300*40	400*400	22.9	3718.1
CC19	S-200*200*20	300*300*25	400*400	22.9	3475.1
CC20	S-200*200*20	300*300*19	400*400	22.9	3408.4
CC21	S-200*200*20	300*300*16	400*400	22.9	3211.5
CC22	S-200*200*20	300*300*12	400*400	22.9	2248.1
CC23	S-200*200*20	300*300*9	400*400	22.9	2423.5
CC25	C-165*20	300*300*40	400*400	20.8	3216.4
CC26	C-165*20	300*300*25	400*400	20.8	2337.3
CC27	C-165*20	300*300*19	400*400	20.8	1756.2
CC28	C-165*20	300*300*16	400*400	20.8	1370.0
CC29	C-165*20	300*300*12	400*400	20.8	1273.0
CC30	C-165*20	Φ300*40[2]	400*400	20.8	2681.3
CC31	C-165*20	Φ300*25	400*400	20.8	2198.1
CC32	C-165*20	Φ300*19	400*400	20.8	1963.9
CC33	C-165*20	Φ300*16	400*400	20.8	1677.8
CC34	C-165*20	Φ300*12	400*400	20.8	1240.7
CC35	S-175*175*20	300*300*40	400*400	21.5	1975.7
CC36	S-175*175*20	300*300*19	400*400	21.5	1667.0
CC37	S-175*175*20	300*300*12	400*400	21.5	1665.0
CC38	S-175*175*20	300*300*40	400*400	21.5	2025.7
CC39	S-175*175*20	300*300*19	400*400	21.5	1723.8
CC40	S-175*175*20	300*300*12	400*400	21.5	1614.1
CC41	S-175*175*20	300*300*40	400*400	21.5	1953.1
CC42	S-175*175*20	300*300*19	400*400	21.5	1660.1
CC43	S-175*175*20	300*300*12	400*400	21.5	1570.0
CC44	S-175*175*20	300*300*40	400*400	21.5	2254.0
CC45	S-175*175*20	300*300*19	400*400	21.5	1642.5

CC46	S-175*175*20	300*300*12	400*400	21.5	1588.6
CC47	S-175*175*20	300*300*40	400*400	21.5	2336.3
CC48	S-175*175*20	300*300*19	400*400	21.5	2038.4
CC49	S-175*175*20	300*300*12	400*400	21.5	1697.4
CC50	S-175*175*20	300*300*40	400*400	21.5	3335.9
CC51	S-175*175*20	300*300*19	400*400	21.5	2636.2
CC52	S-175*175*20	300*300*12	400*400	21.5	2107.0
CC64	S-200*200*20	300*300*50	400*400	24.3	2818.5
CC65	S-200*200*20	300*300*19	400*400	24.3	2482.3
CC66	S-200*200*20	300*300*50	400*400	24.3	3704.4
CC67	S-200*200*20	300*300*19	400*400	24.3	3364.3
CC68	S-200*200*20	300*300*19	400*400	24.3	3730.9
CC69	S-150*150*20	300*300*9	400*400	24.3	1809.1
CC70	S-200*200*20	330*330*28	400*400	24.5	2963.5
CC71	S-200*200*20	330*330*28	400*400	24.5	3238.9
CC72	S-200*200*20	330*330*28	400*400	24.5	3725.0
CC73	S-150*150*20	330*330*28	400*400	24.5	2934.1

Note: b_{bp}: Width of base plate, d_{bp}: Depth of base plate, t_{bp}: Thickness of base plate, b_{rc}: Width of concrete column, d_{rc}: Depth of concrete column.

[1] In the section of steel column, S is SHS column, C is circular column.

[2] The shape of base plate is circle.

Table 4-6 Parameter matrix and experiment results of [4-4]

Specimen ID	**Base plate**	**Loading eccentricity**	**Compression strength**	**Experiment results**	
	b_{bp}*d_{bp}*t_{bp}	e	f_c	N_{exp}	M_{exp}
	All in mm	[mm]	[N/mm2]	[kN]	[kN*m]
CE1	330*330*50	100	24.5	1375.9	137.6
CE2	330*330*50	100	24.5	1486.7	148.7
CE3	330*330*50	100	24.5	1663.1	166.3
CE4	330*330*50	100	24.5	1865.9	186.6
CE5	300*300*50	25	25.7	2255.0	56.4
CE6	300*300*50	50	28.5	2105.0	105.3

CE7	300*300*50	75	28.5	1874.7	140.6
CE8	300*300*50	100	28.5	1294.6	129.5
CE9	300*300*50	-[1]	25.7	539.0	67.8
CE10	300*300*50	25	25.7	2725.4	68.1
CE11	300*300*50	50	28.5	2703.8	135.2
CE12	300*300*50	75	28.5	2175.6	163.2
CE13	300*300*50	100	28.5	1706.2	170.6
CE14	300*300*50	-	25.7	686.0	81.8
CE15	300*300*36	25	25.7	2244.2	56.1
CE16	300*300*36	50	25.7	1789.5	89.5
CE17	300*300*36	75	25.7	1393.6	104.5
CE18	300*300*36	100	28.5	1069.2	106.9
CE19	300*300*36	-	25.7	490.0	60.1
CE20	300*300*36	25	25.7	2683.2	67.1
CE21	300*300*36	50	25.7	2023.7	101.2
CE22	300*300*36	75	25.7	1803.2	135.2
CE23	300*300*36	100	28.5	1288.7	128.9
CE24	300*300*36	-	25.7	490.0	58.9
CE25	300*300*25	25	25.7	1862.0	46.6
CE26	300*300*25	50	25.7	1599.4	80.0
CE27	300*300*25	75	25.7	1178.9	88.4
CE28	300*300*25	100	28.5	831.0	83.1
CE29	300*300*25	-	28.5	392.0	52.1
CE30	300*300*25	25	28.5	2366.7	59.2
CE31	300*300*25	50	28.5	1892.4	94.6
CE32	300*300*25	75	28.5	1339.7	100.5
CE33	300*300*25	100	28.5	1021.2	102.1
CE34	300*300*25	-	25.7	490.0	60.9

Note: b_{bp}: Width of base plate, d_{bp}: Depth of base plate, t_{bp}: Thickness of base plate, e: Loading eccentricity as shown in Figure 4-6

[1] Shear force was applied on the specimens as shown in Figure 4-6.

Chapter 5.
Conclusions

5. Conclusions

In this thesis, the research subject is exposed column bases which are widely used in the low-to-medium rise steel structures. To ensure the anchor rods yielding in the exposed column bases, component design approaches were established.

In Chapter 1, the research background and object were stated. Starting with the earthquake damage on the exposed column bases, the design recommendations of exposed column bases were summarized. For the exposed column base design in Japan, different from other design recommendations, the anchor rods are permitted to be yielded. To ensure the yielding of anchor rods, besides the strict restrain on the material property of anchor rods, prevention of concrete breakout failure and bearing failure of foundation concrete is very important. However, the current recommendations did not clearly state the calculation methods of concrete breakout failure and bearing stress. Thus, the experiment with full-scaled exposed column bases was conducted, by analyzing the experiment results, the design approaches of concrete breakout failure strength and bearing strength were proposed.

In Chapter 2, two phases with 10 full-scale exposed column base specimens were tested with cyclic loading applied. Experiment parameters contained the number of column longitudinal rebar, strength of foundation concrete, strength and embedded length of anchor rods, depth of foundation beam, strength and embedded of beam transverse rebar. As the experiment results, the concrete breakout failure cracks were observed, meanwhile, it was found that the concrete breakout failure strength calculated by the current design recommendation in Japan was around twice the experiment results. On the other hand, the full plastic strength calculated by the AIJ recommendation fit well with the experiment results, which was taken as a premise for the discussion of the bearing strength of foundation concrete. The influence of each parameter on the concrete breakout failure strength and bearing stress were also clarified.

In Chapter 3, design approach of concrete breakout failure is proposed. By analyzing the experiment results the contribution of column rebar and concrete on the concrete breakout failure strength was clarified. In the case of specimens without column rebar,

the concrete breakout failure strength was approximately 1.36 to 1.68 times higher than calculated values, while the strength deterioration caused by concrete breakout failure was not observed. The current design recommendation in Japan overestimates the number of effective column rebar in the evaluation of pull-out strength of anchor rods. Not all of the column rebar in the concrete breakout failure area were contributed. Furthermore, the number of effective column rebar is changed with the position of column. With the proposed reduction method of the number of effective column rebar, in the calculation of maximum strength, the current reduction factor applied to the strength of column rebar could fit well with the experiment results. Regarding the contribution of concrete, the experimental results confirmed its value at the instant which conical cracks occurred and identified the ultimate state. In the design of the tension of anchor rods, to prevent the occurrence of conical cracks, it was proposed that a reduction factor should be applied to the contribution of concrete. Subsequently, after the concrete breakout failure crack occurred, the strength of effective column rebar should also be considered for the ultimate strength. Overall, based on the proposed calculation method for concrete breakout failure strength, it could evaluate the experimental results with good accuracy. To confirm the applicability of the proposed design approach, previous experimental results were also collected, which demonstrated good fitness.

In Chapter 4, a method to get full plastic moment of exposed column bases from the moment-column base rotation hysteresis curve was proposed and confirmed by the experiment results. With this proposed method, by summarizing and analyzing the previous experiment data, the accuracy and applicability of current bearing stress calculation equations in the case of exposed column bases are evaluated. Calculation equations contained the design recommendations in Japan (AIJ method) and United States (ACI method), and a proposal from previous research (K & M method). It was observed that all the evaluation equations tend to underestimate the ultimate strength of specimens when the axial force component $n > 0.4$. However, when $n<0.2$, all the methods tend to overestimate the maximum strength in the case of compressive or tensile axial force applied on the exposed column bases. In the case of compressive axial force,

compared with the tension of anchor rods, the axial force took a significant role in the evaluation results that they were positively correlated. On the other hand, the correlation between the evaluation results and compression stress of concrete was not observed. The accuracy of all the methods was clarified, comparing with all the evaluation methods, AIJ method was the most conservative method with the least number of overestimated specimens. Furthermore, considering the design philosophy in Japan, a more conservative method is proposed. Comparing with K&M and ACI methods, K&M method fit better when considering LRFD design philosophy.

In all, considering the design of exposed column bases in Japan, to ensure the yielding of anchor rods, the design approaches of concrete breakout failure and bearing failure of the foundation concrete were proposed as illustrated in Figure 5-1.

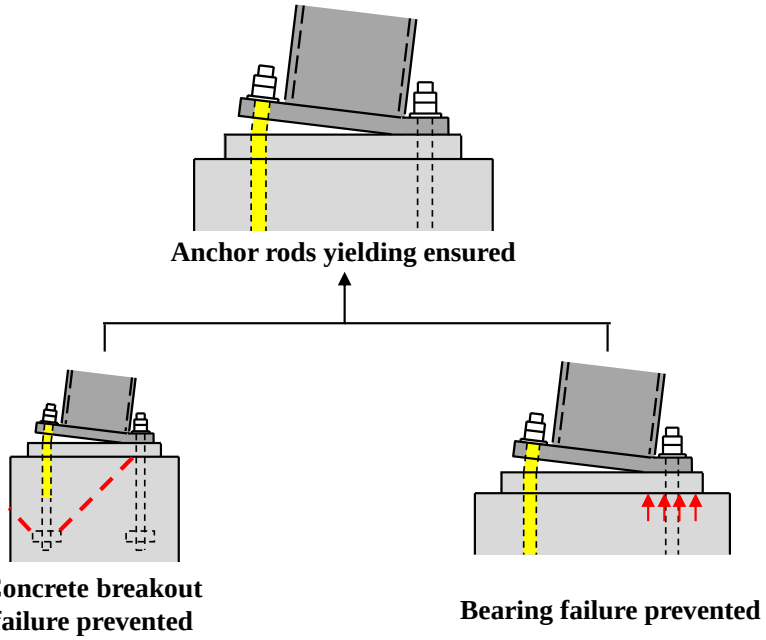

Figure 5-1 Research flow of the thesis

For the concrete breakout failure, the stagewise design approach was proposed. The concrete breakout failure crack could be controlled by considering only the contribution of concrete strength on the concrete breakout failure. Then, after the concrete breakout failure crack occurred, the strength of column longitudinal rebar could be added for the ultimate strength. The number of effective column rebar is also clarified. For the concrete bearing failure, the current evaluation methods are summarized and analyzed by the

database containing previous experiment results. The accuracy and applicability of these methods on different design philosophies were clarified. Furthermore, based on the design philosophies of Japan, considering the simplicity in the design, a more conservative design approach was proposed. Following the above design approaches, the concrete breakout failure and bearing failure of foundation concrete could be prevented. Thus, the yielding of anchor rods could be ensured.

Acknowledgment

Firstly, huge thanks to my supervisor, Prof. Kishiki Shoichi for all of his teaching. I could not appreciate it more and I believe that without his teaching, I could not be me like today. He saved me so many times and hinted at me again and again. I really appreciate that he did not give up on me as I made him disappointed so many times. In addition to academic topics, we also talked about many things in our lives, which also greatly influenced my view of things close to my life. I don't feel that words are enough to convey my appreciation. If I had to sum it up in one sentence, I would say that I feel so lucky to have you as my supervisor.

Great thanks to Professor Motoyui Shojiro, Professor Kono Susumu, associate Professor Nishimura Koshiro, associate Professor Sato Daiki for the time to review this thesis.

Then, I would like to thank Prof. Yamada Satoshi at the University of Tokyo. Thanks for giving me the chance to study in this amazing Lab. I feel a little ashamed that I could not learn more from him because of my laziness. But I will always be grateful and keep making progress in the research way.

Next, I would like to thank associate Prof. Ishida Takanori at Yokohama National University. He is a really nice teacher. Every time I have research questions, he would like to teach me in a very detailed and basic way to make it so easy to understand. He also assisted and educated me during the entire experiment time, particularly in the early days when I was unable to communicate in Japanese, which made me feel quite relieved that if he was around, everything would be alright.

I would like to thank assistant Prof. Tatsumi Nobuhiko. He helped me a lot in my experiment. I feel very comfortable while talking with him. He is really friendly and approachable. He also led me to the way of drip coffee and I can not live without coffee now. Congratulations on your promotion in advance.

I would like to thank associate Prof. Cui Yao at Dalian University of Technology. She is the one who led me to the research way and made me feel the happiness from research. Without her advice and support, I could not be a member of such a great Lab.

I would like to thank associate Prof. Jiao Yu at Tokyo City University. As a senior who graduated from Yamada Lab., she is more like my sister. We discussed not only research but also many anecdotes that happened before I entered the Lab. That made my image of members in the Lab., especially professors, much richer.

Then, one of the most important members to me who used to be in our Lab, our previous secretary Ibayashi Otone san. She is the sweetest person I have ever met. I can not admire her nice too much. She really made my life much easier in the early years when I was unable to communicate in Japanese, and I could get her warm encouragement all the time.

I would like to thank our previous secretary Miyamoto Aki san. Although we have not been staying together for a not long time, she is very warm and introduces many interesting places in Japan. We had a lot of talks about coffee which were very impressive.

I would like to thank our secretary Okubo Motoko san. She is very nice and she could speak Chinese very well which really surprised me. She would like to help us with many things even something I think I am supposed to do myself. Thanks so much for her help so that we could spend more time on the research and other stuff.

I would like to thank our secretary Nagami Eiko san. Thanks for all your help to the Lab., it could be a great relief to Okubo san I guess. I am sorry that we do not have many talks and get to know more about each other, but thanks again for the works.

I would like to thank the staff in SOFTech, Endo Yuko san, and Tanaka Akira san. Thanks for their help for these years with the RA things. I remember many interesting talks with Endo san and she was always being nice to me which made me feel very warm. Tanaka san, we talked a lot about the Tokyo Olympics volunteer things and that was great memories.

As for my research, the experiment took a significant part. Such that, I would like to thank Tokyo Tekko Co., Ltd. for the funding; Asiss Co., Ltd. for making concrete specimens; Fuso Industries and Hirota Tekkojyo for making the experiment jigs. Several days of work in Asiss impressed me a lot, I felt the people`s life pace there, which I have never imaged before. Also in the research group, Adachi san in Tokyo Tekko, Sakuta san, and Kiyohara san in Horie Engineering and architectural Research Institute, we had a lot of discussions about the whole experiment and they offered many useful ideas for the research. I have to say that I truly appreciate their patience with me because I struggled to grasp Japanese in the first few discussions.

The world has changed a lot in these three years, the same for me. I don't think I could have done it without everyone's help, and my words may seem insufficient to express my gratitude. Observing all of the professors get promoted, as well as the Lab members come and leave

made me feel a lot of emotions. Great thanks to the accompany of all of you for a short or long time, that would be my precious memories.

To Fu Xiang, Zheng Haowen, Li Jiaxi: We have been staying together for such a long time, facing many life choices, solving problems related or not related to research, and drinking, chatting, drinking, fighting, drinking, laughing, and drinking. What we have done together seemed no more important, but the time we spend together or on each other makes these years much more meaningful, colorful, and unforgettable. We have talked a lot and I certainly know we have more things to talk about in the future, no matter where we are or what kind of people we will become. Just wish you all the best and good luck with our bright bright future.

To Xiang Yang: We do not spend a lot of time together, while I got to know a lot of knowledge in our major and after our conversations, I have to admit that there is a significant gap between me and a good civil engineer. Especially after you joined our Lab, I am very impressed that you can imagine what is relevant to research through many real-life things. I think you've shown me the way. Thank you so so much and wish you all the best.

To Nakada Shotaro: You are really special, and we get to know each other more with my improvement of Japanese, or your English, and thanks to Ninniku-ya. Thank you for being energetic most times and annoying for few times, it often made waves deep inside and made me think if I should perform more cheerful. But please just continue to be what you like to be and do not care about others' mind. Wish you all the best and hope we could see each other soon in the future.

To Tanaka Susumu: You are the first Japanese person I have invited to my house for a party. I must admit that I mustered the confidence to make a decision. And I was relieved that I did. Thank you for always being nice and friendly to us and I do remember the time we spend at my home and Tohoku Jinja.

To Randy, Aoyagi, Tsukada, Thaileang, Sugawara, Kibishi, Kotaka, Kotaki, Ishigawa, Sakurada, Kurosawa, Jasmine, Tamada, Sok An, Fujioka, Kato, Pei, Liu, Dong, and Chen: Thank you for all your accompany and help in the lovely or hard days. I really appreciate it. It is my pleasure to work with you. Just give my best wishes to all of you and hope everything will go well in the future.

Of course, except the Lab. members, I also received a lot of support from my friends in these years. When I feel sad, confused about the topics or life, or just bored, I will go to them for a talk. It seems not a big deal but really works.

To Xing Guangchao and Wang Shuming: Nothing special but you just have to be in my acknowledgment since my undergraduate thesis, master thesis, and now. Love you 3000 times.

To Wang Zequn: We had more talks after I got my Master's degree, for reasons only we know. Thank you so so much for your help and without you I could be more like me now. All the best to you and really hope to see you soon.

To Deng Shuo(Shou): You saved me on my hardest days. I could not imagine what will I be like without you in those days. Thank you for always being by my side and talking with me. Sorry, I could not be your side when you are having a hard time, but please remember that if you need me just call me.

At the end of 2020, I got to know some new friends. I had a great time with them; everything that occurred was a new experience for me. Thank you for all of your companionship and happiness.

Also, I want to appreciate An Pu, Troye Sivan, Lauv, Jeff Buckley, Frank Sinatra, Sam Fender, Marshmello, Martin Garrix, and bands Hyukoh, Oaeen, No party for Cao Dong, Surl for their music. I really can not live without music. Thank you for making so so many cheering/touching works. Music never dies.

Finally, for the first time, I made a friend.

To Zhang Guohai: Thanks for all of your understanding, support, and always being at my side, I was so so lucky to meet you. I love you.